STRUCTURAL, MECHANICAL, AND BIOCOMPATIBILITY INVESTIGATIONS OF YTTRIUM AND FLUORIDE DOPED NANO HYDROXYAPATITE

A THESIS SUBMITTED TO
THE GRADUATE SCHOOL OF NATURAL AND APPLIED SCIENCES
OF
MIDDLE EAST TECHNICAL UNIVERSITY

BY

BURÇİN BAŞAR

IN PARTIAL FULLFILLMENT OF THE REQUIREMENTS
FOR
THE DEGREE OF MASTER OF SCIENCE
IN
ENGINEERING SCIENCES

JANUARY 2009

Approval of the thesis:

STRUCTURAL, MECHANICAL, AND BIOCOMPATIBILITY INVESTIGATIONS OF YTTRIUM AND FLUORIDE DOPED NANO HYDROXYAPATITE

submitted by **BURÇİN BAŞAR** in partial fulfillment of the requirements for the degree of **Master of Science in Engineering Sciences Department, Middle East Technical University** by,

Prof. Dr. Canan Özgen
Dean, Graduate School of **Natural and Applied Sciences** _____

Prof. Dr. Turgut Tokdemir
Head of Department, **Engineering Sciences** _____

Assist. Prof. Dr. Zafer Evis
Supervisor, **Engineering Sciences Dept., METU** _____

Assist. Prof. Dr. Ayşen Tezcaner
Co- Supervisor, **Engineering Sciences Dept., METU** _____

Examining Committee Members

Prof. Dr. M. Ruşen Geçit _____
Engineering Sciences Dept., METU

Assist. Prof. Dr. Zafer Evis _____
Engineering Sciences Dept., METU

Assist. Prof. Dr. Ayşen Tezcaner _____
Engineering Sciences Dept., METU

Assist. Prof. Dr. Dilek Keskin _____
Engineering Sciences Dept., METU

Assist. Prof. Dr. Caner Durucan _____
Metallurgical and Materials Engineering Dept., METU

Date: 13.01.2009

I hereby declare that all information in this document has been obtained and presented in accordance with academic rules and ethical conduct. I also declare that, as required by these rules and conduct, I have fully cited and referenced all material and results that are not original to this document.

Name, Last name:

Signature:

ABSTRACT

STRUCTURAL, MECHANICAL, AND BIOCOMPATIBILITY INVESTIGATIONS OF YTTRIUM AND FLUORIDE DOPED NANO HYDROXYAPATITE

Başar, Burçin

M. S., Department of Engineering Sciences

Supervisor: Assist. Prof. Dr. Zafer Evis

Co-Supervisor: Assist. Prof. Dr. Ayşen Tezcaner

January 2009, pages 122

In this study, it was aimed to investigate the structural, mechanical and biological properties of nano hydroxyapatite (HA) doped with yttrium and fluoride with different compositions. HAs were synthesized by precipitation method. After sintering at 900^{o}C, 1100^{o}C or 1300^{o}C for 1 hour, the structural properties of HAs were investigated by XRD, FTIR spectroscopy and SEM. High relative densities (above 88 % of relative density) were achieved after sintering. No second phases were observed in XRD measurements. Hexagonal lattice parameters and unit cell volumes of doped HAs decreased indicating the substitutions of ions. Characteristics absorbtion bands of HA and additional bands due to fluoride substitutions were observed in FTIR patterns. SEM images showed that grain sizes decreased with increasing doping amounts and decreasing sintering temperatures. Discs prepared by cold pressing were sintered at 900^{o}C, 1100^{o}C and 1300^{o}C for 1

hour to determine mechanical properties. Mechanical properties of HAs were found to be directly related to the sintering temperatures and amount of dopings.

Biocompatibility of pure and doped HA discs was assessed with in vitro cytotoxicity studies. Cell attachment, proliferation and differentiation state of cells were studied using MTT, ALP and calcium assays and SEM. Cell attachment and proliferation were enhanced with dopings and increasing sintering temperatures. The highest ALP production and calcium deposition were observed on HAs sintered at 1100^{o}C. *In vitro* studies revealed that 1100^{o}C was the sintering temperature for best cell responses. Specifically, 2.5YFHA seemed to be promising as an alternative for pure HA among all doped HAs.

Keywords: Nano Hydroxyapatite, Yttrium, Fluoride, Mechanical Properties, Biological Properties.

ÖZ

İTRİYUM VE FLOR EKLENMİŞ NANO-HİDROKSİAPATİTİN İÇ YAPI, MEKANİK VE BİYOUYUMLULUK İNCELEMELERİ

Başar, Burçin

Yüksek Lisans, Mühendislik Bilimleri Bölümü

Tez Yöneticisi: Yrd. Doç Dr. Zafer Evis

Yardımcı Tez Yöneticisi: Yrd. Doç Dr. Ayşen Tezcaner

Ocak 2009, sayfa 122

Bu çalışmada nano boyuttaki HA'ya çeşitli oranlarda itriyum ve flor elementleri eklenerek iç yapı, mekanik ve biyolojik özelliklerinin incelenmesi amaçlanmıştır. Saf ve iyon eklenmiş HA'lar çöktürme metodu ile sentezlenmiştir. 900^{o}C, 1100^{o}C ve 1300^{o}C'de 1'er saat sinterlendikten sonra içyapılarını incelemek için XRD, FTIR spektroskopisi ve SEM incelemeleri yapılmıştır. Yoğunlukları oldukça yüksek (% 88'in üstünde) malzemeler elde edilmiştir. İkincil faz oluşumlarına rastlanmamıştır. İyon eklenmiş HA'ların hegzagonal latis parametreleri ve birim hücre hacimleri saf HA'ya göre azalmıştır. Bu sonuçlar iyonların yer değiştirdiği ancak HA bozunmadığını göstermektedir. FTIR grafiklerinde HA'nın karakteristik eğrileri ile birlikte florun yer değiştirmesi sonucu oluşan diğer eğrilere de rastlanmıştır. SEM fotoğrafları eklenen elementlerin oranları arttıkça ve sıcaklıklar azaldıkça tane boyutlarının azaldığını göstermiştir.

Soğuk presle hazırlanan diskler 900^{o}C, 1100^{o}C ve 1300^{o}C'de 1'er saat sinterlendikten sonra mekanik özellikleri incelenmiştir. Mekanik özellikler sinterleme sıcaklıkları ve eklenen elementlerin miktarları ile doğrudan ilgilidir

Saf ve iyon eklenmiş HA disklerinin biyouyumlulukları sitotoksisite çalışmaları ile yapılmıştır. Hücre yapışması, çoğalması, ALP ve depolanan miktarları MTT, ALP analizleri ve SEM kullanılarak çalışılmıştır. Eklenen elementler ve artan sıcaklıklar hücrelerin daha iyi yapışmasını ve çoğalmasını sağlamıştır. En yüksek ALP aktiviteleri ve kalsiyum miktarları 1100^{o}C'de sinterlenen malzemeler üzerinde gözlenmiştir. Hücrelerin farklılaşma özellikleri eklenen elementlerin konsantrasyonuna bağlıdır. Hücre çalışmalarında en iyi sonuçlar 1100^{o}C'de sinterlenen HA'larda görülmüştür. Özellikle bu sıcaklıktaki 2.5YFHA'nın saf HA'ya göre en umut verici malzeme olduğu söylenebilir.

Anahtar Sözcükler: Nano Hidroksiapatit, İtriyum, Flor, Mekanik Özellikler, Biyolojik Özellikler

ACKNOWLEDGEMENTS

I would like to express my gratitude to my advisor Assist. Prof. Dr. Zafer Evis and co-advisor Assist. Prof. Dr. Ayşen Tezcaner for their enthusiastic guidance and patience throughout the study. I am so grateful to my advisors for their encouragement and generosities to let me work in their laboratories and to let me benefit from their profound minds and knowledge. It would be very troublesome for me to finish my thesis work if they did not rely on me and not support my works at every stage of this thesis.

I would like to also thank to Assist. Prof. Dr. Dilek Keskin for her guidance throughout this thesis, especially *in vitro* studies.

I must to thank to especially my lab friends Ayşegül Kavas and Özge Erdemli for their instructions and assistance for *in vitro* experiments and their further supports for everything. Moreover, I owe many thanks to my other lab friends Ömer Aktürk, Özlem Aydın, Pınar Sun and Seylan Aygün for their fellowships.

I would like to give my special thanks to my ancient and forever friends Burcu Saka, Dilek Torun, Hacer Selamoğlu, Özlem Sözal and Pınar Bukağıkıran for their always being beside me to support me every time.

My greatest thanks should be for my beloved parents Nezaket Başar, Yaşar Başar and my little brother Berk Başar for their endless supports and encouragements at every stage of my life and this thesis.

Finally, I would like to acknowledge The Scientific and Technological Research Council of Turkey (Project number: 105M271) for the financial support.

TABLE OF CONTENTS

LIST OF TABLES

LIST OF FIGURES

LIST OF ABBREVIATIONS

2.5YFHA : Hydroxyapatite doped with 2.5 % Y^{3+} and 2.5 % F^-

5YFHA : Hydroxyapatite doped with 5 % Y^{3+} and 2.5 % F^-

7.5YFHA : Hydroxyapatite doped with 7.5 % Y^{3+} and 2.5 % F^-

ALP : Alkaline Phosphatase

AMP : Adenosine monophosphate

BCA : Bicinchoninic Acid

DMEM : Dulbecco's Modified Eagle's Medium

DMSO : Dimethyl Sulfoxide

FA : Fluorapatite

FBS : Fetal Bovine Serum

FHA : Fluoridated Hydroxyapatite

FTIR : Fourier Transfer Infrared Spectroscopy

HA : Hydroxyapatite

JCDPS : Joint Committee on Powder Diffraction Standards

MTT : Methylthiazolyldiphenyl-tetrazolium

PBS : Phosphate Buffer Saline

pNPP : p-Nitrophenyl Phosphate

SEM : Scanning Electron Microscopy

TCPS : Tissue Culture Polystyrene

β-TCP : β-Tricalcium Phosphate

XRD : X-Ray Diffraction

CHAPTER 1

1. INTRODUCTION

1.1 Bone

1.1.1 Functions of Bone

Bone is a highly specialized and complex tissue. It has a hierarchical structural organization. The bone and the cartilage together constitute the skeletal system. The basic functions of the bone in the body are summarized in Table 1.1.

Table 1.1. The basic functions of bone in the body (adapted from [1, 2, 3])

	FUNCTIONS
Mechanical	To provide a frame for supporting structurally and providing sites for muscles to attach
Protection	To protect internal vital organs
Movement	To generate and transfer forces locomotion
Chemical/Biological	To reserve ions (Ca^{2+}, PO_4^{3-}, etc.) essential for metabolism, to provide acid-base balance and detoxification
Hematological	To make blood cells in bone marrow.

1.1.2 Bone Structure and Composition

Bone is a natural composite which mainly consists of a ceramic (carbonated non-stoichiometric HA) and a polymer (collagen). Bones have different shapes according to their locations and functions throughout the body as seen in Table 1.2.

Table 1.2. The classification of bones according to shapes in the body

SHAPE	PROPERTIES
Long Bone	- consist of a long shaft (diaphysis) and two articular surfaces (epiphyses), - transmit longitudinal forces, provide support and movement. - e.g. femur, tibia, humerus, phalanges.
Short Bone	- roughly cube-shaped - have a thin layer of compact bone surrounding a spongy interior - provide elasticity, flexibility, shock absorbance and movement - thin and generally curved - e.g. carpals, tarsals.
Flat Bone	- have a spongy bone layer between two compact bone layers - protect internal organs - e.g. skull, ribs, scapula, sternum.
Irregular Bone	- irregular and complicated in shape - consist of thin layers of compact bone surrounding spongy interior - various functions: support, movement, etc. - e.g. vertebrae, some facial bones.

Bone has highly hierarchical levels of arrangement. These levels are: 1) macro level: compact and spongy bone, 2) micro level (from 10 to 50 μm): Haversian systems, osteons, single trabeculae, 3) sub-micron level (1-10 μm): lamellae, 4) nano level (from a few hundred nanometers to 1 μm): fibrillar collagen, embedded mineral, 5) sub-nano level (below a few hundred nanometers): molecular structure of constituent elements such as minerals, collagen, non-collagenous organic proteins [4]. The hierarchically organized structure is illustrated in Figure 1.1.

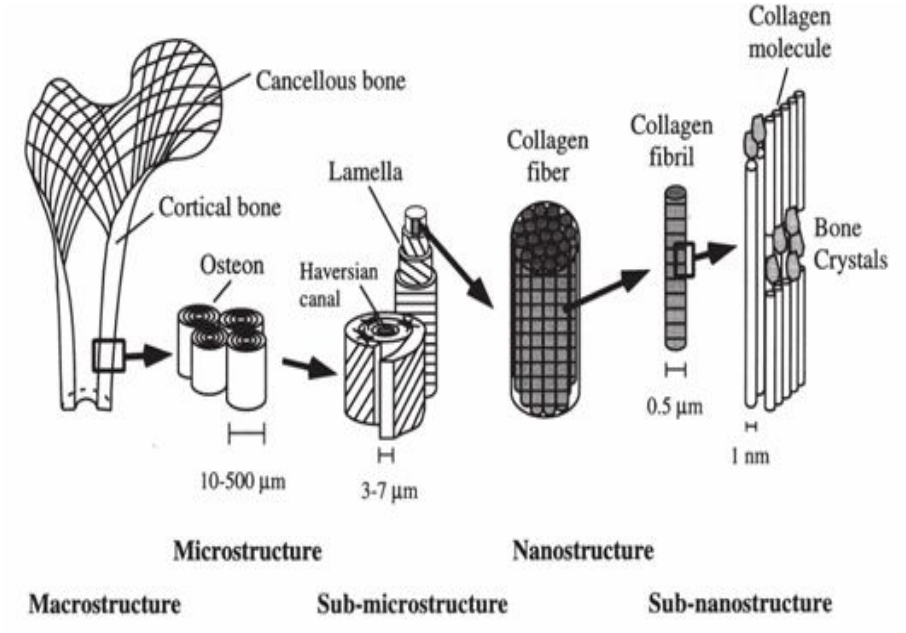

Figure 1.1. Hierarchically organized structure of bone [4].

Compact (or cortical) bone and spongy (or trabecular or cancellous) bone are represented in Figure 1.2.

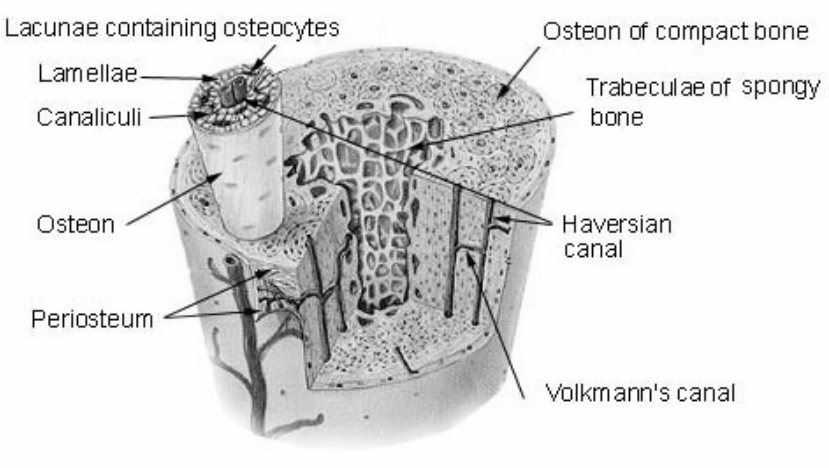

Figure 1.2. Bone structure: compact bone and spongy bone [5].

Trabecular bone has an open cell porous network. It consists of rod and plate-like elements that provide space for blood vessels and marrow. Trabecula which is rod or plate-like structure is known to be the basic functional unit of trabecular bone. These structures are generally not greater than 200 μm in thickness and between 1 μm and 1 mm in length. Cortical bone is denser than trabecular bone; it protects the underlying structures and helps the long bones to resist the stresses on them.

Compact bone consists of mineral (69 wt %) and organic phases (22 wt %) together with water (9 wt %) [6]. 95 wt % of the organic part of cortical bone is collagen type I; the rest is proteoglycans and other non-collagen proteins [7]. The basic functional unit of compact bone is the osteon including the blood vessel and surrounding concentric lamellas. In the center of osteons, there are haversian channels that contain blood vessels and nerve. Additionally, there are other structures namely Volkmann channels, lacunae, and canaliculi [8, 9]. The mineral part of the bone is constituted by calcium phosphates, in the forms of crystallized HA and/or amorphous calcium phosphates (ACP), which contains various ions like Na^+, Mg^{2+}, K^+, CO_3^{2-}, Cl^-, and F^-, listed in Table 1.3 [10-13]. Biological apatites are present in needle or plate forms scattered throughout the organic (collagen) matrix

(Figure 1.3). The widths of crystals are between 1.5 nm and 7.5 nm and their lengths are between 20 nm and 70 nm [6, 7, 12, 14]. Nano-sized dimension and low crystallinity with non-stoichiometric composition, inner crystalline disorder and presence of carbonate ions in the crystal lattice are two important characteristics of biological apatites. [1].

Table 1.3. Comparative composition and crystallographic properties of cortical bone and HA [6, 7, 10-14].

Constituents (wt %)	**Cortical Bone**	**Hydroxyapatite**
Calcium, Ca^{2+}	24.5	39.6
Phosphorus, P	11.5	18.5
Ca/P molar ratio	1.65	1.67
Sodium, Na^{2+}	0.7	Trace
Magnesium, Mg^{2+}	0.55	Trace
Potassium, K^{+}	0.03	Trace
Carbonate, CO_3^{2+}	5.8	–
Fluoride, F^{-}	0.02	–
Chloride, Cl^{-}	0.10	–
Total inorganic	65.0	100
Total organic	25.0	–
Absorbed H_2O	9.7	–
Crystallinity index	33-37	100
Crystallite size	20-70nm x 1.5-7.5 nm	Changes with synthesis method

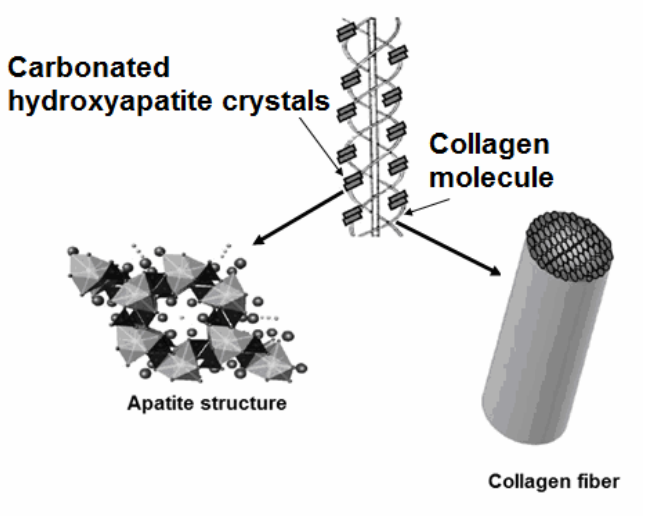

Figure 1.3. Arrangement of carbonate HAs and collagen molecules in the formation of hard tissues [1].

Bone can be considered as "living biomineral" since there are active cells inside them. These are bone lining cells, osteoblasts, osteoclasts and osteocytes [3]. *Bone lining cells*, which are flat and elongated in shape, cover all surfaces of bone. They control the movement of ions (Ca^{2+}, PO_4^{3-}, etc) between the body and the bone. Bone lining cells are considered as inactive osteoblasts and they are derived from osteoprogenitor cells via complex series of changes. *Osteoblasts* are formed from bone lining cells and they are cubodial single nucleated cells on the bone surface. The function of osteoblast is the formation of bone. They initially lay down the collagenous matrix called osteoid. Osteoblasts play a role in the deposition of minerals (mineralization) on this matrix. *Osteoclasts* are bone-resorption cells. They are giant multinucleated cells derived from precursor cells circulating in the blood. They dissolve bone by secreting H^+ and acids for matrix dissolution and enzymes (collagenase) for degradation of the matrix. *Osteocytes* are bone maintaining cells, which are found in the bone. The osteocytes are derived from osteoblasts. They are imprisoned in the matrix during bone tissue production. They survive in hollows of lacunae, and connect with neighboring osteocytes and bone lining cells through

canaliculli. They are responsible in bone formation, matrix maintenance and calcium homeostasis. They possibly act as sensors of mechanical stimuli and they communicate with osteoblasts and osteoclasts.

1.1.3 Biomechanical Properties of Bone

In order to decide which materials should be used as an implant in the body, it is crucial to understand the type and the amount of the stresses formed on the implant site that the implant is going to be inserted. Therefore, the mechanical properties of the bone in the body are needed to be investigated. The candidate materials used as implants should be chosen according to compensation capability for the original one. Not only the biocompatibility within the body but also the mechanical integrity should be taken into consideration for implant material choice. A typical stress-strain curve of a bone is given in Figure 1.4. Additionally, Table 1.4 summarizes some mechanical properties of human cortical bone; these data are collected from cited researches.

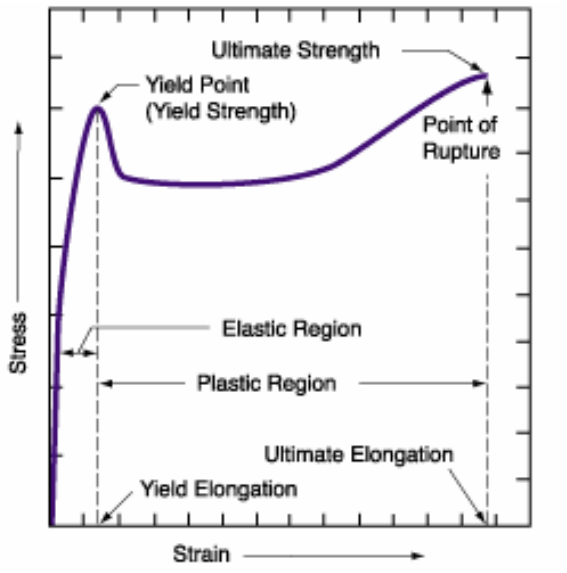

Figure 1.4. A typical stress-strain curve of a bone under tension [15].

Table 1.4. Some mechanical properties of human cortical bone

	Test directions according to bone axis		
	Parallel	**Normal**	**References**
Tensile strength (MPa)	124-174	49	[16, 17]
Compressive strength (MPa)	170-193	133	[16, 17]
Bending strength (MPa)	160	–	[16]
Shear strength (MPa)	54	–	[16]
Young's modulus (GPa)	17.0-18.9 20-27 (random)	11.5	[16, 17, 18, 19]
Fracture Toughness ($MPa.m^{1/2}$)	2-12	–	[20, 21]
Hardness (GPa)	0.396 (no direction stated)	–	[22]
Ultimate tensile strain	0.014-0.031	–	[16, 17]
Ultimate compressive strain	0.0185-0.026	–	[16, 17]
Yield tensile strain	0.007	–	[17]
Yield compressive strain	0.010	–	[17]

1.2 Calcium Phosphates

Calcium phosphates have been used in medical applications throughout last five decades because they show high biocompatibility in the human body. Elemental composition of calcium phosphates, listed in Table 1.5, shows very close resemblance to the minerals of the bone and teeth. However, they are weak against to heavy loads due to their brittleness.

Table 1.5. Calcium phosphates family and their application area listed according to Ca/P ratio.

Ca/P ratio	Name	Abbreviation	Formula	Some Applications
0.5	Calcium metaphosphates (α, β, ϒ)	CMP	$Ca(PO_3)_2$	Fillers in dental composites, cements and adhesive [23]
0.5	Monocalcium phosphate monohydrate	MCPM	$Ca(H_2PO_4)_2{\cdot}H_2O$	Bone cement [24]
0.67	Tetracalcium dihydrogen phosphate	TDHP	$Ca_4H_2P_6O_{20}$	
0.7	Hepta calcium phosphate	HCP	$Ca_7(P_5O_{16})_2$	
1.0	Calcium pyrophosphate (α, β, ϒ)	CPP	$Ca_2P_2O_7$	
1.0	Calcium pyrophosphate dihydrate	CPPD	$Ca_2P_2O_7{\cdot}2H_2O$	
1.0	Dicalcium phosphate	DCPA	$CaHPO_4$	Coating on implant [25]
1.0	Dicalcium phosphate dihydrate	DCPD	$CaHPO_4{\cdot}{\cdot}2H_2O$	Coating on implant [26]

Table 1.5. (continued) Calcium phosphates family and their application area listed according to Ca/P ratio.

Ca/P ratio	Name	Abbreviation	Formula	Some Applications
1.33	Octacalcium phosphate	OCP	$Ca_8(PO_4)_6H_2 \cdot 5H_2O$	Coating of metallic implants [27], scaffold construct [28]
1.50	Tricalcium phosphate (α, β, ϒ)	TCP	$Ca_3(PO_4)_2$	Bone replacement [29], drug delivery [30], bone cement [24]
1.50	Calcium-deficient hydroxyapatite	CDHA	$Ca_9(HPO_4)(PO_4)_5OH$	Scaffold for bone tissue [31]
1.67	Hydroxyapatite	HA	$Ca_{10}(PO_4)_6(OH)_2$	Bone substitute [32], bone cement [33], drug delivery [34], coating of metallic implants [35]
2.0	Tetracalcium phosphate	TetCP	$Ca_4(PO_4)_2O$	Self-setting cement [12]

The most widely studied calcium phosphates are HA and TCP. HA has a great importance in biomedical applications owing to its superior biocompatibility and slow dissolution rate in the body. TCP is also used as a biomaterial; however it has high resorption rate and very poor mechanical properties, accordingly.

1.3 Nano Hydroxyapatite

HA is widely used as a substitute for bones and teeth owing to its excellent biocompatibility [20, 36] and its similar structure with the mineral part of the bone [29]. However, its mechanical properties such as strength, hardness and toughness do not comply with mechanical properties of bone (Table 1.6) and limit its applications in load-bearing areas [24]. HA has been used in non-load bearing areas such as ossicles in middle ear, replacements for tooth roots [13, 20, 37].

Table 1.6. Comparative mechanical properties of cortical bone and HA.

Properties	**Bone**	**HA**
Density (g/cm^3)		3.156
Tensile Strength (MPa)	124-174	40-300
Compressive Strength (MPa)	170-193	300-900
Bending Strength (MPa)	160	115-200
Young's Modulus, E (GPa)	17-27	80-120
Poisson's Ratio		0.28
Hardness (GPa)	0.396	3.79-5.0
Fracture Toughness (MPa $m^{1/2}$)	2-12	0.6-1.0

Hydroxyapatite has calcium and phosphorus elements in its hexagonal structure. These elements are the same elements present in the inorganic parts of the bone and teeth. As a result, the host reactions against HA are minimum. In fact, strong bonds are generated between bone and implant material surface due to the high bioactivity of HA. There have been many attempts to improve the mechanical and biological properties of synthetic HA [38-43]. The special attention was on nano crystalline HA to achieve improvements both biologically and mechanically.

Bone minerals are at nano scale; therefore, the studies and researches on nano HA was accelerated to improve its properties in all aspects.

1.4 Doping of Nano Hydroxyapatite

Doping is the introduction of an element, an atom, an ion or molecule into a material to enhance its various properties. When the foreign elements are introduced into the given material inevitably, they are called impurities. That is to say that a doping element is intentionally added into another material in a given amount, ranging from a few ppm to a few percent.

The general formula of apatites is $X_5(YO_4)_3Z$. X, Y and Z can be various elements and molecules. Table 1.7 summarizes these elements and molecules that can be possibly substituted for X, Y and Z. All these compounds have the same unit cell structure, they are all considered to be hexagonal. In the structure of HA, many elements can be substituted with X and Z. These changes lead to alterations in properties of apatite crystals and material's overall properties, such as mechanical, chemical and biological properties.

Table 1.7. Various elements and molecules possibly substituted in $X_5(YO_4)_3Z$.

Possible Elements or Molecules	
For X	Ca, Sr, Ba, Pb, Na, K, Ni, Cu, Co, Cd, Y, La, Fe, Zn, Mg, Ce
For Y	P, As, V, C, Si,
For Z	OH, F, Cl, O, Br

1.4.1 Doping of Nano HA with Various Ions

1.4.1.1 Cell (*In Vitro*) Studies of Nano HA

In mineral phase of bone, there are many components such as Mg^{2+}, F^-, CO_3^{2-}; therefore, many studies were conducted about the doping of HA with different elements. Various ions have been added into nano HA in order to enhance its biological, mechanical and chemical properties [44-51].

Osteoblast cell attachment studies on HA doped with divalent and trivalent ions (Mg^{2+}, Zn^{2+}, La^{3+}, Y^{3+}, In^{3+} and Bi^{3+}) were performed [51]. Osteoblast attachment on HA doped with Y^{3+} ions was noted to be superior compared to pure HA [44]. For instance, the amount of osteoblast attachment onto the HA doped with Y^{3+} ions was computed as 3000 cell/cm^2. This result was approximately two times higher than that of pure HA. Furthermore, osteoblasts attached faster and in higher numbers onto the HA doped with trivalent ions on the contrary to the divalent ions. The number of attached cells on HA doped with divalent ions was 2200 cell/cm^2, while this value for HA doped with trivalent ions was increased to 2600 cell/cm^2. The biodegradation (weight loss) rate of HA doped with Mg and Zn ions was slower than that of pure material, especially the rate of degradation was minimum for HA doped with magnesium ion The most interesting point was that Bi^{3+} was found to be a promising cation because this cation increased the cellular properties most effectively. Additionally, this cation is already present in the body. In this light, the investigations on HA doped with Bi^{3+} could be accelerated to determine its efficiencies. However, mechanical properties of HA doped with Bi^{3+} need to be analyzed. [48].

1.4.1.2 Microstructural and Mechanical Studies of Doped HA

The inconsistency of known mechanical properties of synthetic HA with those of bone limits the applications of HAs in the body [37]. In order to improve the microstructural and mechanical properties of nano HA, HA with various anionic and cationic substitutions for OH^- and Ca^{2+} have been developed to overcome these limitations.

Magnesium cation is one of the most important ions substituted for Ca in HA [52, 53]. If other ions, such as fluoride or carbonate, are not co-substituted among with Mg in HA, the substitution amount of Mg with Ca in HA is limited up to 0.4 wt% of Mg [53]. It was reported that increasing the concentration of Mg in HA decreased the crystallinity [53, 54], Destabilization of the structure of HA and favoring its thermal conversion into β-TCP was also reported with Mg addition [55-58]. Additionally, attempts have been made on Mg^{2+} and Zn^{2+} substitutions in nano HA. For example, Mg^{2+} and Zn^{2+} ions were doped into the nano HA in order to examine the effects of metal ions on its morphological and sintering characteristics [48]. It was observed that the grain size of HA doped with 1 wt % Mg was smaller than that of pure HA. On the other hand, HA doped with same amount of zinc had larger grains than pure HA. HA doped with 1 wt% Mg and Zn ions and sintered at 1300^oC showed higher Vickers hardness and compression strength than undoped HA [48]. Vickers hardness of undoped HA was about 325 HV, HA doped with 1 wt% Mg^{2+} and with 1 wt% Zn^{2+} was about 380 HV and 350 HV, respectively. According to compression tests, undoped HA had a strength of 211 MPa and compression strengths of doped HA with Mg^{2+} and Zn^{2+} were 281 MPa and 223 MPa, respectively.

HA doped with Al^{3+} cations were studied with regard to microstructure and sintering characteristics [46]. Second phase formations were determined in 2.5, 5, 7.5 mole % dopings of HA, which were then sintered at 1100^oC and 1300^oC. Al^{3+}

substitutions in HA led to an increase in thermal instability and triggered the formation TCP and CaO. In order to avoid second phase formation, it was stated that the amount of Al^{3+} substitution should be less than 5 mole %. Owing to the fact that the diameter of Al^{3+} ion was smaller than that of Ca^{2+}, hexagonal cell volume was diminished. The grain sizes of HA doped with 5 % Al^{3+} changed depending on sintering temperature. It was observed that HA doped with Al^{3+} and sintered at 1300^{o}C had smaller grain size with respect to pure HA.

The studies about doping of HA were not limited to the addition of single cations. In fact, the attempts of co-substitutions were also performed. For example, Si and Mg elements were doped together into HA [59]. The characteristics of the doped material were investigated in terms of morphology, sintering behaviors and biological response [50].

In another study, ZrO^{2+} was added into the HA to substitute for Ca^{2+} [47]. It was reported that the porosity of the sintered material increased with increasing amount of cation doping. Additionally, it increased the degradation of HA. As a result of ZrO^{2+} ion substitution for Ca^{2+} ions, hexagonal lattice parameters of HA have increased. Then this led to high stresses in HA causing biodegradation of HA. Due to the water formation during degradation, additional porosity was then generated. Hereby, HA doped with ZrO^{2+} were stated more porous than pure HA.

Doping of HA was not induced by only addition of cations, but also by anions. According to another study, F^{-} and Cl^{-} ions were co-substituted [49]. Contrary to apatite structure, lattice parameters altered in an increasing manner. All HA prepared with these anions in changing portions exhibited crystal sizes that were smaller than 50 nm. This confirmed that it was consistent with crystal size of natural HA.

1.4.2 Fluoride Doping

When fluoride ions partially replace OH^- ions in HA, fluoridated hydroxyapatite (FHA) is obtained. If F^- ions completely replace OH^- ions in HA, it is called fluorapatite (FA).

FHA is considered as a new alternative biomaterial for bone applications due to its low solubility, high thermal stability and biological potential [60-64]. Fluorine in saliva and blood plasma is necessary for dental and skeletal development and fluorine is known to be very important in suppressing dental caries [50, 65]. It was also noted to stimulate proliferation and differentiation of bone cells [61]. Moreover, it has been used in treatment of osteoporosis [62]. However, the amount of fluoride ions added in HA need to be carefully controlled for bone applications, because high content of F^- may cause adverse effects such as osteomalacia [66]. High concentration of fluoride ions may also inhibit the cell proliferation by releasing Ca^{+2} ions in HA due to decreased solubility [67]. Addition to the reports that high concentrations of fluoride led to abnormal tissue growth [68], poor mechanical properties occurred at high amount of additions of fluoride into HA, but lower fluoride levels improved the mechanical properties of HA, such as hardness, fracture toughness, elastic modulus and brittleness [69]. Therefore, the optimum fluoride concentrations in HA for biomaterial applications were reported as 0.033-0.4 mol F^-/mol apatite by previous studies [67, 70].

1.4.3 Yttrium Doping

In natural bone, apatite crystals are in nano scale. Doping of nano HA with various elements has been reported to be advantageous. However, there has been limited study in the literature about the microstructure and especially about the mechanical properties of HA doped with yttrium. For example, substituted yttrium ions (Y^{3+}) into bioceramics have been reported to modify the microstructural

and biological properties of the materials [71-74]. Yttria stabilized zirconia was introduced for medical applications due to its improved toughening mechanism that provided the use of the material under stress without fracture [71].

Owada *et al* [72]., studied the humidity-sensitivity of Y-doped calcium oxyhydroxyapatite ($Ca_{10-X}Y_X(PO_4)_6(OH)_{2-X}\ O_X$). They stated that the ratio of surface hydroxyl groups per unit surface area of sintered samples increased with increasing Y amounts. Moreover, the electrical conductivity of Y-doped HA was enhanced with respect to that of pure HA [72]. Additionally, Newnham stated that the Y-doped HA has a high affinity to water molecules [73]. Since electrical conductivity and hydrophilicity are important characteristics for bone regeneration, Y-doped HA was considered to be advantageous for orthopedic applications [74].

Despite the findings for physical properties of yttrium, there was little knowledge about the biocompatibility properties of yttrium for orthopedic applications until Webster *et al.* studied the osteoblast response to pure and Y-doped HA [51]. Before this research, yttria stabilized zirconia was reported to have no cytotoxicity when used in animal studies [75]. It was also stated that the osteoblast adhesion was increased with concentration (2-7 % mole) of Y in HA. The rate of adhesion with 2 % mole Y^{3+} was found 28 % greater than that with pure HA [76]. In that study, effects of doping of cadmium, zinc and magnesium ions into HA were also investigated in terms of cell attachment. The findings stated that the greatest amount of cell adhesion after 4 hours incubation was on HA doped with 2 % moles of Y^{3+} among HA doped with 2% mole of those ions [76].

Webster *et al.* [51], investigated the effect of divalent (Mg^{+2}, Zn^{+2}) and trivalent (Y^{+3}, In^{+3}, La^{+3}, Bi^{+3}) dopants on characteristics of HA pertinent to orthopedic and dental applications. The osteoblast adhesion after 4 hours of incubations was the greatest on HA doped with Y^{3+} and In^{3+} but there were no statistical differences between other HA formulations. However, osteoblast response

to HA doped with trivalent dopants was significantly greater than that to HA doped with divalent dopants. Additionally, alkaline phosphate (ALP) activity, an indication of osteoblast differentiation, was measured after 7 and 21 days incubations. It was reported that undoped HA seemed to have greater ALP activity than HA doped with Y^{+3}. A significant difference between ALP activities at 7 days and at 21 days was not found for HA doped with Y^{+3} [51].

Osteoblast response to Y^{3+} doped nanocrystalline HA as coating was studied. Beside the benefits of nano structure of HA, substitution of yttrium enhanced the functions of cells cultured on HA [74]. Osteoblast response was enhanced with increasing amount of Y^{3+} added into bulk HA [76]. Osteoblast adhesion was not significantly different between Y^{3+} doped and undoped nano crystalline HA after 4 hours post seeding. This was attributed to that there may be a minimum limit to improve the osteoblast adhesion and this limit was not reached in this study (yttrium was added 1.3 % moles) [74]. On the contrary, ALP activity and calcium deposition by osteoblasts cultured on Y^{3+} doped nano HA was improved in comparison to pure HA.

1.5 Aim of the Study

The objective of this study was to synthesize nano-sized pure and Y^{3+} and F^- doped HA to investigate their microstructural, mechanical and biological properties. HA was doped with Y^{3+} and F^- ions to enhance its biological and mechanical properties. Pure and doped nano size HAs sintered at different temperatures were prepared in powder form to investigate their crystal structure and bonding characteristics by X-ray diffraction (XRD) and Fourier Transform Infrared (FTIR) spectroscopy, respectively. Scanning electron microscopy (SEM) was performed to study the grain sizes of the materials. Mechanical properties of the discs were investigated by diametral tension and micro-hardness tests.

Biocompatibility of pure and doped HA discs was assessed with cytotoxicity studies using Saos-2 cells. Cells were seeded on doped and undoped discs. Cell adhesion and proliferation on discs after 1 day, 3 days and 5 days of culturing were studied using MTT viability assay and SEM examinations. ALP assays and SEM. Alkaline phosphatase activity (ALP) and mineralization (Ca deposition) assays was performed after 7 and 14 days to investigate the differentiation state of seeded cells on pure and doped nano HA discs.

CHAPTER 2

2. MATERIALS AND METHODS

2.1 Materials

2.1.1 Precursors Used For Synthesis

Calcium nitrate tetra hydrate ($Ca(NO_3)_2 \cdot 4H_2O$) and di-ammonium hydrogen phosphate ($(NH_4)_2HPO_4$) (Merck, Germany) were used to synthesize HA. In order to prepare yttrium and fluorine doped HAs, yttrium nitrate ($Y(NO_3)_3 \cdot 5H_2O$) and ammonium fluoride (NH_4F) (Sigma-Aldrich, USA) were used. Ammonia (NH_3) solution (Merck, Germany) was also used in the synthesis of HAs.

2.1.2 Cell Culture Studies

L-ascorbic acid, β-gleycerophosphate, dexamethasone, sodium azide (NaN_3), triton X-100, p-nitrophenyl phosphate (pNPP) substrate solution, bicinchoninic acid solution, cupric sulfate pentahydrate and o-cresolphathalein complexone were obtained from Sigma, USA. Dulbecco's Modified Eagle Medium (DMEM) (high and low glucose) and fetal bovine serum (FBS) were purchased from Biochrom, Germany. Penicilin-streptomycin, sodium pyruvate solution, bovine serum albumin and trypsin-EDTA were the products of PAA laboratories GmbH, Austria. Dimethly sulfoxide (DMSO) (molecular biology grade) was obtained from AppliChem, Germany. Methylthiazolyldiphenyl-tetrazolium (MTT) bromide, glutaraldehyde and Adenosine mono phosphate (AMP) were purchased from Sigma-Aldrich, Germany. Calcium carbonate was the product of Fluka

Chemical GmbH (Switzerland). 96 % ethanol and 37 % hydrochloric acid (HCl) were obtained from Ryssen (France) and Merck (Germany), respectively.

2.2 Methods

2.2.1 Synthesis of HA Powders and Discs

2.2.1.1 Synthesis of Pure HA

Nano-HA was synthesized by precipitation method [46, 47]. The steps of the synthesis process were illustrated in Figure 2.1. Calcium nitrate tetra hydrate and di-ammonium hydrogen phosphate were used as precursors. After two different solutions were prepared by these precursors, they were mixed together. 0.6 M $Ca(NO_3)_2 \cdot 4H_2O$ and 0.3 M $(NH_4)_2HPO_4$ were separately prepared in distilled water. The Ca/P ratio was kept at 1.67. Prepared solutions were stirred for one hour. After stirring for 1 hour, ammonia solution was added into both solutions to bring the pH level to 11-12. Calcium nitrate solution was drop wise and spontaneously added into di-ammonium hydrogen phosphate solution. A milky solution was obtained at the end of the mixing. This final mixture had a pH level of 11-12 with the addition of ammonia solution. After 2-3 hours of stirring, the mixture was heated until boiling to increase the reaction rate. After the boiling, the solution was left to stirring for 24 hours. After the stirring, the mixture was filtered with a fine filter paper. At the end of this process, a wet cake was obtained. The wet cake was dried in an oven at 200^{o}C to remove excess water. After the drying, the sample was calcined at 600^{o}C for half an hour to get rid of gases accumulated during precipitation. After the calcination, sintering was applied at 900^{o}C, 1100^{o}C and 1300^{o}C in air for 1 hour. The samples were heated and cooled in the furnace.

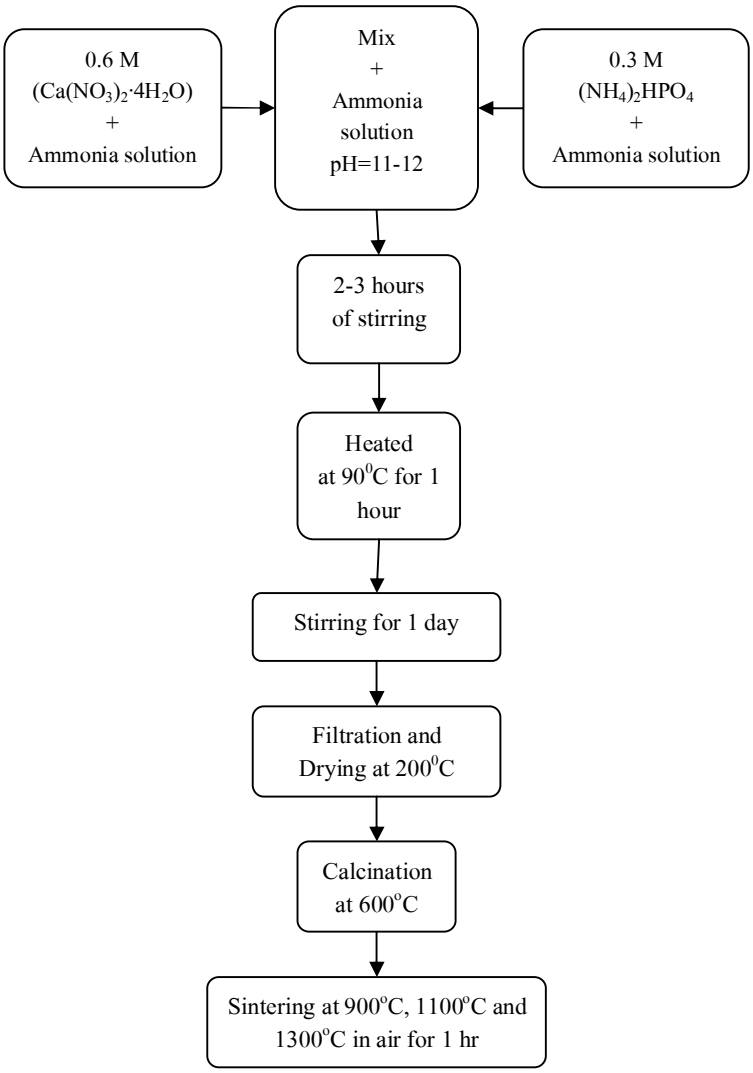

Figure 2.1. Illustration of the synthesis process of HA.

2.2.1.2 Synthesis of Doped HAs

The main precursors were same for doped HA. Additionally, yttrium nitrate and ammonium fluoride were used. Doped HA was prepared for three different material composition. Yttrium nitrate was added into calcium nitrate solution in 3 different mole compositions: 2.5 mole %, 5 mole % and 7.5 mole % of calcium nitrate. In conformity with former studies [67, 70], the concentration of fluoride ions added in HA synthesized in this study was determined as 0.260 mol F^-/mol HA.

Ammonium fluoride was added into di-ammonium phosphate solution to obtain a mole ratio of 2.5 mole % of di-ammonium phosphate. The designations of pure and doped HAs depending on the composition are summarized in Table 2.1. The amounts of main precursors were lowered to achieve the substitutions of added materials into HA structure. Therefore, the moles of the precursors used to prepare the solution were changed according to the compositions as seen in Table 2.2.

The same procedure used in preparation of pure HA was performed to prepare doped HA. The proportion of elements additions were adjusted according to atomic percentage of precursors. After the solutions were mixed, the products were stirred, filtered and dried. The dried and calcined materials were sintered at temperatures of 900^{o}C, 1100^{o}C and 1300^{o}C for 1 hour.

Table 2.1. Summary of sample designations of pure and doped HAs.

Sample Designation	Description
Pure HA	undoped HA
2.5YFHA	2.5% Y^{+3}-2.5% F^{-}-HA
5YFHA	5% Y^{+3}-2.5% F^{-}- HA
7.5YFHA	7.5% Y^{+3}-2.5% F^{-}-HA

Table 2.2. Moles of materials used for preparation of pure and doped HAs.

	$Ca(NO_3)_2 \cdot 4H_2O$	$(NH_4)_2HPO_4$	$Y(NO_3)_3 \cdot 6H_2O$	NH_4F
HA	0.076	0.045	0	0
2.5YFHA	0.073	0.045	0.0019	0.0019
5YFHA	0.071	0.045	0.0038	0.0019
7.5YFHA	0.069	0.045	0.0057	0.0019

2.2.1.3 Preparation of Pure and Doped HA Discs

Calcined doped and undoped powders at 600°C were cold pressed into a die (13 mm in diameter) at 330 MPa for 60 seconds with a hydraulic cold press equipment (Carver Inc., Wabash, India). 4 different compositions were used in the preparation of the samples. Discs were sintered at 900°C, 1100°C and 1300°C for 1 hour.

2.2.2 Characterization Methods

2.2.2.1 Structural Analysis

2.2.2.1.1 Density Measurement

Density of the materials was determined by the geometrical method. After the discs were sintered, the densities of the materials were calculated. Green and sintered densities were defined separately. Thickness, diameter and weight of the discs were measured using a caliper and precision balance. Volume and density of the discs were determined by using the following formulas:

$$V = \left(\pi \cdot \frac{D^2}{4} \right) \cdot t \tag{2.1}$$

$$d = \frac{w}{V} \quad (2.2)$$

where:

V= disc volume; t= disc thickness; D= disc diameter; w= weight; d= density.

The green densities and the sintered discs' densities were calculated in the same way as above. Porosity of the materials was calculated comparing experimental densities with theoretical density of HA (3.156 g/cm^3). Hence relative density and porosity of the green and sintered materials were determined.

2.2.2.1.2 X-Ray Diffraction Analysis

Phases present in the samples were investigated by X-ray diffraction (XRD) method using a Rigaku DMAX 2200 machine. XRD was performed on the samples with a Cu-Kα radiation at 40 kV/ 40 mA and samples were scanned from 20^o to 60^o in 2θ with a scan speed of 2.0^o/min. Joint Committee on Powder Diffraction Standards (JCPDS) files were used for comparison with the positions of diffracted planes taken from XRD results. The amount of phases present in pure and doped HA was calculated by using relative intensity measurements of diffracted planes.

2.2.2.1.2.1 Lattice Parameters of Pure and doped HA

HA has a hexagonal unit lattice structure. The hexagonal lattice parameters of hexagonal pure and doped HA were calculated by successive approximations.

In order to calculate the lattice parameter 'a' for the hexagonal crystal system of HA, the Bragg's equation was based. The following formula was used to calculate 'a' [77]:

$$a_0 = \left(\frac{\lambda}{2\sin\theta}\right)\sqrt{\left(\frac{4}{3}(h^2 + hk + k^2) + \left(\frac{a}{c}\right)^2 l^2\right)} \quad (2.3)$$

where:

a_0: the calculated lattice constant; λ: x-ray wavelength; θ: the Bragg angle for corresponding (hkl); a/c: the last calculated ratio in successive approximation.

If the value of the term "$\frac{4}{3}(h^2+hk+k^2)$" was larger than the value of the term "$(\frac{a}{c})^2 l^2$" for a reflection of (hkl), this formula was used to calculate a_0. Furthermore, if the value of the term "h^2+hk+k^2" was less than the value of "l^2", it was used to calculate c_0. To minimize the error caused by incorrect axial ratio, another formula was used to calculate c_0 [77]:

$$c_0 = (\frac{\lambda}{2\sin\theta})\sqrt{(\frac{4}{3}(\frac{c}{a})^2(h^2+hk+k^2)+l^2)} \quad (2.4)$$

The volume of the hexagonal unit cell of the materials was calculated according to the following formula:

$$V = 2.589(a^2)c \quad (2.5)$$

2.2.2.1.2.2 Particle Size Determination

The particle sizes of sintered pure and doped HA were determined from XRD patterns. The reflections from the planes (002) and (300) were used to calculate particle sizes. The Scherrer equation was used to determine the "D" values [78]:

$$D = \frac{K\lambda}{\beta_{1/2}\cos\theta} \quad (2.6)$$

In this formula, "K" expresses a constant changing with crystal properties and was chosen as 0.9. "λ (=1.514 Å)" and "θ" are x-ray wave-length and the diffraction angle, respectively. The value of "$\beta_{1/2}$" is measured as the width at half maximum intensity of XRD peaks for the planes (002) and (300).

2.2.2.1.3 Scanning Electron Microscopy (SEM) Analysis

A JEOL JSM-6400 (JEOL Ltd., Japan) SEM at a voltage of 20 kV was used to examine the samples. Before the examination, the samples were first polished with SiC papers (Buehler Ltd., USA) from 240 to 1200 grit. Final polishing was performed with 1μm monocrystalline diamond suspension (Buehler Ltd., USA) and the samples were finally etched with a 0.5 M HF acid for 2 minutes. At the end, they were coated with gold.

2.2.2.1.3.1 Grain Size Determination

Grain size determination of the samples was performed using SEM images of pure and doped HAs sintered at 900°C, 1100°C and 1300°C. The intercept method was used with a 20 cm circumference circle to find out the grain sizes of HAs. Grain sizes from SEM images were determined using following formula [79]:

$$G_{av} = \frac{L}{N * M} \tag{2.7}$$

where:

G_{av}: average grain size; L: circumference of the circle (20 cm); N: number of intersections along circumference line, M: magnification.

2.2.2.1.4 Fourier Transform Infrared Spectroscopy (FTIR)

FTIR spectra were used to identify the presence of OH^- and F^- bonds formed in the doped and undoped HA structure. The samples were first crushed in mortar and pestle. Ceramic powders and potassium bromide (KBr) were mixed with 1 to 300 weight ratio. The prepared powder mixture was cold pressed to obtain transparent pellets. The spectra records were performed from 1400 cm^{-1} to 400 cm^{-1}

using a 512 scan on FTIR spectrometer (Brukers IFS 66/S; Bruker Optics, Germany).

2.2.2.2 Mechanical Testings

2.2.2.2.1 Diametral Tensile Testing

Pure and doped HA discs (6 discs for each group) with a diameter of approximately 10 mm and a thickness of about 2.7 mm were used. In this method, a cylinder is compressed in a lying position between two flat plates. The maximum tensile stress is formed across the flat surface diameters of cylinders and a plane from one end of the cylinder to another. Maximum tensile stress is generated normal to loading direction across the loading diameter. The schematic view of the diametral test setup was illustrated in Figure 2.2.

Universal testing machine (LS500; Llyod Instruments, UK) was used to perform the diametral testing. The speed of the machine was 2 mm/min during the test. The following formula was used to calculate the tensile strength of the sample [80, 81]:

$$S = \frac{2F}{(\pi \cdot D \cdot t)} \tag{2.8}$$

where:

F: failure force; D: sample diameter; t: sample thickness.

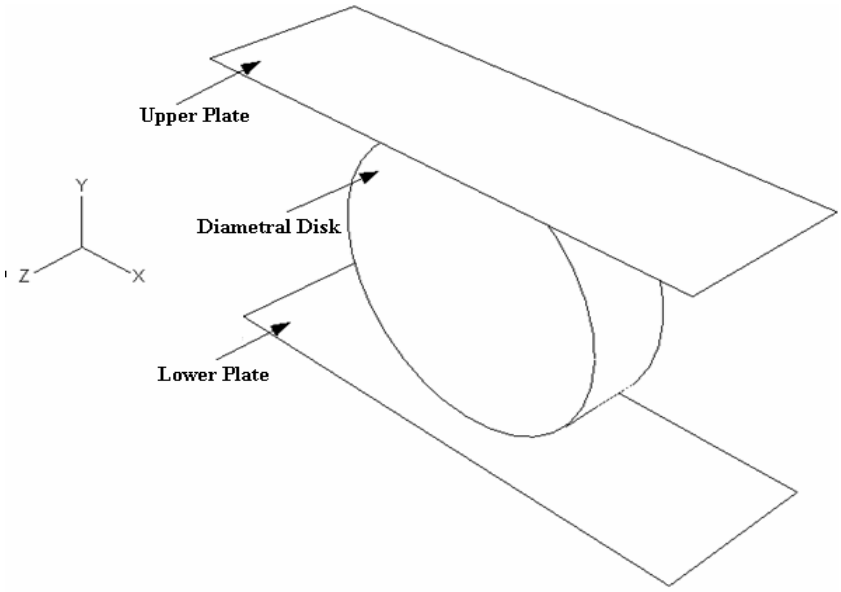

Figure 2.2. Schematic view of the diametral test setup.

2.2.2.2.2 Vickers Micro-hardness

The micro-hardness of the samples was determined by a Vickers micro-hardness tester (HMV-2, Shimadzu, Japan). The sintered discs were used to determine the micro-hardness of the materials. A diamond indenter was applied with a load of 200 g for 20 seconds onto the surface of the discs. The diagonal indent shape formed after the indentation was measured to determine the micro-hardness of the samples. 20 measurements were performed on each sample. For the calculation, the following formula was used:

$$HV = 0.001854 \frac{P}{d^2} \tag{2.9}$$

where;

HV: Vickers hardness (GPa); P: Applied load (N); d: diagonal indent length (mm).

2.2.2.2.2.1 Fracture Toughness

Fracture toughness of the samples was determined according to the length of the cracks generated by the indentations applied during the micro-hardness test. Two widely used equations were used to calculate the fracture toughness. Depending on the size of the cracks formed by indentation, one equation was preferred for calculation.

The shapes of the cracks were presented in Figure 2.3. Halfpenny shape cracks were formed when the ratio of c/a was greater than 3. On the contrary, the Palmqvist shaped was observed when the ratio of c/a was less than 3. When Halfpenny shaped cracks were generated, the Evans and Charles equation was used to calculate the fracture toughness [82]:

$$K_{1c} = 0.0824 \frac{P}{C^{1.5}} \tag{2.10}$$

where:

P: applied load (N); C: crack length (m).

If c/a ratio was less than 3, Palmqvist shape crack was observed. Then, Palmqvist equation was used for the calculations [83]:

$$K_{1c} = 0.035\left(\frac{H^{0.6}E^{0.4}}{\phi^{0.6}}\right)\left(\frac{a}{(c-a)^{0.5}}\right) \tag{2.11}$$

where:

H: Hardness; E: Young's Modulus; ϕ: the coefficient related to the material constraint ($\phi \cong 3$).

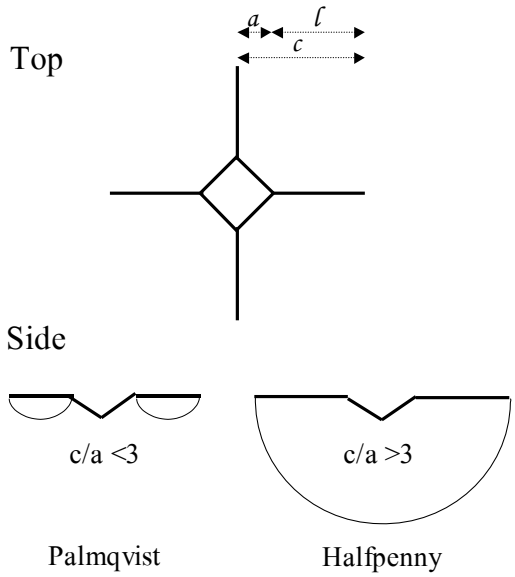

Figure 2.3. The top and side view of an illustration of the Palmqvist and Halfpenny shape cracks generated by Vickers micro-hardness indentation.

2.2.2.3 *In Vitro* Studies

2.2.2.3.1 Cell Attachment and Proliferation

After sintering at 900^{o}C, 1100^{o}C and 1300^{o}C, pure and doped HA discs were sterilized at 200^{o}C for 2 hrs. Saos-2 cells in Dulbecco's modified Eagle medium (DMEM) were seeded on discs at an initial cell seeding density of 5x10^{4} cells/disc. The growth medium consists of DMEM with high glucose supplemented with 10 % fetal bovine serum (FBS), 1 % penicillin-streptomycin and 0.1 % sodium pyruvate. Saos-2 cells were cultivated for 1, 3 and 5 days at 37^{o}C in carbon dioxide incubator (5215, Shel Lab., USA). The medium was replaced every 3 days. MTT bromide assay was used to study the attachment efficiency and proliferation of cells on discs. Shortly, discs were incubated with MTT for 4 hrs at 37^{o}C in a carbon dioxide incubator. MTT was taken up by viable cells and was reduced to insoluble purple formazan crystal by dehydrogenase enzymes. At the end of the incubation, MTT

solution was removed, discs were rinsed with PBS. Dimethyl sulfoxide (DMSO) solution was added onto discs to solubilize formazan crystals formed inside the cells. Absorbance at 550 nm was read with a μOuant™ microplate spectrophotometer (Biotek Instruments Inc, USA).

The attachment efficiency of Saos-2 cells onto discs was determined with respect to the Tissue Culture Polystyrene (TCPS) as follows:

$$\text{Attachment Efficiency (\%)} = \frac{\text{OD read at 550 nm for discs after 24 hr}}{\text{OD read at 550 nm for TCPS after 24 hr}} \qquad (2.12)$$

2.2.2.3.2 Morphology of Cells

The morphology of cells on the discs was investigated by SEM (JSM-6400, JEOL Ltd., Japan) after 1 and 5 days of incubation periods. For SEM analysis, the cells were fixed with 2.5 % glutaraldehyde in PBS for 1 hr. After rinsing with distilled water, they were dehydrated with ethanol series (70, 80, 90 and 100%) and dried in air in the laminar flow. The discs were coated with gold before examination.

2.2.2.3.3 Alkaline Phosphatase (ALP) Assay

Cells were seeded on discs with a density of $4x10^4$ cells/disc and were incubated in osteogenic differentiation medium (DMEM supplemented with 10 % FBS, 1 % penicillin-streptomycin, 0.1 % sodium pyruvate, 50 μg/ml ascorbic acid, 10 mM β-glycerophosphate and 10^{-8} M dexamethasone for 7 and 14 day incubation periods. The medium was refreshened every 3 days.

The intracellular ALP activity was measured colorimetrically by monitoring the conversion of *p*-nitrophenyl phosphate (pNPP) to *p*-nitrophenol. ALP enzyme hydrolyzes pNPP to *p*-nitrophenol and an inorganic phosphate as the following:

$$p\text{-nitrophenyl phosphate} \xrightarrow{\text{ALP}} p\text{-nitrophenol} + \text{phosphate} \qquad (2.13)$$

For ALP activity assay, the protocol was briefly as follows: after 7 and 14 day incubations, the cells on discs were lysed with 600 µl of 0.1 % Triton X-100 containing 0.1 % w/v sodium azide as protein preservative in distilled water on ice [84, 85]. The cell lysates were frozen and thawed three times to disrupt cell membranes. 100 µl pNPP substrate solution was added into 20 µl aliquots of each cell lysate. After 15 minutes incubation at 37^{o}C, the absorbance of each sample was measured at 405 nm by using µOuant^{TM} microplate spectrophotometer. *P*-nitrophenol formed was determined from the calibration curve constructed in the range of 25-250 µM (Figure A.1 in Appendix A). ALP activity was normalized by the protein content of the cell lysates. The specific ALP activity was expressed as nmol/mg protein/min.

The protein content was determined by bicinchoninic acid (BCA) assay which was based on the reduction of the cupric (Cu^{2+}) ion to cuprous (Cu^{1+}) ion by the protein. BCA-assay was performed by using the same aliquots prepared for ALP assay. Substrate solution was composed of a mixture of 1 ml of copper sulfate reagent (2 g cupric sulfate in 50 ml water) and 50 ml of BCA reagent. 1 ml of Copper-BCA reagent was added into 50 µl aliquots of each cell lysates. After 30 minutes incubation at 37^{o}C, the absorbances at 562 nm were determined by using a µOuant^{TM} microplate spectrophotometer. The protein content of each lysate was determined by a standard curve obtained with bovine serum albumin in the range of 0-1.2 mg/ml (Figure B.1 in Appendix B).

2.2.2.3.4 Calcium Deposition Analysis

The same cell lysates in ALP protocol were used to determine Ca content produced by cells seeded on discs after 7 and 14 day incubations. Calcium o-cresolphthalein complexone method [86, 87] was used to determine the amount of calcium deposited on discs. 100 µl samples from cell lysates were added into 1 ml color reagent and 1 ml buffer. Color reagent was prepared by mixing of 25 mg o-cresolphthalein complexone powder (Sigma, USA) into 250 ml distilled water and 15 ml concentric HCl. Buffer was constituted by 37.8 ml Adenosine monophosphate (AMP) reagent and 250 ml distilled water in pH 10.7. After mixing of aliquots with reagents, they were incubated at room temperature for 15 minutes. The absorbances at 540 nm were determined by using a µOuant™ microplate spectrophotometer. Calcium amount formed was determined from the calibration curve constructed in the range of 0-12.5 mg/dl (Figure C.1 in Appendix C). Calcium content deposited was normalized by the protein content of the cell lysates. The content of calcium was expressed as Ca/mg protein.

2.2.2.3.5 Statistical Analysis

All the data were illustrated as the mean ± standard deviations. One-way analysis of variance (ANOVA) was done with Tukey's Multiple Comparison Test for the post-hoc pair wise comparisons using SPSS-15.0 Software (SPSS Inc., USA). Differences were considered as significant for $p \leq 0.05$.

CHAPTER 3

3. RESULTS AND DISCUSSION

3.1 Structural Analysis

3.1.1 Density of the Samples

Green densities (densities of compacts before sintering) and densities after sintering of the pure and doped materials are represented in Table 3.1. The relative densities of all sintered materials were higher than 88 % (Table 3.1), which could be interpreted that densification was highly succeeded for all the sintering temperatures.

Among the HAs sintered at 900^{o}C, their green densities were around 50% of the theoretical density (3.156 g/cm^{3}). After the sintering, these densities reached to at least 88 % of the theoretical density. There were no huge differences between densities of pure and doped HAs; the densest sample was 2.5YFHA with a 93.7 % of the relative density. The least one was 7.5YFHA sintered at 900^{o}C with an 88.5 % relative density, but it was still highly dense.

Green densities of HAs sintered at 1100^{o}C were also about 50% of the theoretical density. Like HAs sintered at 900^{o}C, densities of these samples increased up to 88% of the theoretical density after sintering. No significant changes were observed between densities of pure and doped HAs.

When HAs were sintered at 1300^{o}C, green densities being around 50% of theoretical one went up to densities with 90% of that. The highest densities among all HAs was obtained after this sintering temperature. Substitutions into pure HA

did not result in significant fluctuations in densities.

Table 3.1. Green and sintered densities of pure and doped HAs.

Sintering Temperature (^oC)	Material ID	Green density (g/cm^3)	Density after the sintering (g/cm^3)	Relative Density* (%)
900^{o}C	HA	1.59	2.94	93.1
	2.5YFHA	1.59	2.96	93.7
	5YFHA	1.58	2.88	91.2
	7.5YFHA	1.59	2.79	88.5
1100^{o}C	HA	1.57	2.95	93.5
	2.5YFHA	1.51	2.88	91.4
	5YFHA	1.54	2.85	90.2
	7.5YFHA	1.55	2.80	88.8
1300^{o}C	HA	1.60	2.97	94.2
	2.5YFHA	1.51	2.98	94.3
	5YFHA	1.50	2.98	94.4
	7.5YFHA	1.55	3.05	96.6

* Relative density was calculated with respect to theoretical density (3.156 g/cm^3) [48].

Although high densities were obtained, fully dense HAs could not be achieved in this study, as seen Table 3.1. Pressureless sintering at 1100^{o}C for 1 hour was assessed for sintering of HAs due to the reports in literature stated that 1100^{o}C was required for the best HA system [38, 88, 89]. In contrast, nano-crystalline HA powders could be fully densified by pressureless sintering at 1000^{o}C for 2 h, while conventional HA could not be sintered to above 70 % of theoretical density via pressureless sintering [90]. Additionally, nano HA powders could be sintered at lower temperatures (900^{o}C) with pressure-assisted sintering (load=100 MPa) for shorter time periods (30 min) [90]. Therefore, denser HA with finer grains could be achieved without any decomposition. In the current study, even tough no

pressure-assisted sintering was performed, highly dense HA could be obtained at even lowest temperature of 900^{o}C. Furthermore, no second phase formations occurred at 1300^{o}C with lower amount addition of yttrium and fluoride ions (2.5YFHA). Pure and doped HAs sintered at 1300^{o}C were nearly fully densified in spite of implementation of air sintering and short sintering time in this study. These results might originate from the contributing effects of yttrium and fluoride dopings. Since yttrium and fluoride co-substitution into HA have been never attempted up to this work, only individual effects of these ions on densification and sintering behaviors of HA were available in literature. The densities of the all materials increased with increasing the sintering temperature in the current study. When they were sintered at higher temperatures, denser materials were obtained as seen in Table 3.1. These results are in agreement with the reports of Gross *et al.* [63] stated that density of HA decreased with the fluoridation. Also the similar results for yttrium doped HA were stated that degree of bulk porosity of HA increased with an increase in amount of yttrium. While, at the same sintering temperature, the dopings led to decrease in densities, the densities of pure and doped HAs increased with increasing temperatures from 900^{o}C to 1300^{o}C in this work. There were no significant differences in densities of HAs sintered at 900^{o}C and 1100^{o}C, however, relative densities of pure and doped HAs sintered at 1300^{o}C reached to 94 % of theoretical density.

3.1.2 X-Ray Diffraction

XRD of the pure and doped HA powders after the sintering were investigated to determine which phases were present. The XRD spectra of pure and Y^{+3} and F^{-} doped HAs are shown in Figures 3.1-3.4.

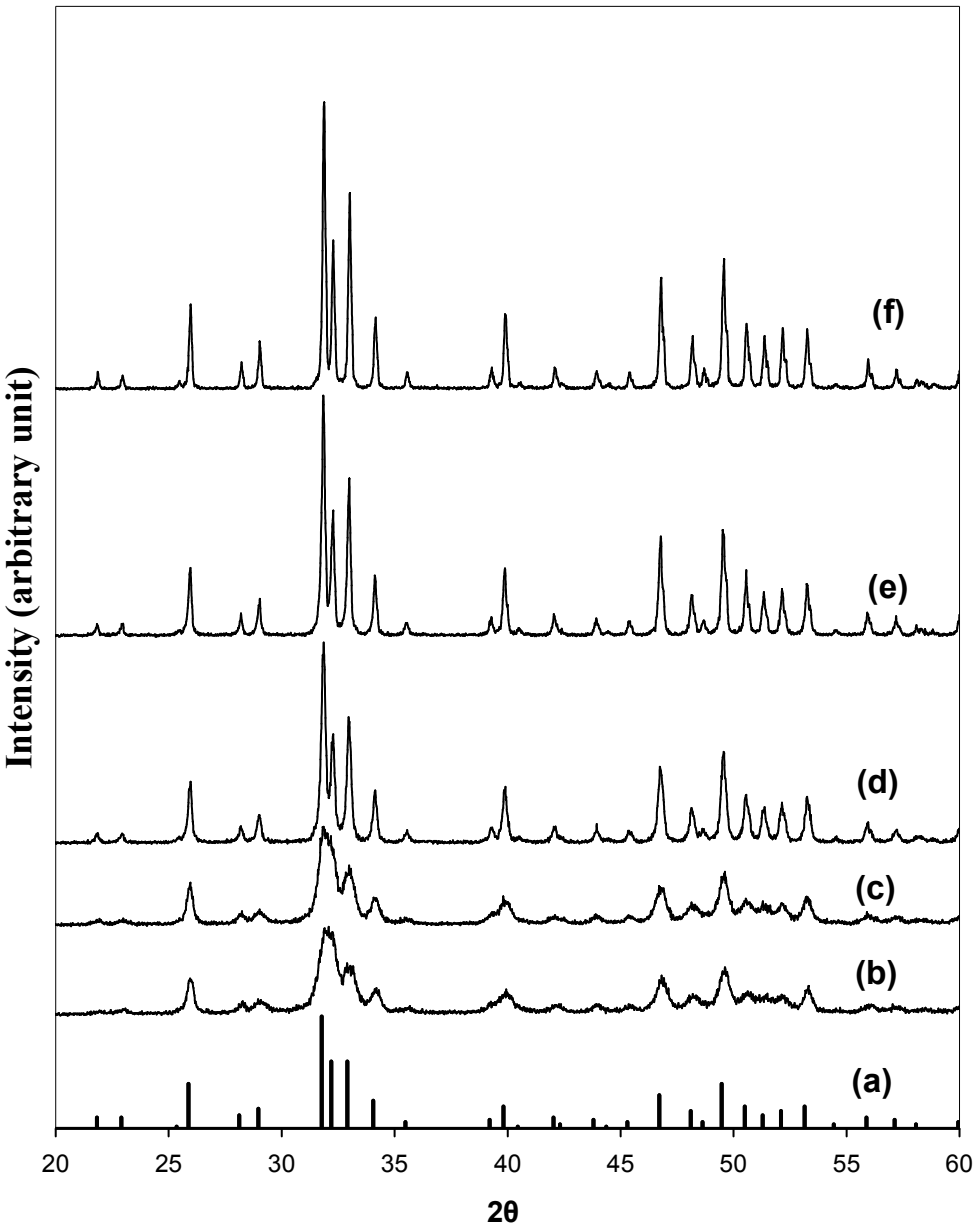

Figure 3.1. XRD spectra of pure HA a) Standard (JCPDS#: 9-432); b) dried at 200°C; c) calcined at 600°C for 0.5 hour and sintered for 1 hour at d) 900°C; e) 1100°C; and f) 1300°C.

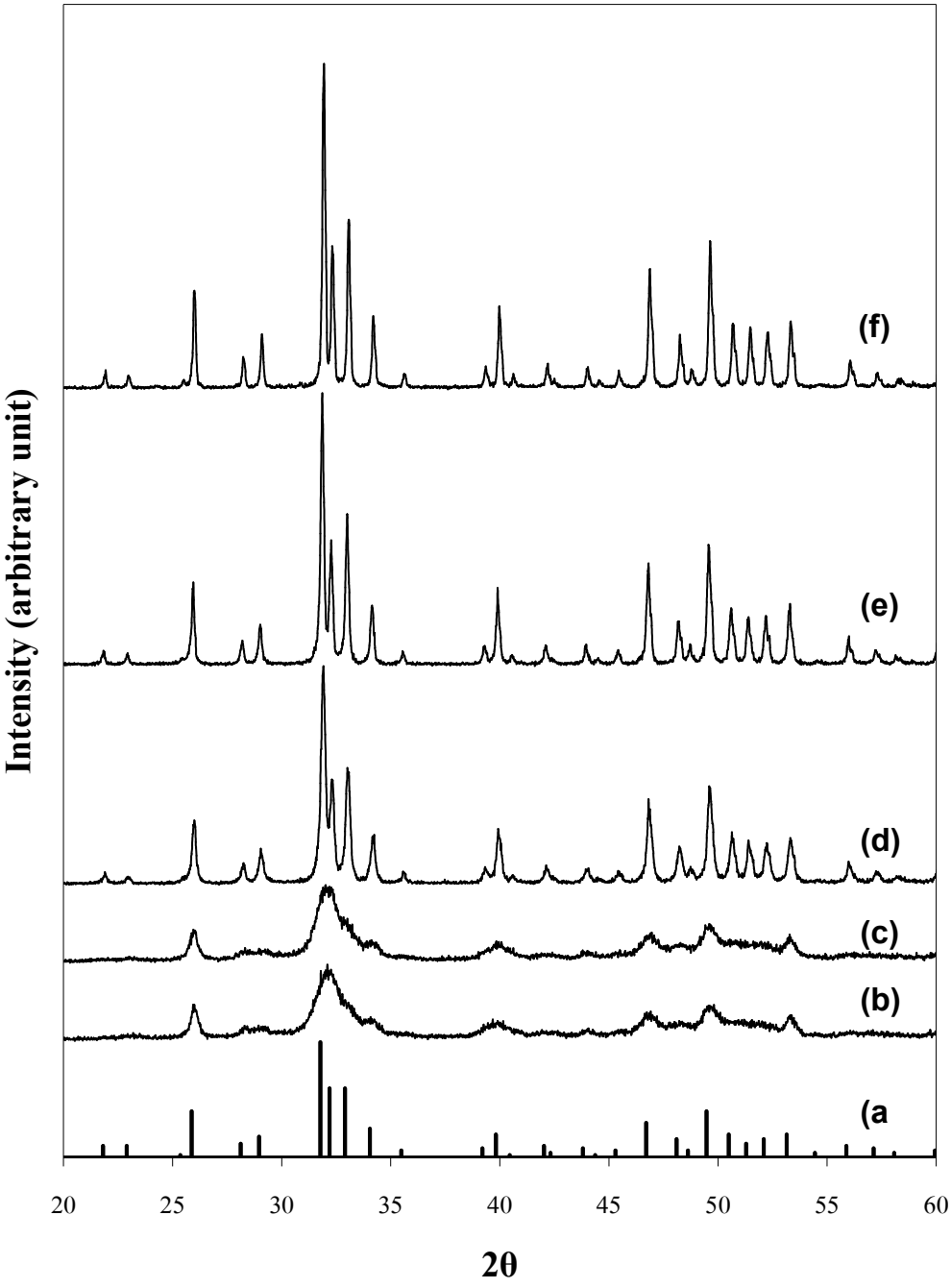

Figure 3.2. XRD spectra of 2.5YFHA a) Standard (JCPDS#: 9-432); b) dried at 200^{o}C; c) calcined at 600^{o}C for 0.5 hour and sintered for 1 hour at; d) 900^{o}C; e) 1100^{o}C; and f) 1300^{o}C.

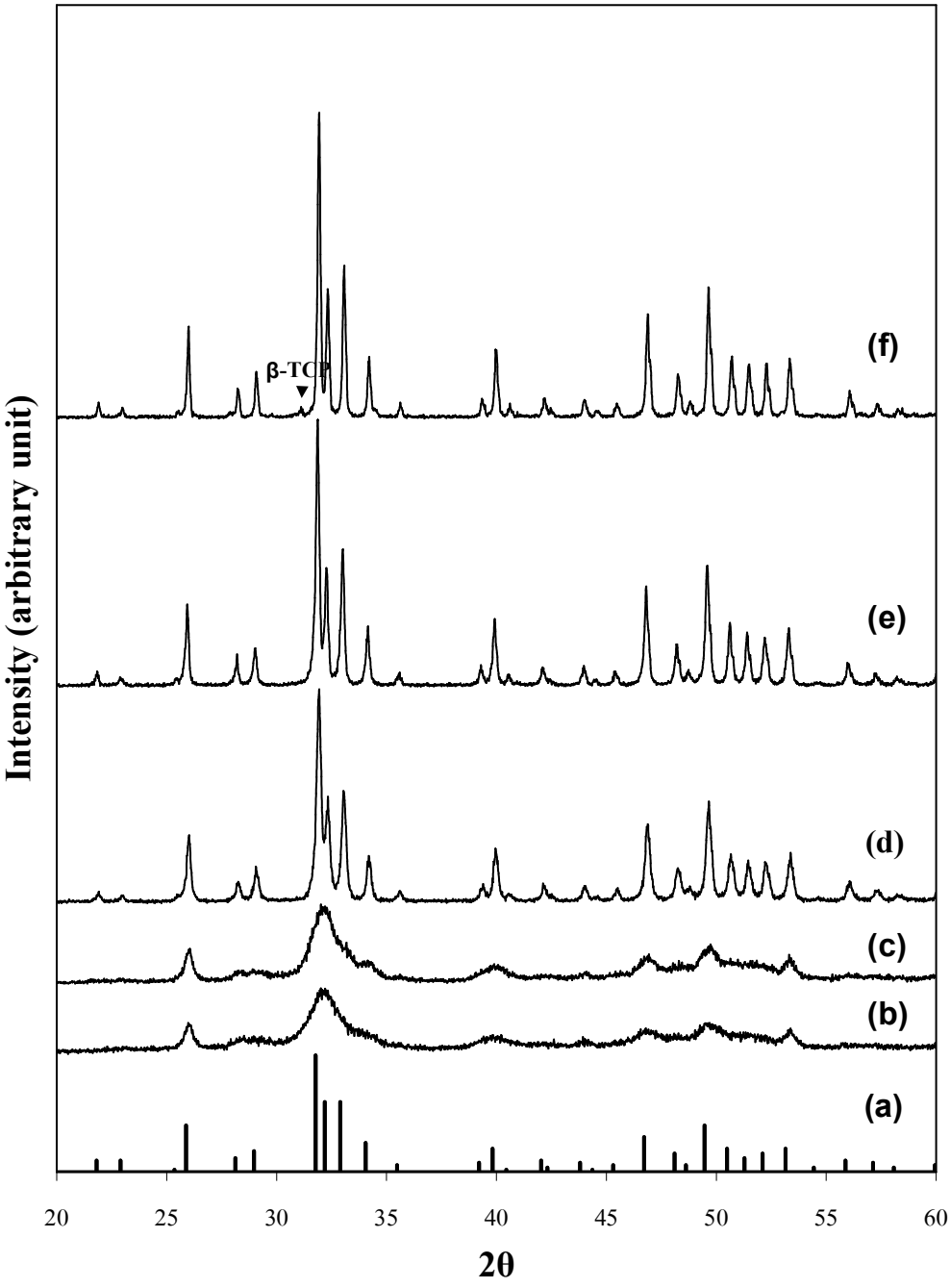

Figure 3.3. XRD spectra of 5YFHA a) Standard (JCPDS#: 9-432); b) dried at 200^{o}C; c) calcined at 600^{o}C for 0.5 hour and sintered for 1 hour at d) 900^{o}C; e) 1100^{o}C; and f) 1300^{o}C.

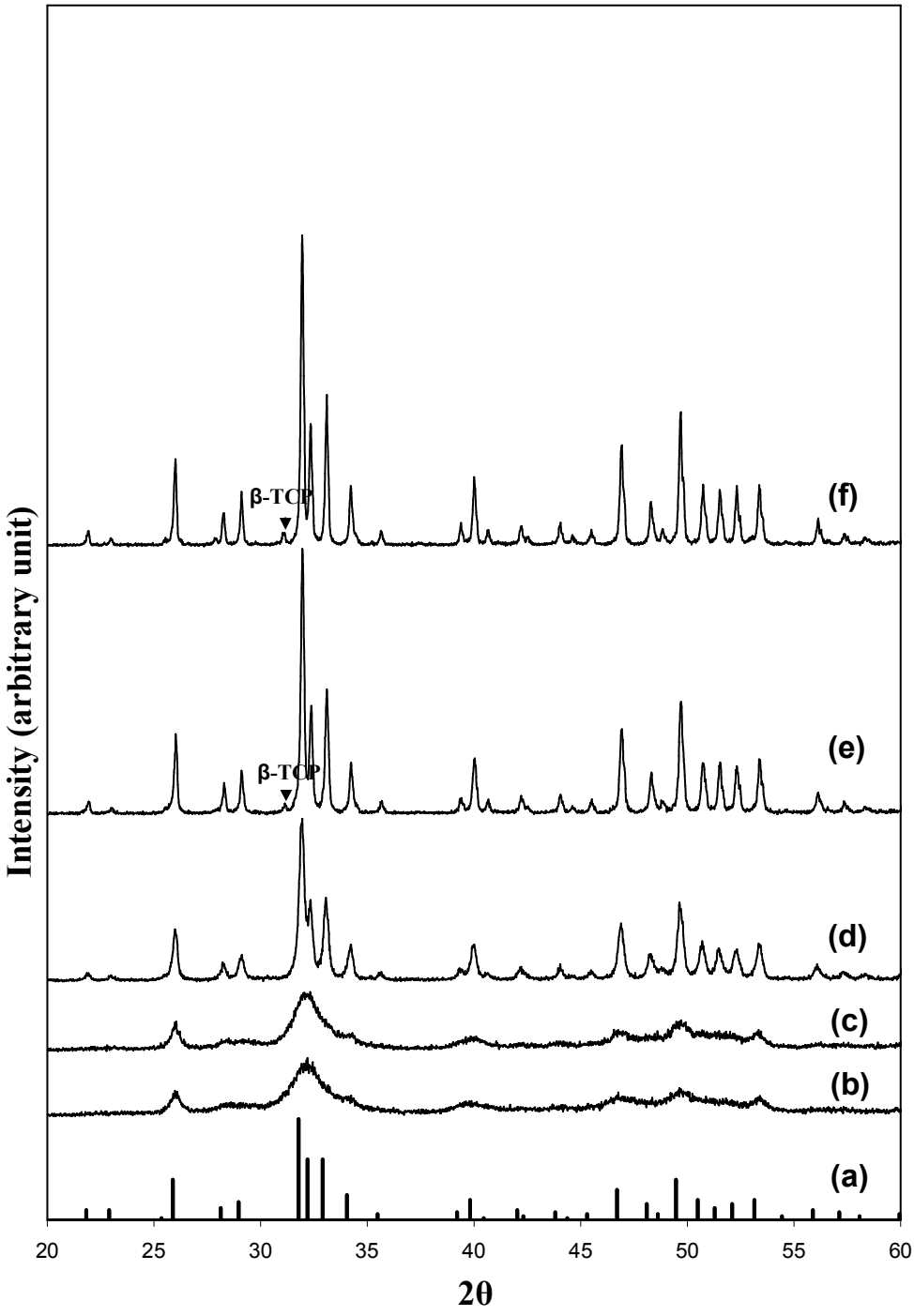

Figure 3.4. XRD spectra of 7.5YFHA a) Standard (JCPDS#: 9-432); b) dried at 200^{o}C; c) calcined at 600^{o}C for 0.5 hour and sintered for 1 hour at; d) 900^{o}C; e) 1100^{o}C; and f) 1300^{o}C.

In all the XRD spectra of pure and doped HAs, XRD peaks became narrower as the sintering temperature increased. This shows that the crystallinity of the samples gradually increases with increasing the sintering temperature. The XRD peaks of the samples calcined at 200°C and 600°C patterns are so extended that the materials at these temperatures have low crystallinity degree and very small particle size. At 900°C, the peaks become sharper than those at lower temperatures, additionally new peaks can be observed in the pattern. Furthermore, the peak intensity rises up when the temperature increases. The highest crystallinity for all samples appears to be found at 1300°C due to its XRD pattern being the most intense and narrow.

Conventional HA with micron size grains decomposes into unwanted second phases at temperatures exceeding 1150°C in ambient atmosphere as shown in Reaction 3.1 [86].

$$Ca_{10}(PO_4)_6(OH)_2 \rightarrow 3Ca_3(PO_4)_2 + CaO + H_2O \quad (3.1)$$

In this study, nanocrystalline HA were produced by the precipitation method. Therefore, it was not expected formation of any second phases in the material even at higher sintering temperatures, because XRD studies indicated that nanocrystalline HA materials were thermally stable up to 1300°C [91-94]. XRD peaks confirmed the purity of HAs, since no other phases except HA were observed as dominant phase for all of the samples with various compositions and at different sintering temperatures.

In Figure 3.1, XRD spectra of pure HA dried at 200°C, calcined at 600°C for 0.5 hour and sintered for 1 hour at 900°C, 1100°C and 1300°C are seen. The width of the peaks at 200°C and 600°C were extended, it indicates that crystallites in the materials are very tiny in nature, and the crystallinity degree of the powders is low.

The new and sharper peaks appeared in the spectra with increasing temperature. The sharp and more intense peaks indicated that the materials became more crystalline with increasing temperature. All peaks closely matched with JCPDS file number 9-432 for HA; no other phases were observed in the patterns regardless of the temperature. This could be interpreted in terms of formation of stoichiometric and thermally stable HA at the end of the synthesis in this study [95].

In Figure 3.2, XRD spectra of 2.5YFHA dried at 200^{o}C, calcined at 600^{o}C for 0.5 hour and sintered for 1 hour at 900^{o}C, 1100^{o}C, and 1300^{o}C are presented. The intensities and sharpness of the peaks were gradually mounting up with increasing the temperature. The broader peak patterns at 200^{o}C and 600^{o}C pointed the smaller crystal sizes and lower crystallinity degree, as in former figure. The XRD patterns for 2.5YFHA also closely fitted with the JCPDS file number 9-432 for HA. No secondary phases other than HA were detected in the patterns suggesting that added elements went into solid solution in HA and ions were substituted into the lattice of pure HA. No severe fluctuations in the XRD peak positions due to the addition of yttrium and fluoride ions into HA were determined in the XRD patterns of 2.5YFHA, except that the positions of the peaks were slightly shifted to the right with respect to the positions of pure HA peaks (Figure 3.1). This could be due to the substitutions in the lattices. For example, the most intense peak (in the vicinity of (211) plane) for all sintering temperatures in pure HA was detected at around 2θ=31.8; whereas for 2.5YFHA it was observed at around 2θ=31.9. No second phase in the XRD peaks may indicate the perfect substitution of yttrium and fluoride ions within HA. Even at 1300^{o}C, 2.5YFHA did not decompose into any other phases, maintaining its stoichiometry and stability.

In Figure 3.3, XRD spectra of 5YFHA dried at 200^{o}C, calcined at 600^{o}C for 0.5 hour and sintered for 1 hour at 900^{o}C, 1100^{o}C, and 1300^{o}C are shown. XRD patterns were found to match with the JCPDS file number 9-432 for HA. Addition

of Y^{+3} and F^{-} ions did not cause any severe fluctuations in XRD patterns of 5YFHA. However, very trace amounts of β-TCP at 2θ=31.12 were detected in the pattern of 5YFHA sintered at 1300°C. Any other considerable observation was not distinct in the rest. The positions of the peaks in the XRD spectra were also slightly shifted to the right compared to the pure HA pattern. The increase in the percentage of the added yttrium did not harshly affect the pattern of the material, regardless of the temperature. The broadening of the peaks was also increasing with temperature rises.

In Figure 3.4, XRD spectra of 7.5YFHA dried at 200°C, calcined at 600°C for 0.5 hour and sintered for 1 hour at 900°C, 1100°C, and 1300°C are shown. The XRD peaks of 7.5YFHA at 200°C, 600°C and 900°C were free from any second phases. However, very small intensities of β-TCP were detected at 2θ=31.14 and 2θ=31.04 for 7.5YFHA sintered at 1100°C and 1300°C, respectively. In general, the patterns of 7.5YFHA were in agreement with the JCPDS file number 9-432 for HA.

The Ca/P ratios of synthesized pure HA, 2.5YFHA, 5YFHA and 7.5YFHA were 1.69, 1.62, 1.58 and 1.53, respectively. Except that of pure HA, these were below of stoichiometric ratio of 1.67. The presence of small amounts of β-TCP in the XRD patterns of 5YFHA sintered at 1300°C and 5YFHA and 7.5YFHA sintered at 1100°C and 1300°C could be attributed to these non-stoichiometric ratios of the materials. Pure HA and 2.5YFHA sintered at all sintering temperatures did not have any second phases in XRD patterns in spite of their non-stoichiometric structure. These results exhibited that higher amount of additions at higher sintering temperature led to decomposition of HA into β-TCP, as seen in Reaction 3.1.

Apart from small exceptions, all peaks in the XRD graphs belonged to the characteristic XRD peaks of HA. Peak patterns showed that the crystallinity and peak intensities of all of the samples became higher with increasing the sintering temperatures. Moreover, second phase formations were unclear and, if any, in trace

amounts depending on nano-size nature of HAs and thermal stability of materials due to the dopings into HA synthesized in this study.

3.1.2.1 Lattice Parameters of Pure and Doped HA

Lattice parameters of pure and doped HAs synthesized in this study were calculated with successive approximations method. Lattice parameters of pure HA produced were assumed as reference lattice parameters, then the alterations in lattice lengths and volume were calculated. Lattice parameters of pure HA and HA doped with Y^{+3} and F^- sintered at different temperatures and the changes in lattice parameters of "a" and "c" and hexagonal unit cell volumes are presented in Table 3.2.

Addition of substitution elements into HA at all sintering temperatures led to reduction in lattice parameters, consequently in volume of hexagonal unit cells (Table 3.2). Both a-axis and c-axis contracted, but the reductions in lattice parameters were more apparent for unit cell parameter "a". These results showed that ions doped into HA were successfully substituted into HA. As a result, changes and shifting in the microstructure of doped HAs were observed. Ion sizes of both Y^{3+} and F^- are smaller than those of Ca^{2+} and OH^- ions. The addition of these ions resulted in the shrinkage of lattices. Ionic radii of Y^{3+} and Ca^{2+} ions are 0.9 Å and 1.0 Å, respectively [96]. The F^- and OH^- ions have ionic radii of 1.32 Å and 1.68 Å, respectively [11, 97]. The contractions in the lattice parameters are believed to be resulted mostly from F^- ions rather than Y^{3+} ions. Because the difference between ionic radii of OH^- and F^- ions is more significant than that of Y^{3+} and Ca^{2+} ions.

In general, as the amount of yttrium doping increased, the contradictions in "a" and "c" also increased. These results were consistent with previous study of Ergun *et al.* [45], which stated that the lattice parameters of HA decreased with the increasing additions of yttrium ions up to 7 mol % and Y^{3+} substitute for Ca^{2+} in

the HA lattice. Similarly Webster *et al.* [51] demonstrated the reductions in "a" and "c" lattices of HA doped with 5 wt % yttrium and the substitutions of yttrium for calcium. While the addition of yttrium leads to alterations in both a-axis and c-axis, fluoride ion addition causes only a-axis to change [63, 98]. As a result a-axis was more sensitive to changes in fluoride content compared to c-axis. By then, the changes in "c" axis in this study must be resulted from the addition of yttrium. Therefore, hexagonal unit cell volumes of doped HAs were smaller than those of pure HAs as seen in Table 3.2. Increasing the amount of doped elements into HA resulted in further decreases in lattice parameters and unit cell shrinkages.

Table 3.2. Hexagonal lattice parameters "a" and "c" and changes in lattice parameters and unit cells volumes for HA, 2.5YFHA, 5YFHA and 7.5YFHA sintered at a) 900°C; b) 1100°C and c) 1300°C.

a)

	a (Å)	c (Å)	Δa (Å)	Δc (Å)	ΔV (Å^3)
HA	9.417	6.879	0.0000	0.0000	0.0000
2.5YFHA	9.400	6.869	-0.0163	-0.0097	-7.6997
5YFHA	9.396	6.865	-0.0208	-0.0144	-10.2626
7.5YFHA	9.394	6.865	-0.0227	-0.0141	-10.8004

b)

	a (Å)	c (Å)	Δa (Å)	Δc (Å)	ΔV(Å^3)
HA	9.413	6.875	0.0000	0.0000	0.0000
2.5YFHA	9.406	6.874	-0.0077	-0.0011	-2.8201
5YFHA	9.408	6.877	-0.0057	0.0022	-1.3998
7.5YFHA	9.384	6.860	-0.0294	-0.0150	-13.2709

c)

	a (Å)	c (Å)	Δa (Å)	Δc (Å)	ΔV (Å^3)
HA	9.412	6.876	0.0000	0.0000	0.0000
2.5YFHA	9.391	6.866	-0.0215	-0.0096	-9.3962
5YFHA	9.393	6.867	-0.0191	-0.0087	-8.4005
7.5YFHA	9.387	6.866	-0.0248	-0.0106	-10.7022

3.1.2.2 Particle Size Determination

Particle sizes of pure and doped HAs sintered at 900°C, 1100°C and 1300°C were determined from XRD results by using Scherrer equation. Table 3.3 shows the summary of particle sizes of pure and doped HAs sintered at various temperatures.

From Table 3.3, it was concluded that increasing the sintering temperatures caused the grain sizes of the materials to become larger. The decrease in grain size with increasing amounts of Y^{3+} and F^- ions additions into HA was also noticeable. Among all HAs, 7.5YFHA sintered at 900°C had the smallest grain size, while the grain size of pure HA sintered at 1300°C was the largest.

Table 3.3. Particle sizes of pure and doped HAs sintered at various temperatures.

		Particle Size (nm)	
		D (002)	**D (300)**
900⁰C	HA	50.07	45.23
	2.5YFHA	57.23	45.24
	5YFHA	50.08	42.86
	7.5YFHA	34.84	37.01
1100⁰C	HA	61.63	45.23
	2.5YFHA	53.41	50.89
	5YFHA	50.07	50.89
	7.5YFHA	50.08	45.25
1300⁰C	HA	61.63	47.89
	2.5YFHA	53.41	54.29
	5YFHA	53.85	54.85
	7.5YFHA	61.63	45.24

However, the grain sizes calculated by Scherrer equation were significantly different from calculations using SEM images, as seen in the section 3.1.4 SEM examinations. Calculations using SEM images were performed according to real images of the grains. However, particle sizes calculated by Scherrer method were measured theoretically. Therefore, it should be noted that they could not be so reliable compared to measurements from SEM images.

3.1.3 FTIR Analysis

FTIR spectra of pure and doped HAs sintered at 900^{o}C, 1100^{o}C, 1300^{o}C are represented in Figures 3.5-3.8. For all samples, the main characteristic peaks of HA were observed. The frequencies and assignments of reference HA and FA are presented in Table 3.4.

OH^- libration bands around 630 cm^{-1} were only intense for pure HA sintered at 900^{o}C and 1100^{o}C. Bands assigned to PO_4^{3-} group were around 962, 474, 1087 and 601 cm^{-1}. The patterns of doped HAs were similar to that of pure HA, except some additional F^- bands indicating substitutions of added ion with OH^- ions into HA. OH^- libration band at around 630 cm^{-1} which were clearly seen in pure HAs were erased or almost disappeared in the spectra of doped HAs, except 2.5YFHA. F^- bands at around 700 and 858 cm^{-1} appeared in the patterns of doped HAs, as shown in Figures 3.6-3.8. The main characteristic absorbtion bands of HA were preserved with increasing the temperatures, only some additional bands showing the substitutions with ions in HA were added in the FTIR spectra.

Table 3.4. Frequencies and assignments of FTIR spectra for reference HA and FHA [52, 99].

Material	Assignments	Mode	Frequencies (cm^{-1})
HA	OH^- stretching		3572
	OH^- libration		630
	PO_4^{3-}	v_3	1087, 1046, 1072 (sh), 1032 (sh)
		v_1	962
		v_4	474, 462 (sh)
	CO_3^{2-}		1547, 1457, 1415
	Ca-PO_4		290, 275, 228
	Ca-OH stretching	v_3	355, 343
FHA	Ca-F	v_3	325, 336
	Ca-PO_4		280, 230
	PO_4^{3-}	v_2	962, 460
		v_3	1090, 1040
		v_4	601, 575

sh: shoulder; v_1: stretching mode; v_2: doubly bending mode; v_3: triply degenerate antisymmetric stretching mode; v_4: triply degenerate bending mode.

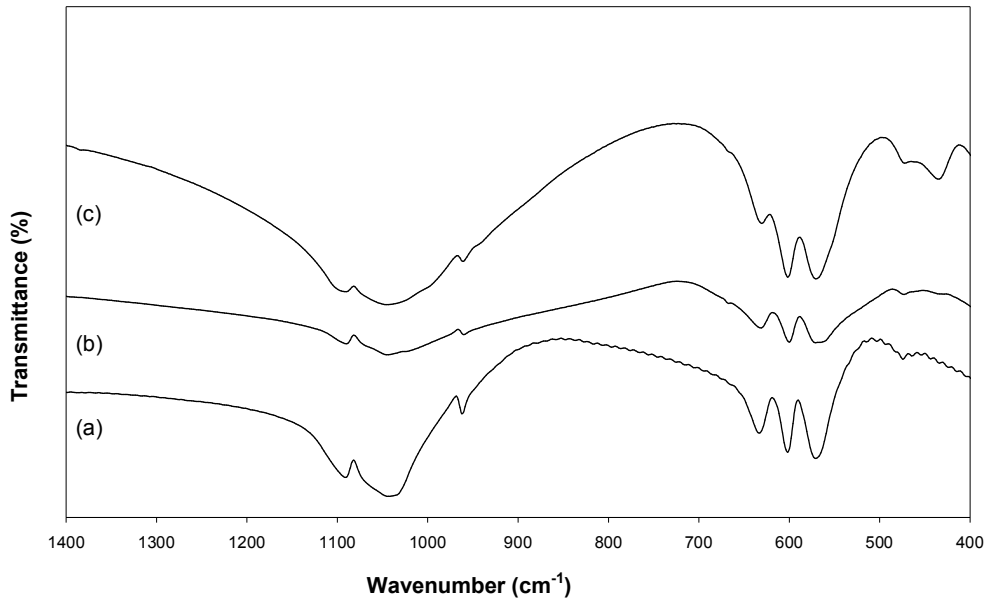

Figure 3.5. FTIR patterns of HA sintered at a) 900°C; b) 1100°C; c) 1300°C.

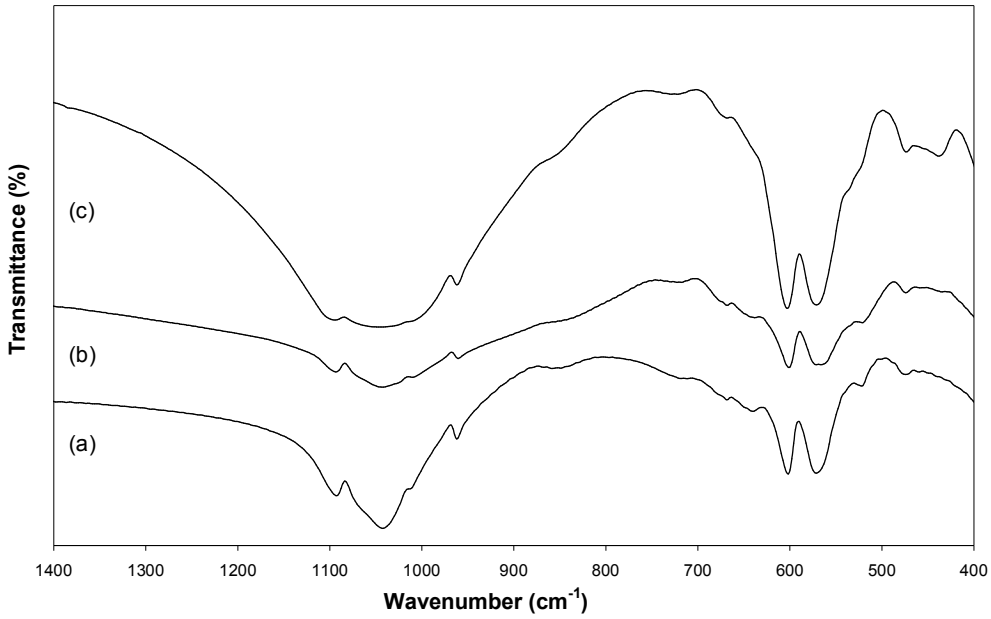

Figure 3.6. FTIR patterns of 2.5YFHA sintered at a) 900°C; b) 1100°C; c) 1300°C.

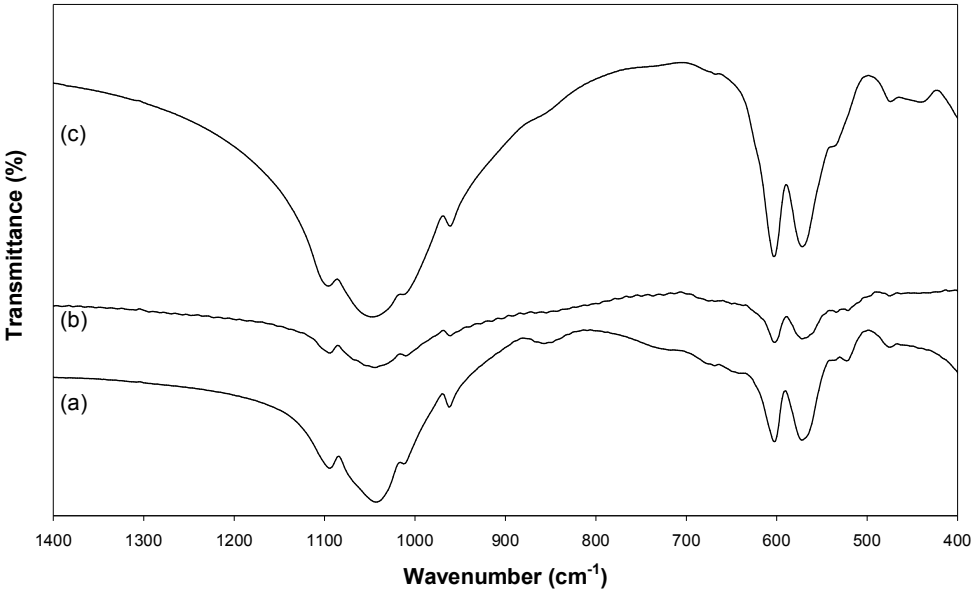

Figure 3.7. FTIR patterns of 5YFHA sintered at a) 900°C; b) 1100°C; c) 1300°C.

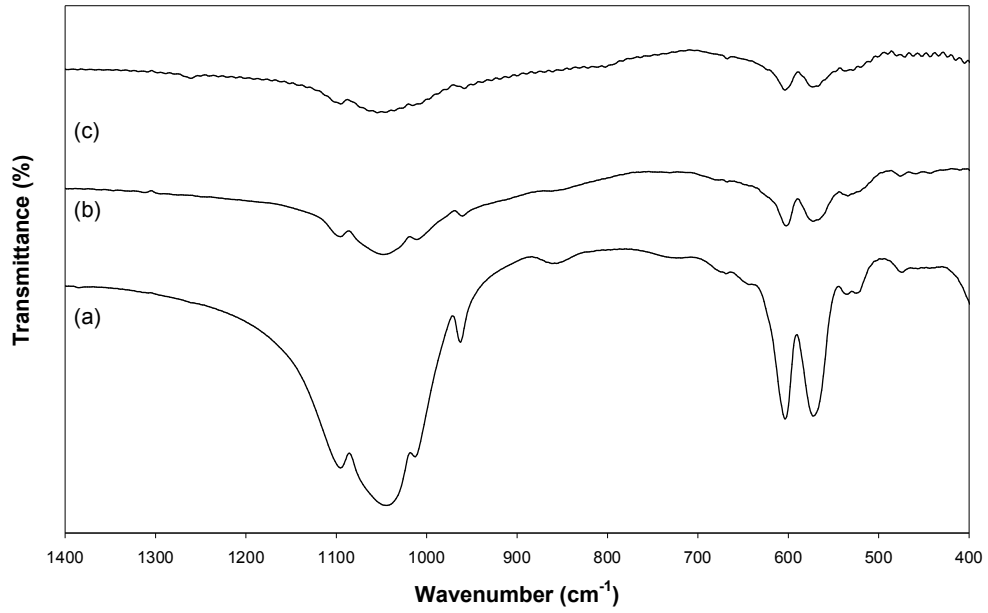

Figure 3.8. FTIR patterns of 7.5YFHA sintered at a) 900°C; b) 1100°C; c) 1300°C.

3.1.4 SEM Examinations

SEM images of pure and doped HAs sintered at 900°C, 1100°C and 1300°C are given in Figures 3.9-3.12.

As seen in SEM images, temperature and amounts of dopants had important effects on grain sizes of the samples. SEM examinations revealed that HAs sintered at low temperatures below 1300°C had more uniform microstructures and equiaxed fine grains. However, as the sintering temperature reached to 1300°C, grain sizes exhibited severe growths. Nevertheless, it was observed that the addition of Y^{3+} and F^- ions into HA prevented the grain growth up to some extent. In Table 3.5, the effect of dopings and sintering temperatures on pure and doped HAs are summarized. HAs sintered at 900°C and 1100°C were observed to be nano in size. But after the sintered at 1300°C, very high fluctuations in grain sizes were observed compared to other sintering temperatures (Table 3.5). It can also be concluded that nano sized HAs were successfully produced at the end of the sinterings, except at 1300°C.

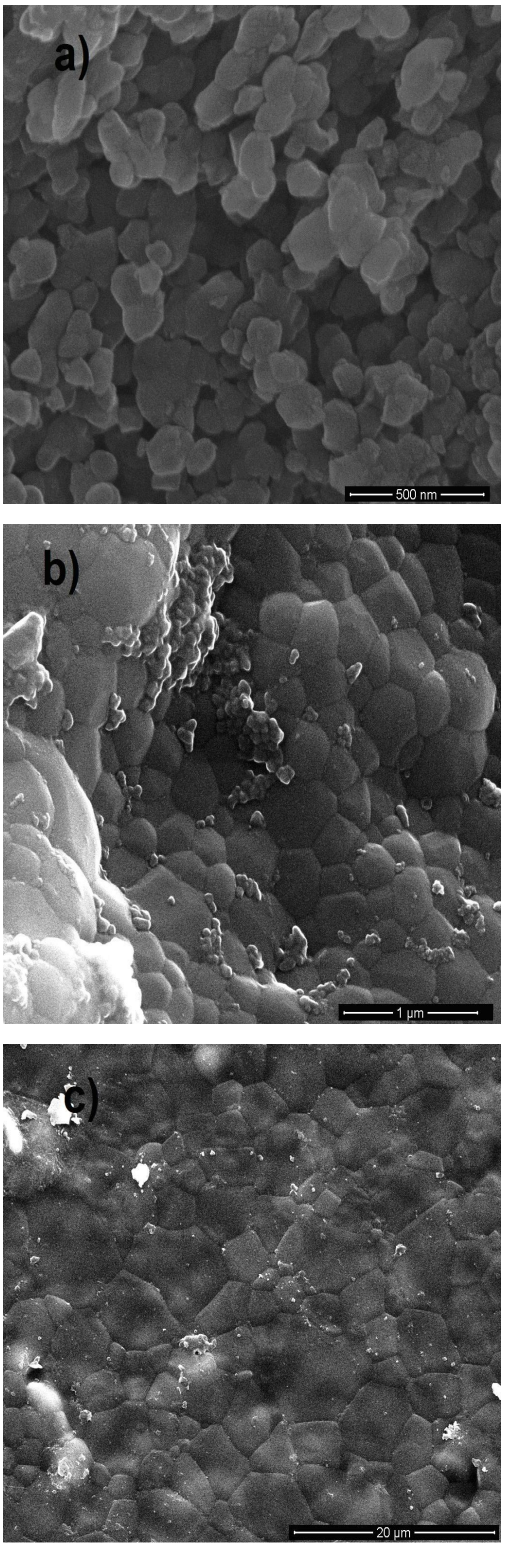

Figure 3.9. SEM images of pure HAs sintered at a) 900^{o}C; b) 1100^{o}C; c) 1300^{o}C.

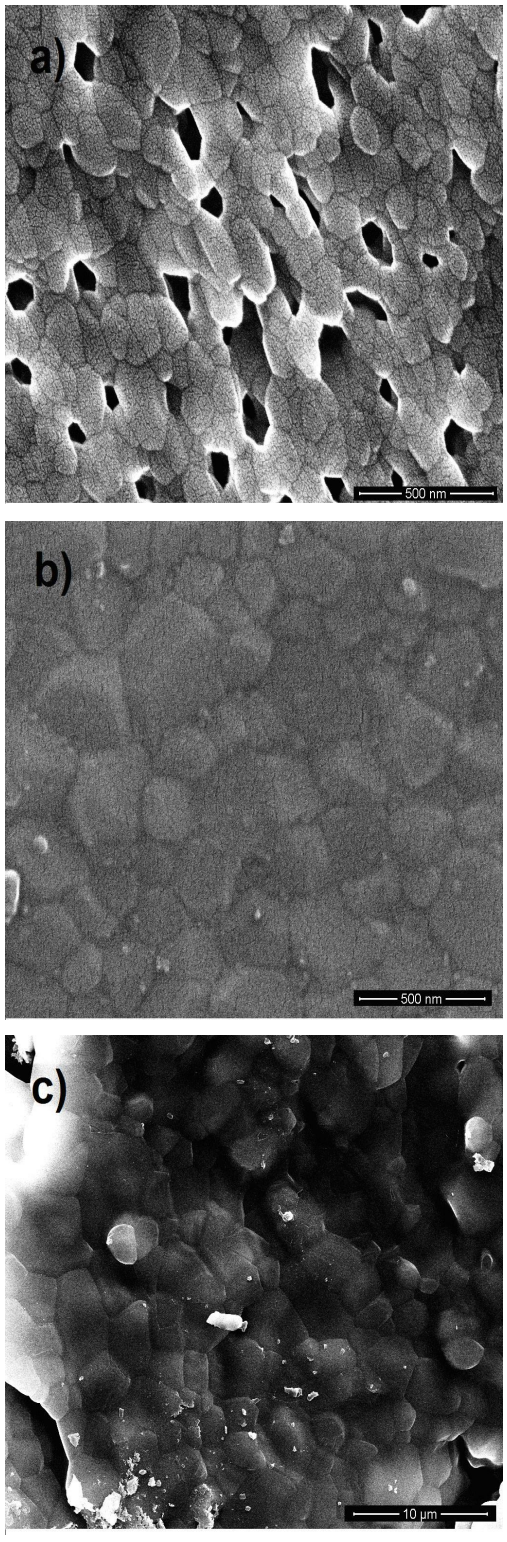

Figure 3.10. SEM images of 2.5YFHAs sintered at a) 900^{o}C; b) 1100^{o}C; c) 1300^{o}C.

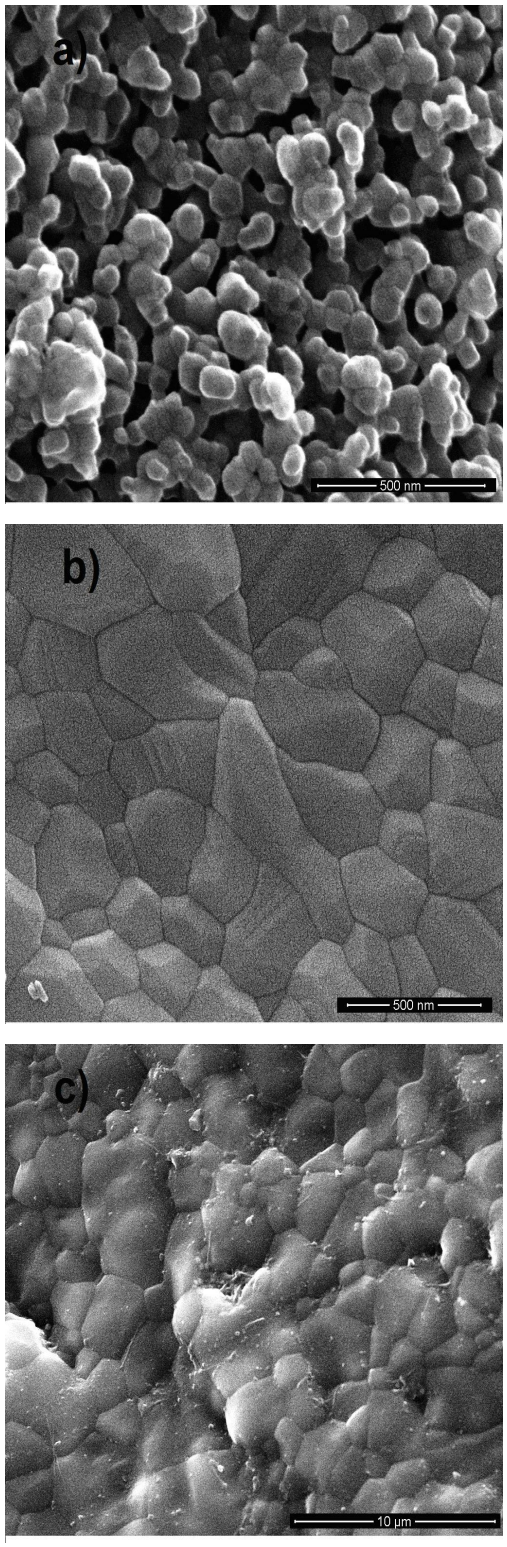

Figure 3.11. SEM images of 5YFHAs sintered at a) 900^{o}C; b) 1100^{o}C; c) 1300^{o}C.

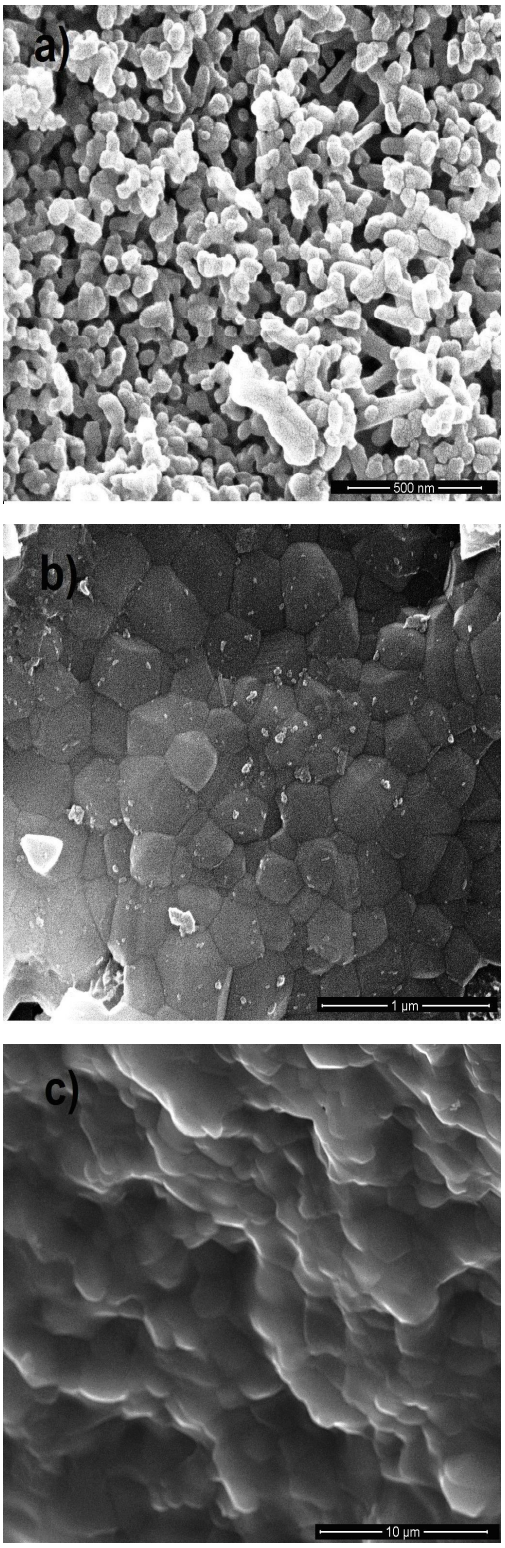

Figure 3.12. SEM images of 7.5YFHAs sintered at a) 900^{o}C; b) 1100^{o}C; c) 1300^{o}C.

Table 3.5. Average grain sizes of pure and doped HAs sintered at various temperatures (determined from SEM images).

	Average Grain Size (nm)		
	900°C	***1100°C***	***1300°C***
HA	86.6	271.0	3487
2.5YFHA	82.6	224.0	2409
5YFHA	56.3	204.8	1832
7.5YFHA	51.4	200.7	1641

Pure HA had the largest grain size for all sintering temperatures compared to doped HAs. Decrease in grain sizes at the same sintering temperatures could be attributed to the dopings. Initially, the grain sizes increased slowly by a factor of between 2 and 4, when sintering temperature went to 1100°C from 900°C. However, when sintered at above 1100°C, the grain sizes increased by a factor of between 8 and 12. Similarly, Ramesh *et al.* [100] reported that the average grain size increase by a factor of more than 7, from 0.88 μm at 1150°C to 7.13 μm at 1300°C. It was demonstrated that since higher temperatures were able to provide the activation energy of HA for grain growth, when sintered above 1250°C, considerable grain growth (by a factor of about 6) occurred compared to other samples sintered at lower temperatures [101]. In the present study, it was clearly seen that increasing temperature caused the grain size of pure HA to grow 40 fold from 86.6 nm at 900°C to 3487 nm at 1300°C. For doped HAs, the same trends were observed with temperature changes. However, the increasing of grain sizes of doped HAs from 900 to 1300°C occurred in a decreasing manner. In other words, the additions of ions resulted in a decrease in grain sizes. As the amount of doped ions increased, the grain size decreased for HAs sintered at the same temperature. Accordingly, the material with the smallest grain size was 7.5YFHA with 51.4 nm sintered at

900°C due to low sintering temperature and high amount of dopings. With the addition of Y^{3+} and F^- ions, nano sized HA was obtained even at 1100°C. Previous reports announced that the grain sizes of HA dope with fluoride ions increased with increasing degree of fluoridation [63, 102], while addition of yttrium into HA led to decrease in the grain sizes of the materials [45, 51]. Therefore, decreases in grain sizes measured in this study could be attributed to yttrium dopings into HA.

Finally, it was seen that the particle sizes determined from SEM images were significantly different, from those calculated by XRD graphs, especially for the grain sizes of materials sintered at 1300°C. This could probably be due to theoretical approach of the Scherrer equation. These results indicated that using of theoretical equations for determining the grain sizes of materials with micron sized grains could not be reliable due to grain size limitations. So, the results calculated from SEM images might be assumed to be more adequate and acceptable than those from XRD patterns.

3.2 Mechanical Testings

3.2.1 Diametral Strength

The bending test method is generally preferred for measuring the strength of ceramics. However, bending tests need to have pre-made bar or rod samples in great amount and also those tests easily distinguish the effects of surface imperfections on the strength. The alternative method for this test is the diametral strength test which was previously studied; it was preferred for the simplicity in practice and availability in test sample preparation [78, 103, 104]. Diametral strength test has been widely used for measuring the diametral strength of ceramics [104-109]. This method was first introduced to measure the tensile strength of the concrete whose strength could not be determined by conventional methods [110-112].

Recently, the diametral test has been widely applied in testing the teeth prosthesis materials and mostly cements used in dentistry [113-115]. Diametral strength test is proper for biomedical materials used in dental and orthopedic applications. Because the stresses formed in vivo for dental implants is similar to thaose generated by diametral compression test [105, 116, 117].

In Figure 3.13, changes in diametral strengths of pure and doped HA discs sintered at 900°C, 1100°C and 1300°C are illustrated. Also, diametral strength as a function of relative density is given in Figure 3.14. In general, there are many factors (porosity, second phases, grain sizes, etc) affecting diametral strength of the materials.

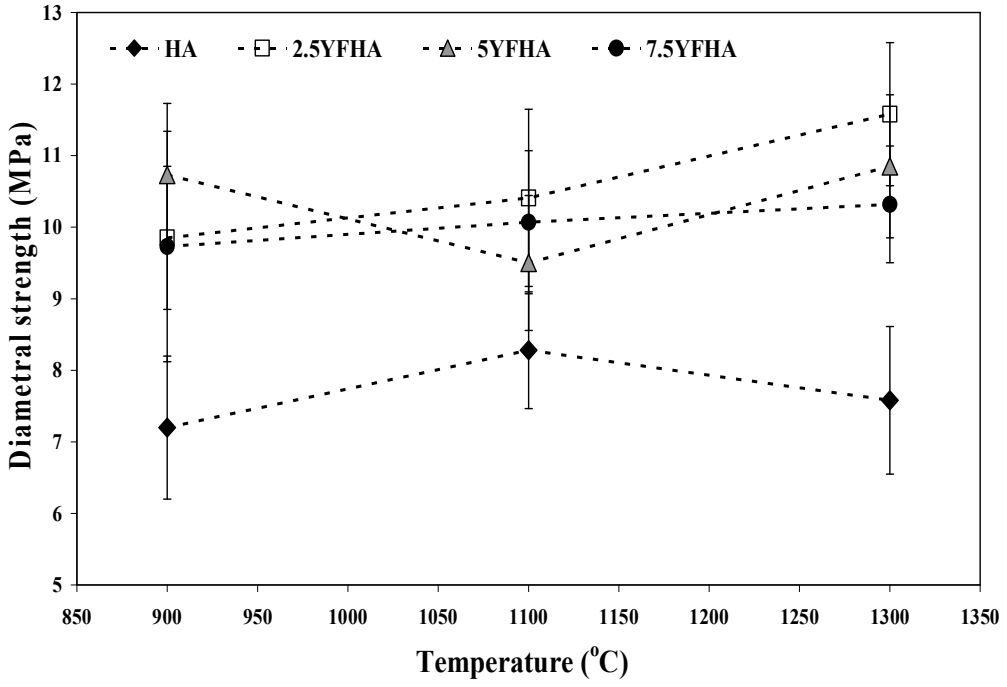

Figure 3.13. Diametral strength of doped and undoped HA sintered at various temperatures.

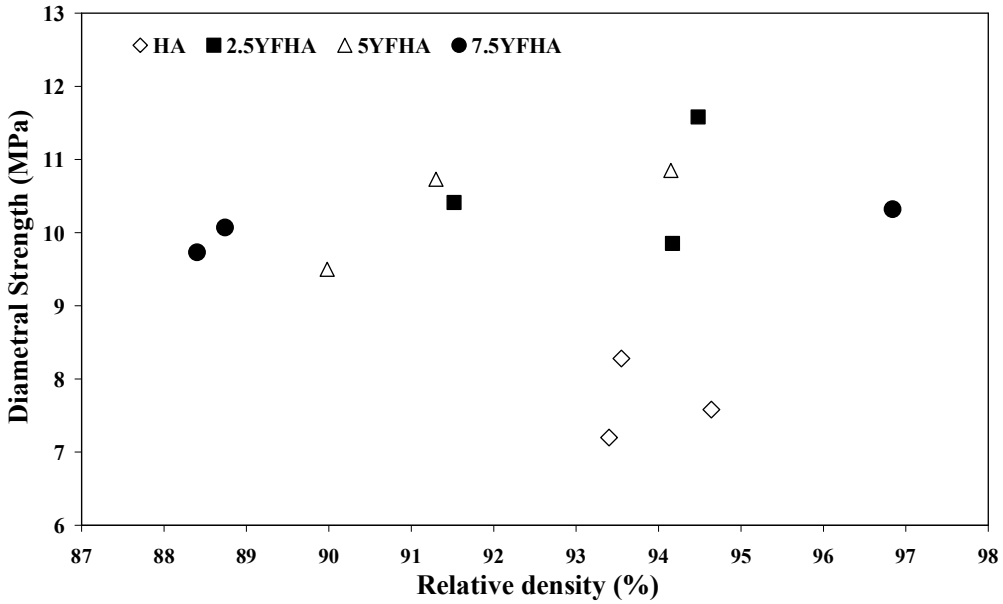

Figure 3.14. Diametral strength of doped and undoped HA with various density.

The diametral strengths of HAs produced in this study varied between 7.2-12.0 MPa (Figure 3.13). The samples tested by diametral method had densities between 88.4-96.8 % of the theoretical density of HA, as seen in Figure 3.14. The diametral discs mostly broke into two pieces. However, few of them splitted into three or more pieces probably due to the inhomogeneous distribution of the pores in the samples tested. The previous studies have reported that diametral strength values could vary with the parameters like amount porosity in the sample, Poisson's ratio of the material, contact area during test, diameter and the thickness of the disc and distribution of the pores [109, 118]. Previous studies stated that diametral strength of HA was between 1-35 MPa [78, 109, 119-122]. Actually, this is a very broad range, because many factors should be considered to determine the diametral strength. Thomas *et al.* [78] pronounced that diametral tensile strength of 100 % dense HA was calculated as 35 MPa, indicating that densification of HA was prominent at the diametral strength of the material. While the diametral strength of porous HA with 45-50 % open pore structure was 1-2 MPa [119], fully dense

HA with diametral strength of 35 MPa could be achieved [78]. An experimental study was performed to find out the influence of porosity on diametral strength of HA with porosities ranging 1-32 %, indicating that the diametral strength of HAs increased with increasing the densification of HA [109]. For example, diametral strength of HA with 10 % porosity was about half of the diametral strength of fully dense one [109].

As seen in Figure 3.13, increasing sintering temperatures generally resulted in an increase in the diametral strength. The only dissimilar trend was observed for pure HA sintered at 1300^{o}C; its diametral strength was prone to decrease when its sintering temperature exceeded 1100^{o}C. This could be due to the excessive grain growth and formation of β-TCP after the sintering at 1300^{o}C as seen in Figure 3.9.

In addition to improving effect of higher sintering temperature, the dopings had also positive influence on diametral strengths of the materials. As shown in Figure 3.13, the diametral strengths of HAs increased with increasing amounts of substitutions into HA. 7.5YFHA had the lowest diametral strength among all doped HAs sintered at 1300^{o}C. Pure HA sintered at 900^{o}C had the smallest diametral strength with 7.2 MPa, among all other HAs. Moreover, 2.5YFHA sintered at 1300^{o}C had the highest diametral strength (11.6 MPa). As seen in Figure 3.13, 2.5YFHA had a consistent pattern in terms of diametral strength at different sintering temperatures. Diametral strength of 2.5YFHA sintered at 900^{0}C, 1100^{o}C, 1300^{o}C increased gradually with increasing sintering temperatures.

The distribution of diametral strength of sintered HAs with respect to relative density of HAs is represented in Figure 3.14. From previous studies, the dominant factor affecting the maximum diametral strength of HA was the amount of porosity of the material [78, 109, 118]. However, there might be other factors affecting the diametral strength of HA such as grain size, presence of impurities, distribution of porosities, and presence of second phases. As seen in Figure 3.14,

decreasing porosity was not enough for HA to have smaller diametral strength. For example, pure HA with 6.6 % porosity, not the least, had the smallest diametral strength with 7.2 MPa and doped HAs with even higher porosities had higher diametral strength than pure HAs. 7.5YFHA with the highest porosity tested in this study, sintered at 900^0C (lowest sintering temperature), had a greater diametral strength with 9.7 MPa. 2.5YFHA with 94.3 % relative density sintered at 1300^oC had the highest diametral strength with 11.6 MPa. Indeed all doped HAs sintered at various temperatures had higher diametral strengths than pure HAs with different porosities and sintered at different temperatures. This showed that the ions doped into HA had a significant role in improvement of the mechanical strength of HA sintered at any temperature. It could be concluded that the amount of substitutions, besides the amount of porosity in the samples, was also critical to verify the diametral strength of HA. Since no secondary phases were observed in the microstructure of HAs, changes in mechanical properties of HAs could not be attributed to the decomposition of HA shown in Reaction 3.1. In order to optimize the mechanical properties of HA, the percentage of doping should be carefully arranged. As seen in Figures 3.13 and 3.14, severe increases in the proportion of substitutions limited the densification of the material even at high temperatures and mechanical stability was disrupted with firm fluctuations in doping amount. However, those properties could be improved if moderate additions of dopants were fixed. In terms of diametral strength, amount of second phases in the microstructure, 2.5YFHA could be the material to be investigated in more detail.

3.2.2 Vickers Micro-Hardness Testing

In order to study the mechanical effects of dopings into HA sintered at various temperatures, micro-hardness of the samples was also determined. The effect of temperature and dopings on microhardness was given in Figure 3.15. It can be noted that the lowest microhardness value of 3.3 GPa was measured for 5YFHA sintered at 900^{o}C, whereas the maximum microhardness value of 5.9 GPa was achieved for 7.5YFHA sintered at 1300^{o}C. Sintering effects on the mechanical properties of HA have been widely investigated. Vickers microhardness of pure HA ranged from 1.17 GPa to 6.86 GPa for various sintering temperatures [93, 101, 123].

An increasing trend in microhardness values was observed with increasing sintering temperatures. All HAs, regardless of dopings, had the highest micro hardness after the sintering at 1300^{o}C due to the high relative densities of the HAs. These results suggest that the sintering temperature had a significant influence on the microhardness of HAs probably due to the densification the materials with increasing the sintering temperatures. Since pure HA is very brittle to be used in load bearing areas in the body, the hardness of HA needs to be moderated to acceptable values for its use in load bearing areas.

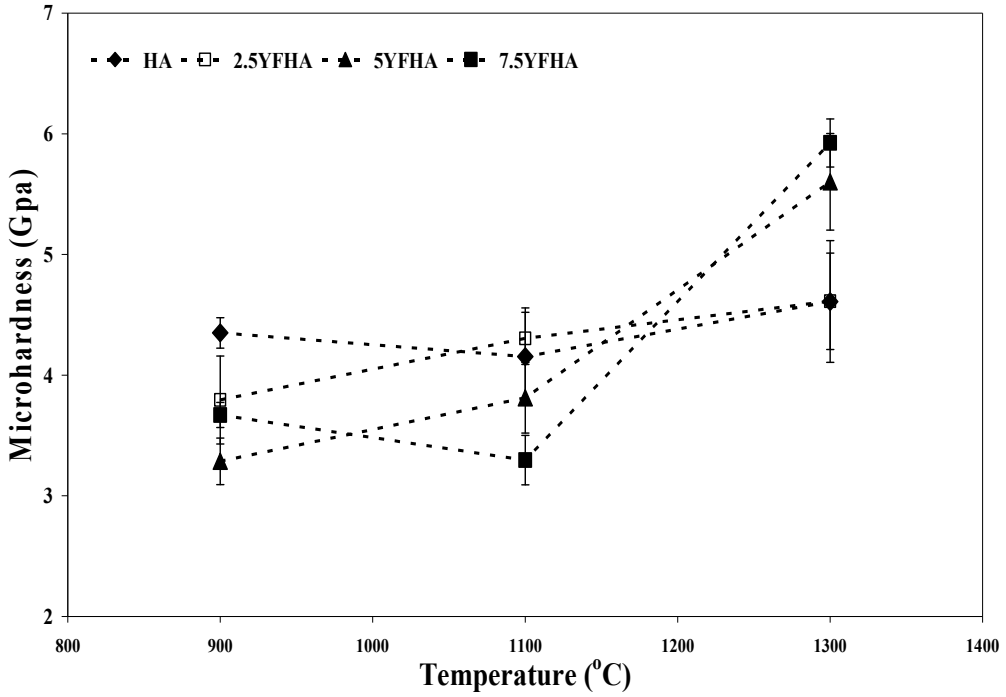

Figure 3.15. The change in microhardness of pure and doped HAs with various compositions as a function of sintering temperature

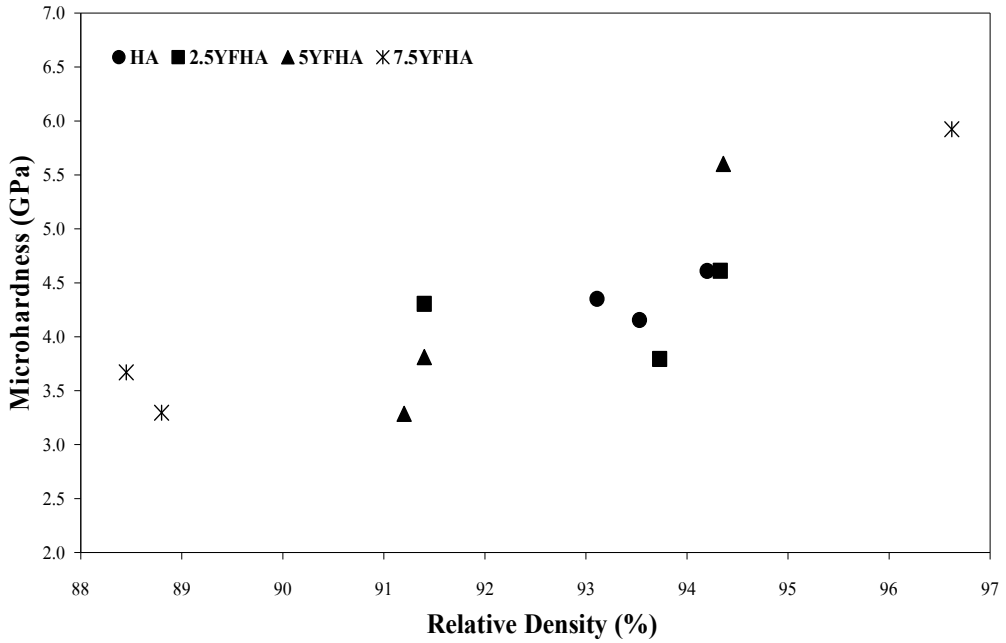

Figure 3.16. The change in microhardness of pure and doped HAs with various compositions as s function of densities of HAs.

Essentially, the main difference in microhardness values of HAs was made by the addition of dopings into HA. The effect of co-substitutions of yttrium and fluoride dopings on microhardness was studied to optimize the amount of the additions. All pure HAs synthesized in this study had microhardness values around 4 GPa. Microhardness values of doped HAs sintered at 900^{o}C were about between 3.3 to 3.8 GPa. The similar pattern was also observed for doped HAs sintered at 1100^{o}C; almost all doped HAs, except 2.5YFHA, had lower microhardness than pure HA. Only the microhardness of 2.5YFHA was slightly higher than that of pure HA at 1100^{o}C. However, doped HAs sintered at 1300^{o}C had higher microhardness values than pure HA sintered at that temperature. As the amount of dopings into HAs sintered at 1300^{o}C increased, the microhardness of the HAs also increased (4.6, 5.6, 5.9 GPa). But the general tendency of change for microhardness was towards decreasing with increasing of the amount of dopings into HA. Besides the amount of dopants, there must have been a correlation between hardness and the relative density and the grain size at various temperatures. The dominant parameter for changes in microhardness values was the amount of porosities differing with the amount of dopants (Figure 3.16). HAs sintered at 1300^{o}C did not show severe differences in their degree of porosities with increasing amount of additions. But for HAs sintered at 900^{o}C and 1100^{o}C, increase in amount of dopings caused the relative density to slightly decrease, also it was noted that the grain sizes decreased with increasing proportions of dopants, as seen in Tables 3.3 and 3.5. In addition to the lower degree of porosity, the grain sizes of pure and doped HAs sintered at 1300^{o}C increased abruptly, which could be interpreted that the high relative density and larger grain size might have been the governing parameters concerning the microhardness values.

3.2.2.1 Fracture Toughness

In Figures 3.17 and 3.18, fracture toughness of pure and doped HAs versus sintering temperature and densities are represented, respectively. The fracture toughness values attained with various temperatures and doping amounts ranged between 1.0-2.1 $MPa \cdot m^{1/2}$. The maximum fracture toughness of $MPa \cdot m^{1/2}$ was measured for 2.5YFHA sintered at $1100^{o}C$ (2.1 $MPa \cdot m^{1/2}$). The lowest fracture toughness value of 1.0 $MPa \cdot m^{1/2}$ was calculated for 5YFHA sintered at $900^{o}C$. In literature, fracture toughness values for pure HA sintered at various temperatures was found to vary in the range of 0.96- 1.45 $MPa \cdot m^{1/2}$ [93, 101, 124]. Therefore, HAs synthesized in this study could be have higher fracture toughness compared to those in literature. Correlated to the previous graph of microhardness vs. temperature, it was shown that harder materials had lower fracture toughness, naturally. As the sintering temperatures were increased, the fracture toughness of pure HA became lower due to the increase in relative density. However, the fracture toughness of Y^{3+} and F^{-} doped HAs sintered at $900^{o}C$ and $1100^{o}C$ increased with the increasing sintering temperatures. Additions into pure HA prevented the fracture toughness from severe decrease, which was resulting from increasing temperatures. However, at the higher sintering temperatures such as $1300^{o}C$, lower fracture toughness values were determined than those at $900^{o}C$ and $1100^{o}C$, probably due to the severe grain growths in HAs sintered at $1300^{o}C$.

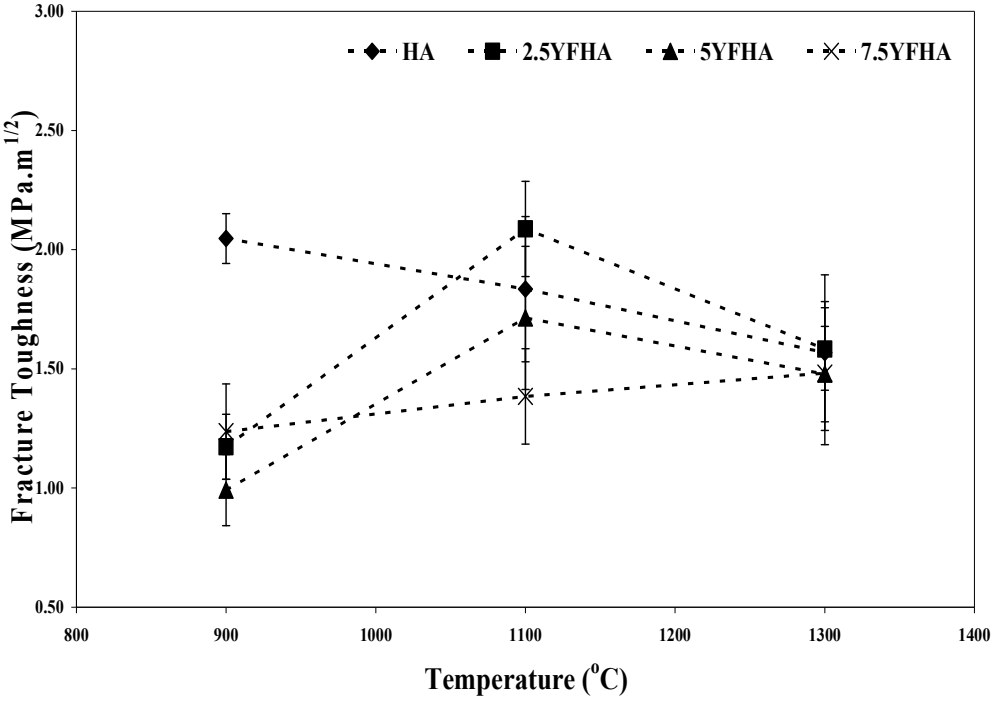

Figure 3.17. The effect of temperature and dopings on fracture toughness of HAs.

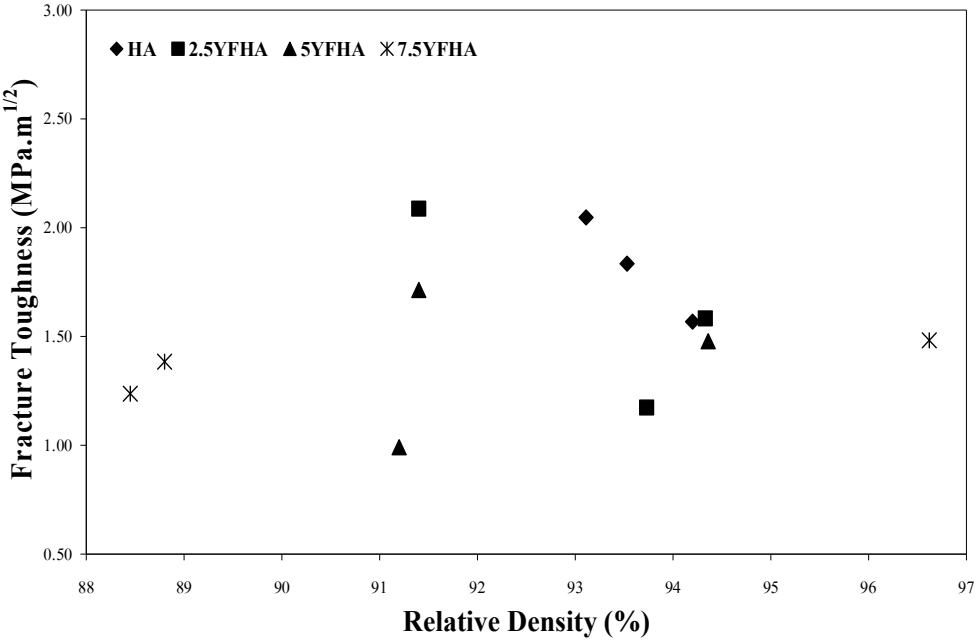

Figure 3.18. The effect of density and dopings on fracture toughness of HAs.

3.3 *In Vitro* Analysis

3.3.1 Cell Attachment and Proliferation

In the present study the fluoride and yttrium was incorporated into HA and the effects of dopants and sintering temperature on the cell behavior was investigated in terms of cell attachment and proliferation. The results of MTT viability assay are shown in Figures 3.19-3.22. Figure 3.19 represents the attachment percentage of Saos2 cells on pure and doped HAs after 24 hr incubation. As seen in Figure 3.19, cell attachment efficiency on all HAs, except pure HA sintered at 1300^{o}C, was above 70 %. The adhesion of Saos-2 cells on all discs was high suggesting that the surface property of both pure and doped HAs was suitable for attachment of Saos-2 cells. Previous studies showed that the fluoride content of HA had a positive effect on cell attachment and proliferation when it reached to a certain amount [67, 70]. Below that level, it had no contribution to cell adhesion [67]. The fluoride content of the doped HAs used was lower than the optimum range suggested being suitable for implantation. It was previously shown that fluoride incorporation within the surface of the material led to Ca^{2+} adsorption on the surface due to formation of lower zeta potential. This resulted with higher adhesion of osteoblast-like cells [67]. Adsorption Ca^{2+} on the surface affects the adsorption of extracellular matrix (ECM) proteins through which osteoblast-like cells attach on the surface of underlying material [125].

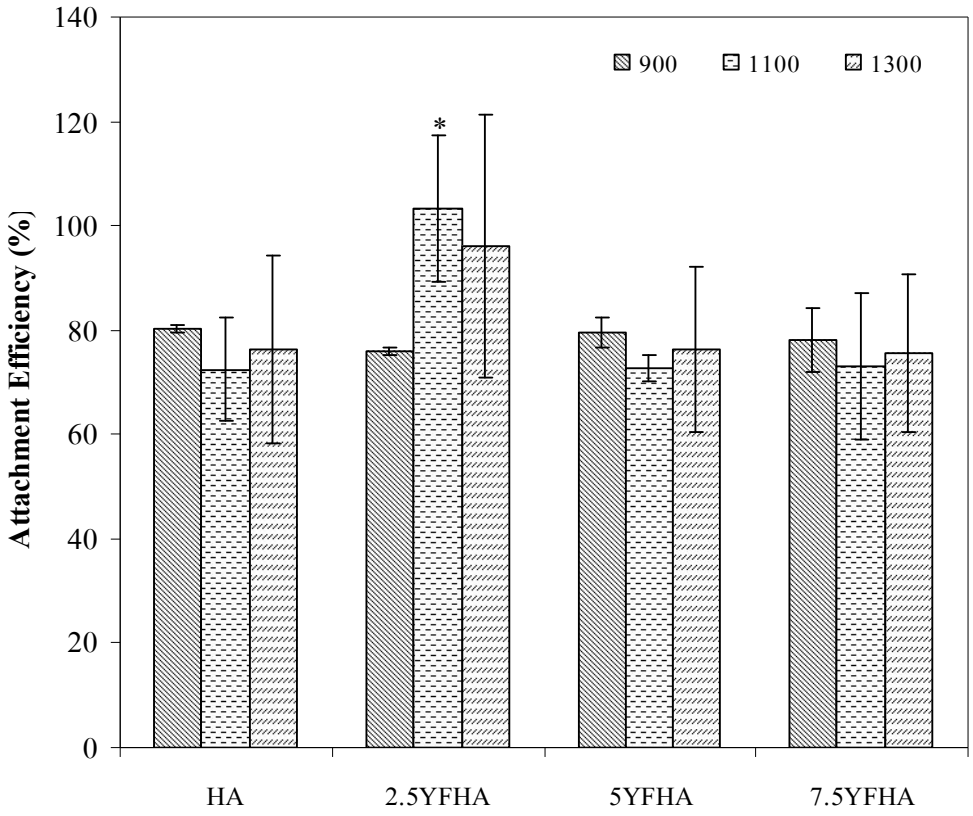

Figure 3.19. Cell attachment on HAs sintered at various temperatures after 24 hour incubation (attachment efficiencies were measured with respect to TCPS when seeding density was $5x10^4$ cells/disc; * incubated for 1 day; statistically different from other HAs sintered at 1100^oC).

The highest cell adhesion among all discs was observed on 2.5YFHA (103±14 %) sintered at 1100^oC. Additionally, cell attachment efficiency observed was also statistically greater than pure HA and other doped HAs sintered at the same temperature suggesting the positive effect of this level of yttrium incorporation along with 2.5 % fluoride doping. Webster *et al.* [76] investigated the effect of various dopants and the amount of yttrium on the mechanism of osteoblast adhesion of HA substrates. They stated that 2 mol % yttrium doped HA had the greatest cell adhesion percentage among all other doped HA after 4 hr incubation, and increasing

amount of yttrium doping into HA also enhanced the osteoblast adhesion. In another study of Webster *et al.* [51], osteoblast adhesion on 5 wt % Y^{3+} and In^{3+} doped HA after 4 hr incubation was the greatest among pure HA and all other doped HAs. It was also recently shown that osteoblast adhesion was not significantly promoted on yttrium doped nanocrystalline HA coatings on titanium substrate in which yttrium doping was less than 2 mol % [74]. This indicated that there could be a minimum level of yttrium doping to promote osteoblast adhesion. In the present study, it was also observed that 2.5 % yttrium addition to fluoridated HA maximized the cell adhesion for all sintering temperatures in comparison to pure HA and doped HAs. Even at very high temperature (1300^{o}C) with micron-sized grains and less amount of yttrium, cell adhesion was above 80 %.

Furthermore, surface structure and grain size of the materials could also have a contributing effect on cell adhesion. Previous studies have concluded that the osteoblast adhesion on especially pure HA, alumina and titania improved with small grain sizes [126-129]. Consistently, the cell adhesion on pure HA sintered at 1300^{o}C with micron grain size was the minimum. However, no decrease in cell adhesion was observed on doped HAs with larger grain sizes. This could probably be due to the contributing factors of yttrium and fluoride ions dopings.

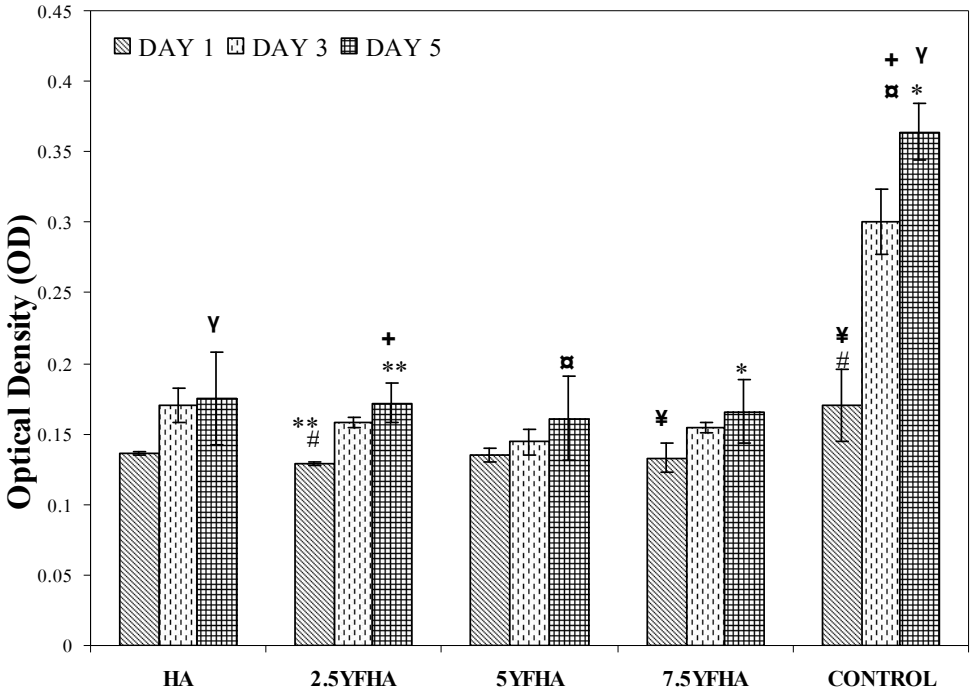

Figure 3.20. Cell proliferation on pure and doped HAs s sintered at 900°C; cells were seeded on TCPS as control (significant differences between groups *, **, ¥, γ, ¤, + $p<0.05$).

Figure 3.20 shows that cells proliferated on all pure and doped HAs sintered at 900°C. Saos-2 proliferation for all these discs was similar. On the other hand, cell proliferation on control surface was greater than all pure and doped HA discs. This could be due to differences in their surface properties (i.e. roughness, wettability, chemical composition, etc). When MTT readings for incubation days 1 and 5 were compared in the same group a significant difference was observed for only 2.5YFHA.

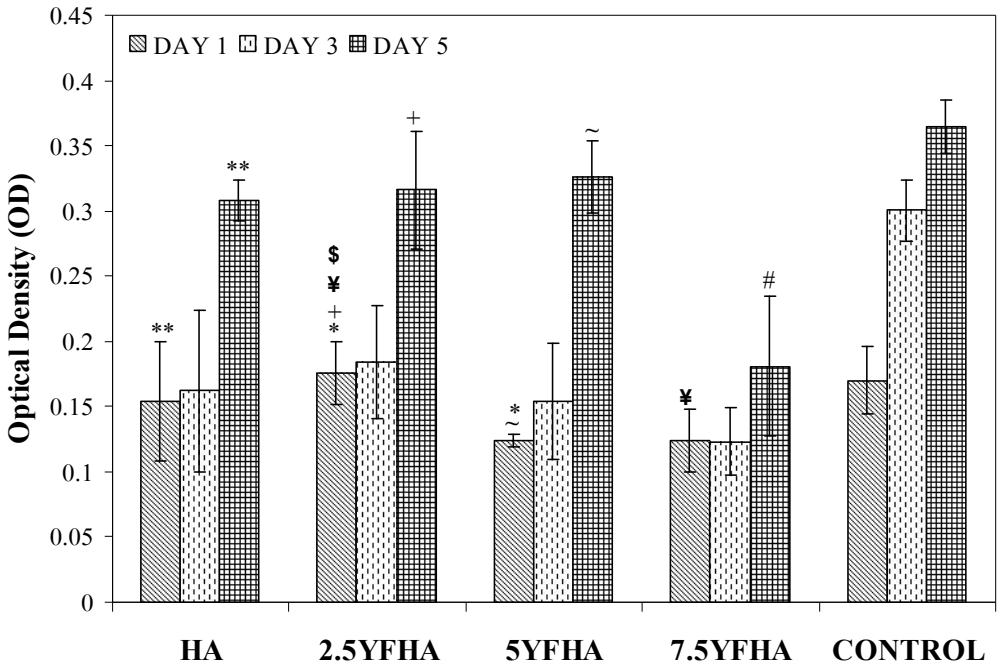

Figure 3.21. Cell proliferation on pure and doped HAs sintered at 1100°C, cells were seeded on TCPS as control (significant differences between groups *, **, ~, ¥, + $p<0.05$; # 7.5YFHA significantly lower than other doped HAs at day 5 $p<0.05$; $ 2.5YFHA significantly higher than other pure and doped HAs at day 1 $p<0.1$).

Figure 3.21 shows that cell proliferated on all HAs sintered at 1100°C. Cell proliferation did not reveal significant difference between first and third days. Cell proliferation on 7.5YFHA was statistically lower than on all other pure and doped HAs and control after 5 days of culture. There was no statistically significant difference in MTT readings for pure HA, 2.5YFHA and 5YFHA after 5 day incubation. Additionally, the cell proliferation on pure HA, 2.5YFHA, 5YFHA was comparable with the control group. The fluoride content was the same (2.5 mol %) for all doped HA, yttrium percentage in HA was changing from 2.5 to 7.5 mol %. Yttrium content of 2.5 and 5 % promoted cell proliferation in comparison to pure HA. Previous studies suggested that there could be a minimum level of doping for improvement in cell adhesion [74, 76]. In addition to these findings, the results in

the current study suggest that there could be a maximum level of yttrium addition over which could slow down the cell growth. Accordingly, yttrium content with 7.5 mol % could exceed this maximum level resulting in less proliferation on 7.5YFHA.

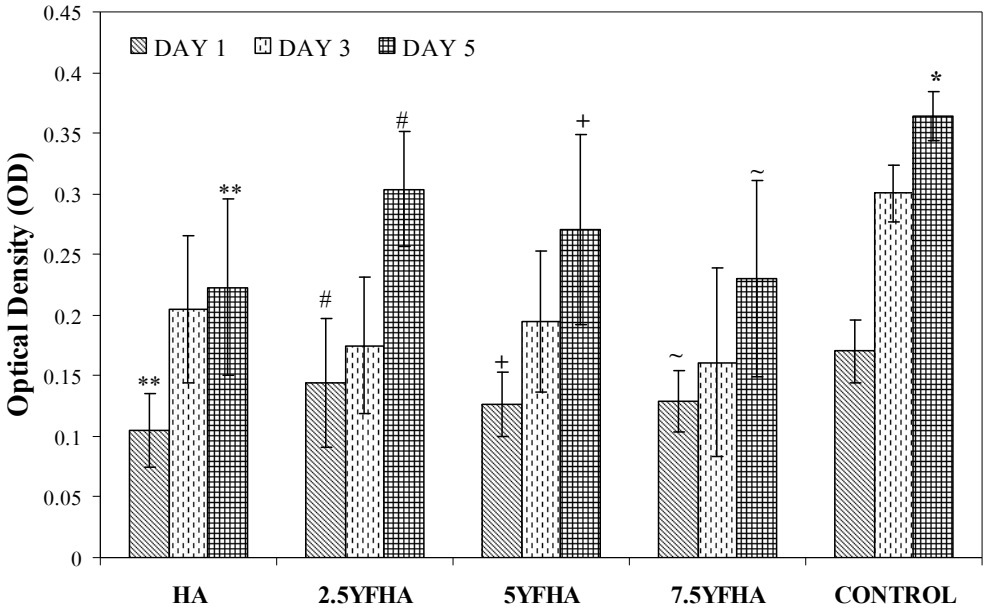

Figure 3.22. Cell proliferation on HAs sintered at 1300°C during 5 day incubation cells were seeded on TCPS as control (significant differences between groups **, #, +, ~: $p<0.05$; * control significantly higher than pure and doped HAs at day 5 $p<0.05$).

Figure 3.22 shows that cell also proliferated on all pure and doped HAs sintered at 1300°C. MTT readings for first and fifth days revealed a statistical difference within for all groups. Cell attachment 2.5 and 5 % yttrium doped HAs was comparable with control, but still numerically lower. As seen in Figure 3.22, cell densities on HAs increased with culture time. Cells proliferation on 2.5YFHA was the highest among all pure and doped HAs after 5 day culture.

The sintering temperature affected proliferation on yttrium and fluoride doped HAs (Figures 3.20-3.22). At day 5, the lowest MTT read for all HAs sintered at 900°C was significantly lower than that for HAs sintered at 1100° and 1300°C. The only exception was 7.5YFHA sintered at 900°C which was significantly lower than only for 7.5YFHA sintered at 1300 °C. The degree of proliferation of cells on pure and doped HAs was similar at 1100 °C and 1300 °C. After cells were attached on HAs, the fastest proliferation was observed on HAs sintered at 1100° and 1300°C. Additionally, 2.5YFHA showed the highest MTT readings at days 1 and 5 for all sintering temperatures among all other pure and doped HAs. Generally, increasing amount of yttrium to 7.5 % in HA led to decreases in the proliferation of cells, at both 1100 °C and 1300 °C sintering temperatures. These results were in contradictory with reports pronouncing that increasing concentrations (from 2 mol % to 7 mol %) of yttrium improved the adhesion of cells [76]. However, yttrium was not the only addition into HA, as done in previous research [76]; yttrium and fluoride were attempted to be co-substituted into HA in this study. Therefore, the contradiction could be aroused by this difference. Previous studies have reported that cell adhesions on especially pure HA improved with decreasing grain sizes [130] and nano-sized bioceramics were known to be better for cell adhesion and proliferation compared to micron-sized bioceramics [126, 127]. The current study revealed that cells highly adhered and proliferated even on larger grain-sized HAs when doped with yttrium and fluoride ions.

3.3.2 SEM Examinations

Figures 3.23-3.34 represent the SEM images of cells cultured on pure and doped HA discs after incubations of 1 and 5 days. Generally, SEM images of pure and doped HAs sintered at different temperatures exhibited that Saos-2 cells on HAs discs attached to the surfaces and proliferated on those surfaces, in

agreement with MTT results given in previous part. After 24 hour of incubation, the cells demonstrated stretched-out morphology. Pseudopodia of cells were clearly distinguished in Figures 3.25(a), 3.26(a), 3.28(a) at day 1. Even after 1 day of incubations, cells were almost fully stretched-out throughout the surfaces of HAs. Beside individual cells, loan of cells were also observed on the surfaces at day1, as seen in Figures 3.23(a)-3.34(a). At day 5, cells on discs were fully spread out and they could hardly be recognized and distinguished from the beneath surface due to their high integration and sprawling like a carpet. Lawn of cells, being one after the other, was predominantly observed rather than individual cells. Lawn of cells was so intensive that the surfaces of the materials were slightly after 5 day of incubations. Additionally, some images showed that more than one ply of cells occurred on some surfaces, as seen in Figure 3.27(b), 3.28(b), 3.30(b), 3.31(b). Also clumps of cells were observed in Figures 3.27(a) and (b), 3.28(a) and (b), 3.30(a), 3.31(a) and (b), 3.32(b) and 3.33(b). In parallel with MTT assay, better images were taken especially for 2.5YFHA sintered at 1100^{o}C and 1300^{o}C; the plies and loan of cells were well observed and even after day 1. This suggested that the surface of 2.5YFHA had better surface properties and better physiological compatibility than the rest of HAs tested in this study.

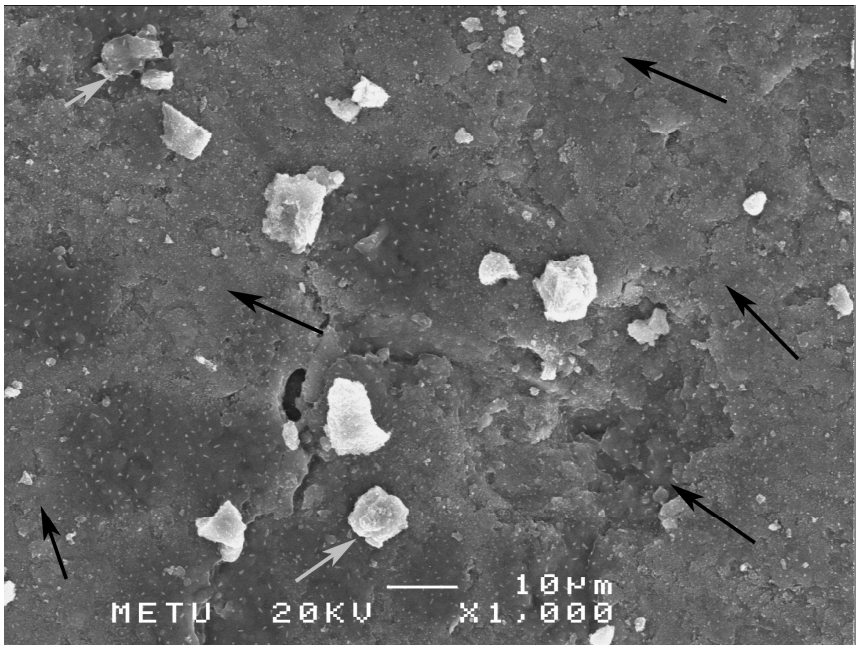

a) HA sintered at 900°C (day 1)

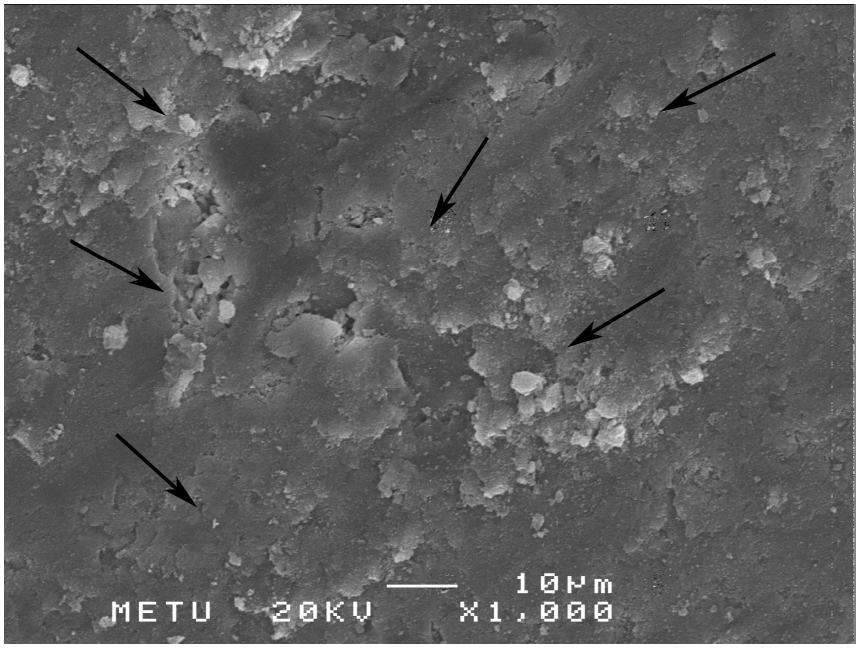

b) HA sintered at 900°C (day 5)

Figure 3.23. SEM images of HA sintered at 900°C after 1 and 5 days (black and white arrows show the lawn of cells and individual cells, respectively).

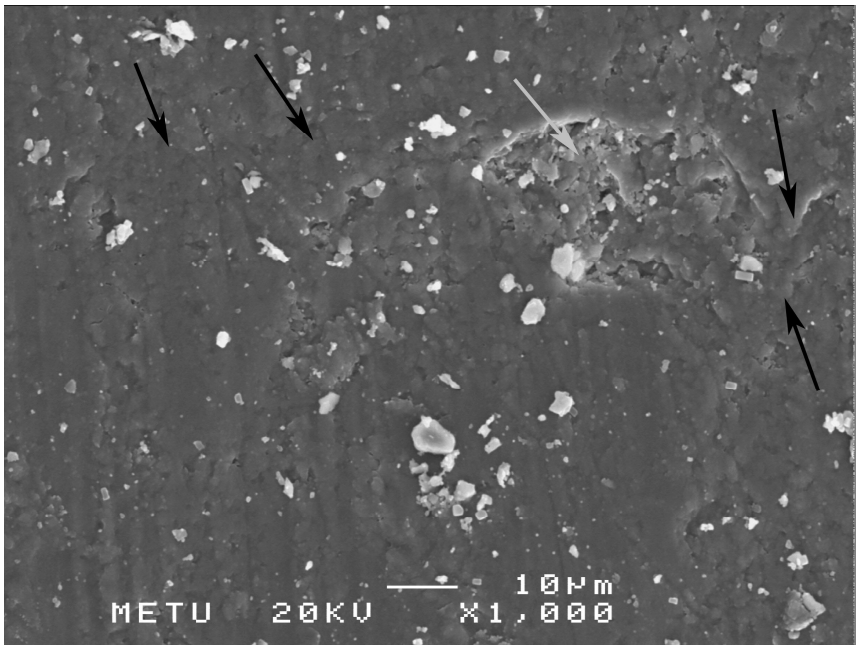

a) HA sintered at 1100°C (day 1)

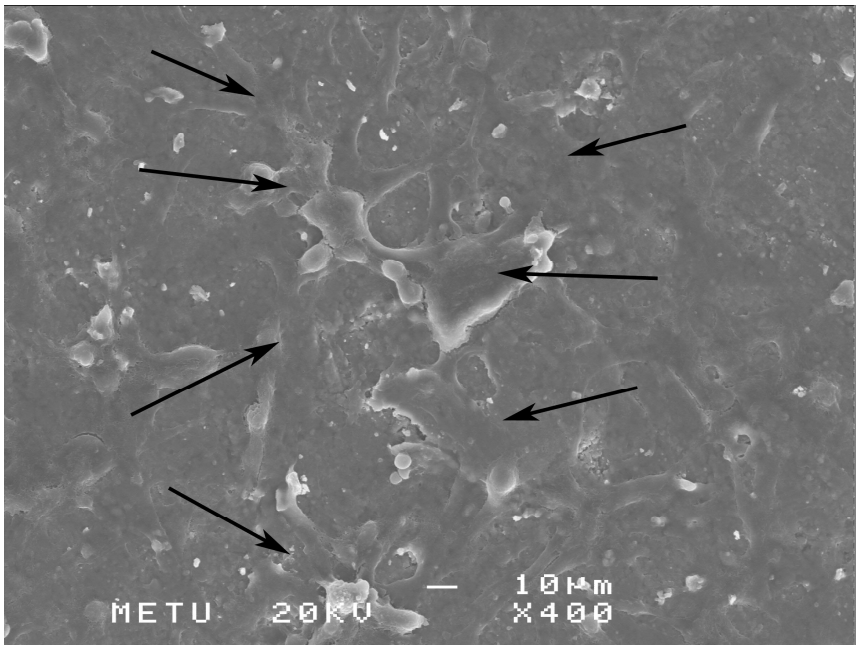

b) HA sintered at 1100°C (day 5)

Figure 3.24. SEM images of HA sintered at 1100°C after 1 and 5 days (black and white arrows show the lawn of cells and the surface of the material, respectively).

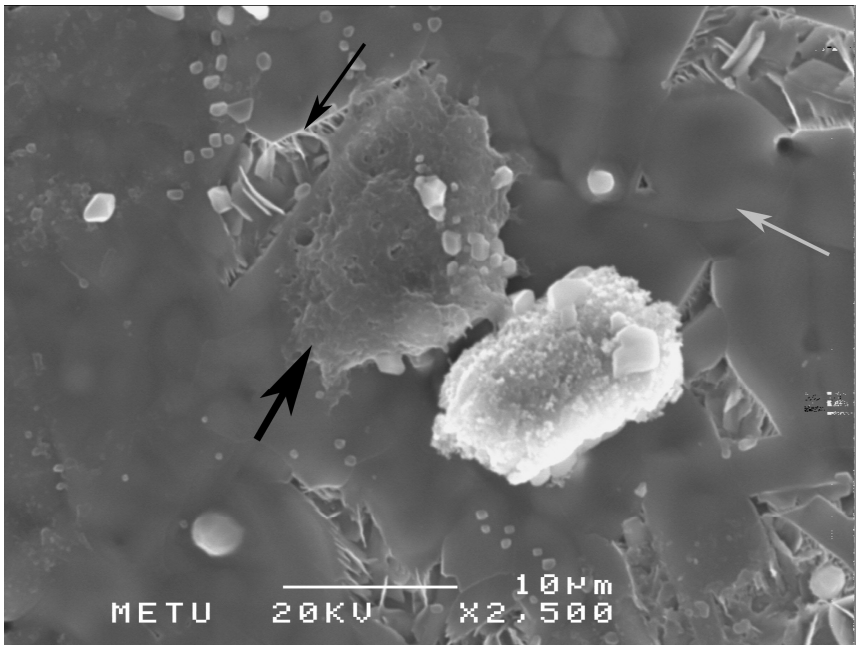

a) HA sintered at 1300°C (day 1)

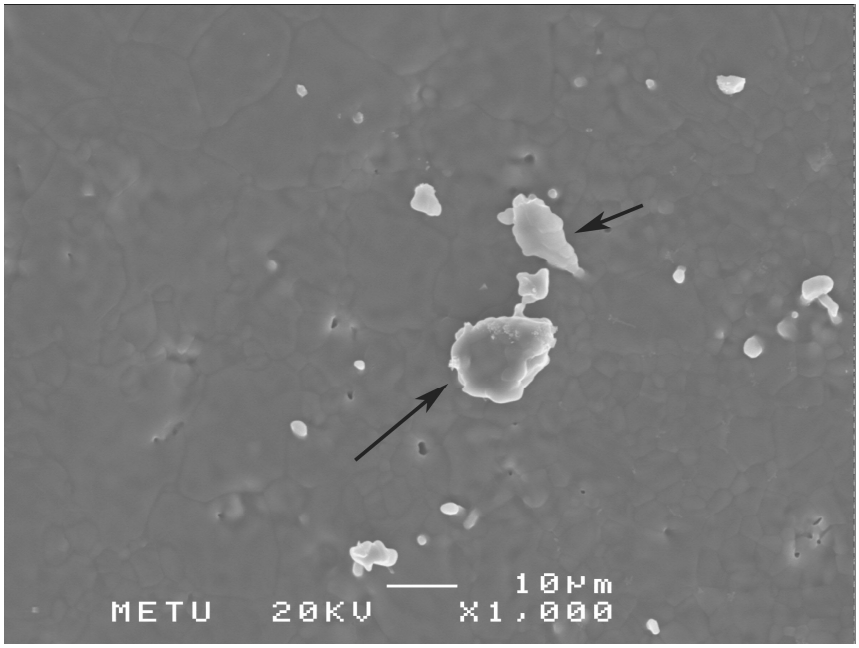

b) HA sintered at 1300°C (day 5)

Figure 3.25. SEM images of HA sintered at 1300°C after 1 and 5 days (black and white arrows show the individual cells and grains of the material, respectively; small black arrow in (a) shows the pseudopodia of the cell attached to the surface).

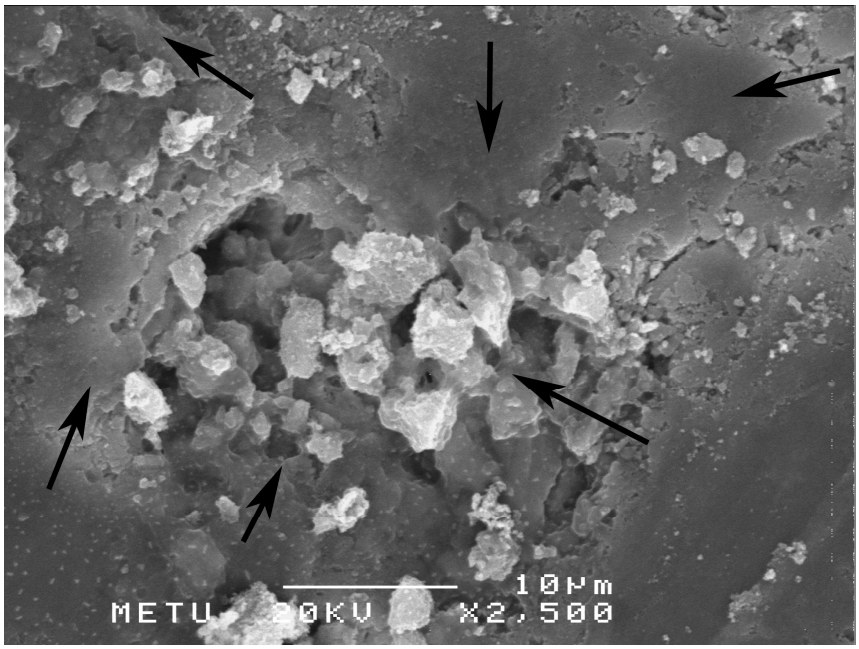

a) 2.5YFHA sintered at 900°C (day 1)

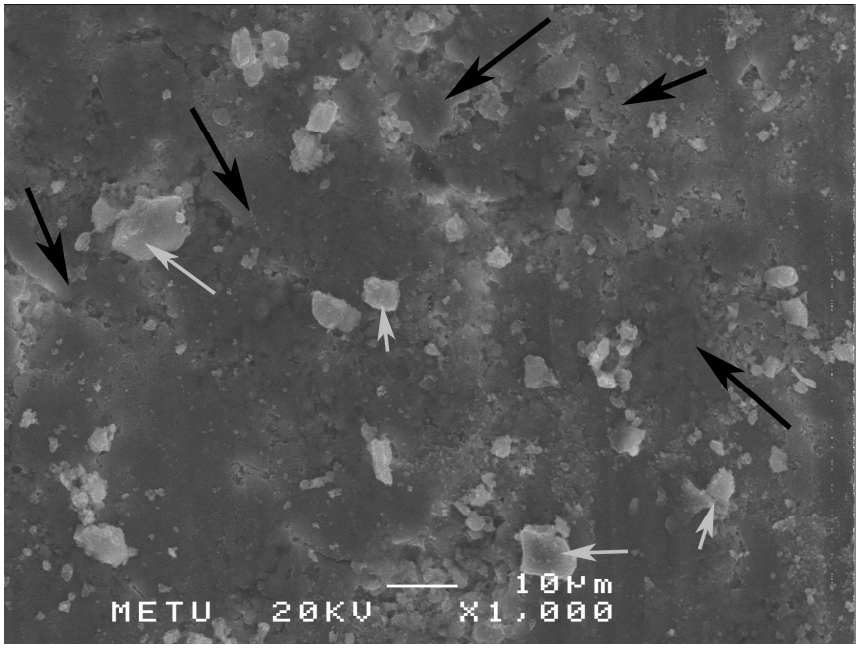

b) 2.5YFHA sintered at 900°C (day 5)

Figure 3.26. SEM images of 2.5YFHA sintered at 900°C after 1 and 5 days (black and white arrows show the lawn of cells and individual cells, respectively).

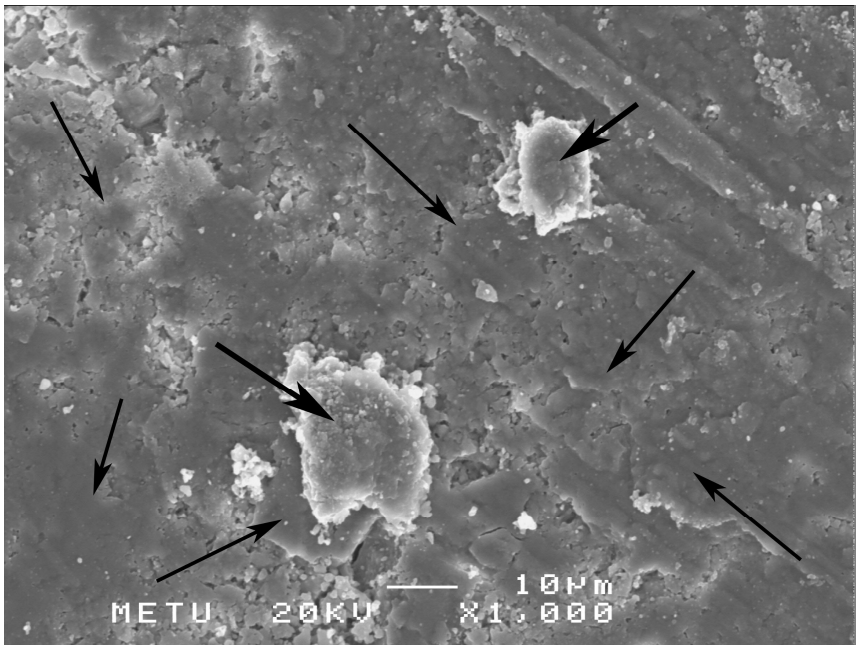

a) 2.5YFHA sintered at 1100°C (day 1)

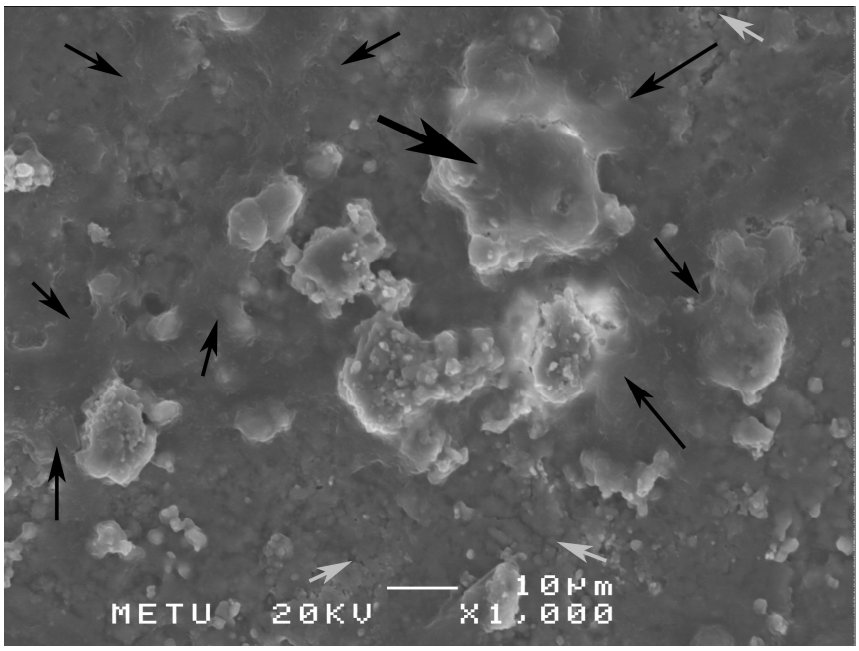

b) 2.5YFHA sintered at 1100°C (day 5)

Figure 3.27. SEM images of 2.5YFHA sintered at 1100°C after 1 and 5 days (black and white arrows show the lawn of cells and grains of the materials, respectively).

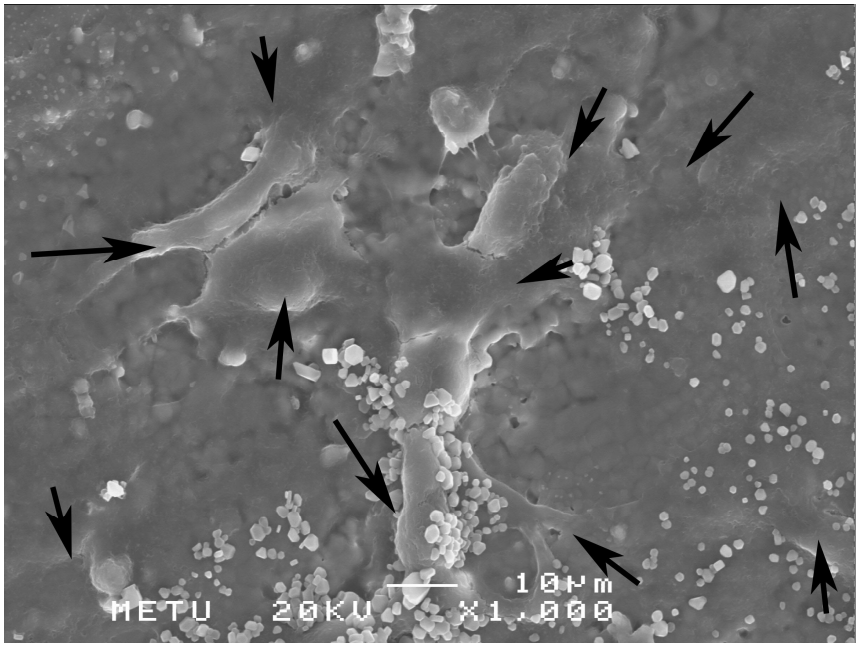

a) 2.5YFHA sintered at 1300°C (day 1)

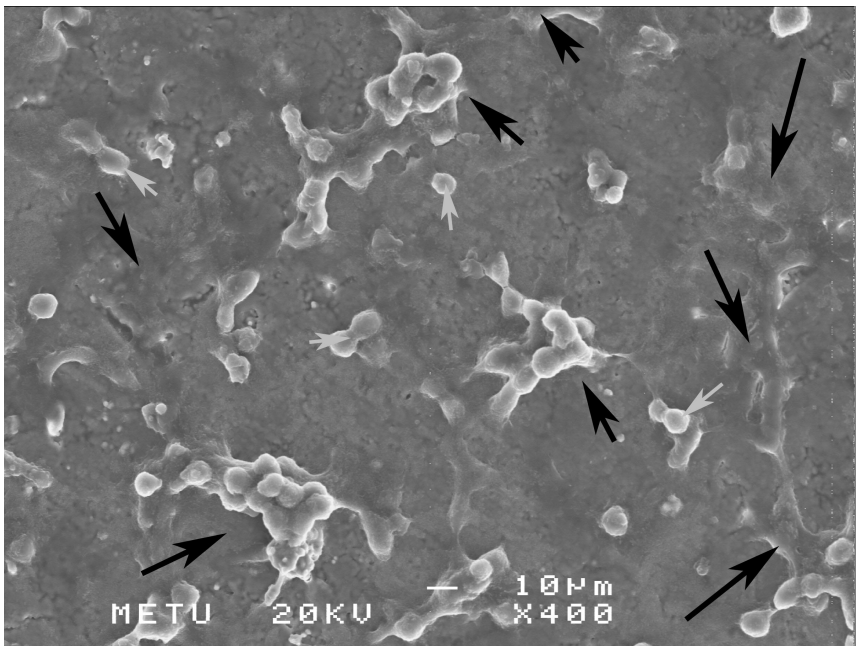

b) 2.5YFHA sintered at 1300°C (day 5)

Figure 3.28. SEM images of 2.5YFHA sintered at 1300°C after 1 and 5 days (black and white arrows show the lawn of cells and individual cells, respectively).

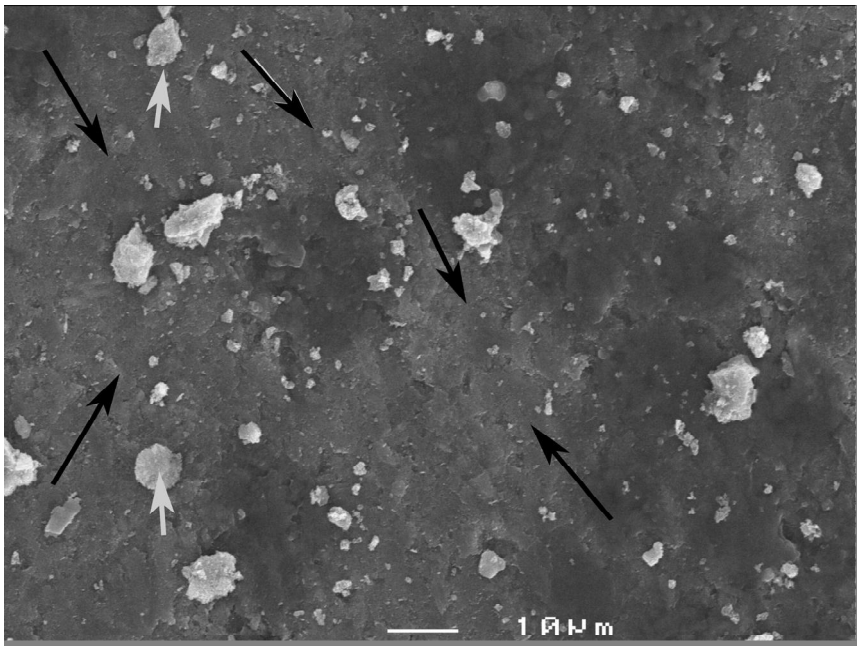

a) 5YFHA sintered at 900°C (day 1)

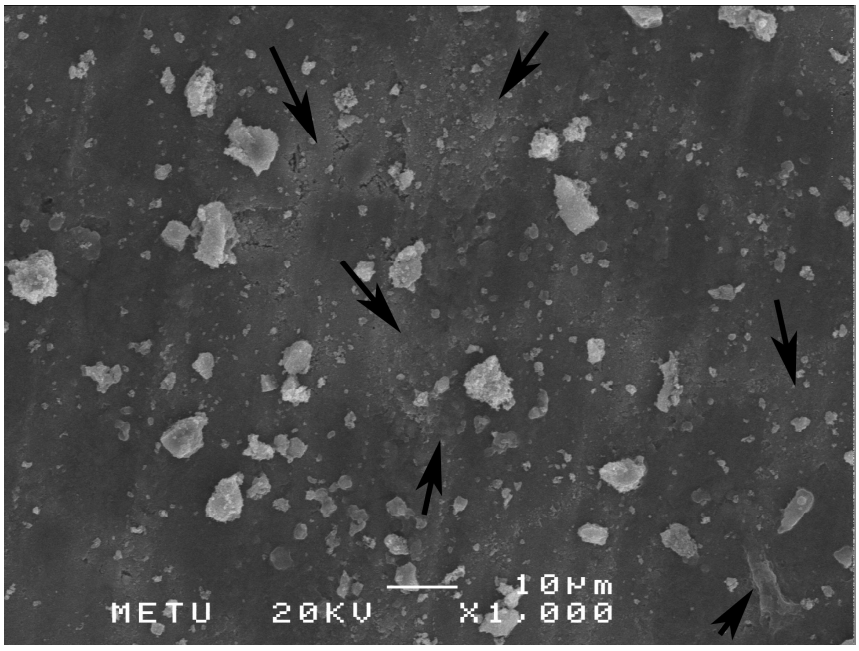

b) 5YFHA sintered at 900°C (day 5)

Figure 3.29. SEM images of 5YFHA sintered at 900°C after 1 and 5 days (arrows show the lawn of cells).

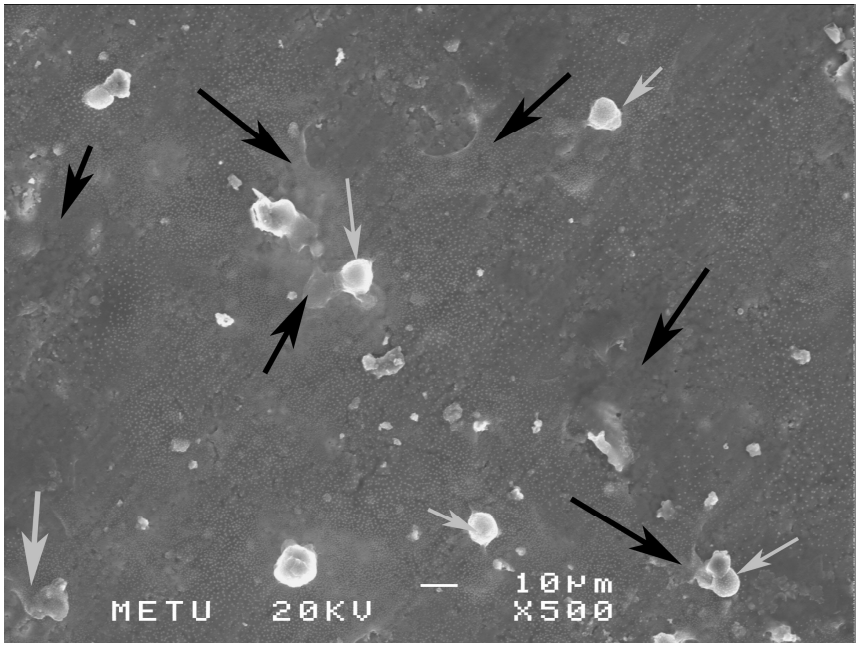

a) 5YFHA sintered at 1100°C (day 1)

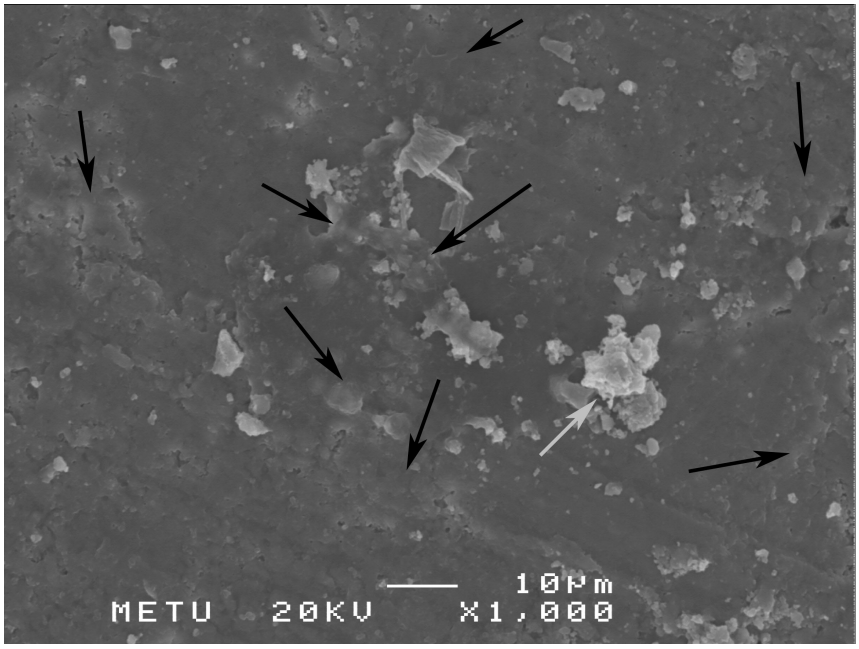

b) 5YFHA sintered at 1100°C (day 5)

Figure 3.30. SEM images of 5YFHA sintered at 1100°C after 1 and 5 days (black and white arrows show the loan of cells and individual cells, respectively).

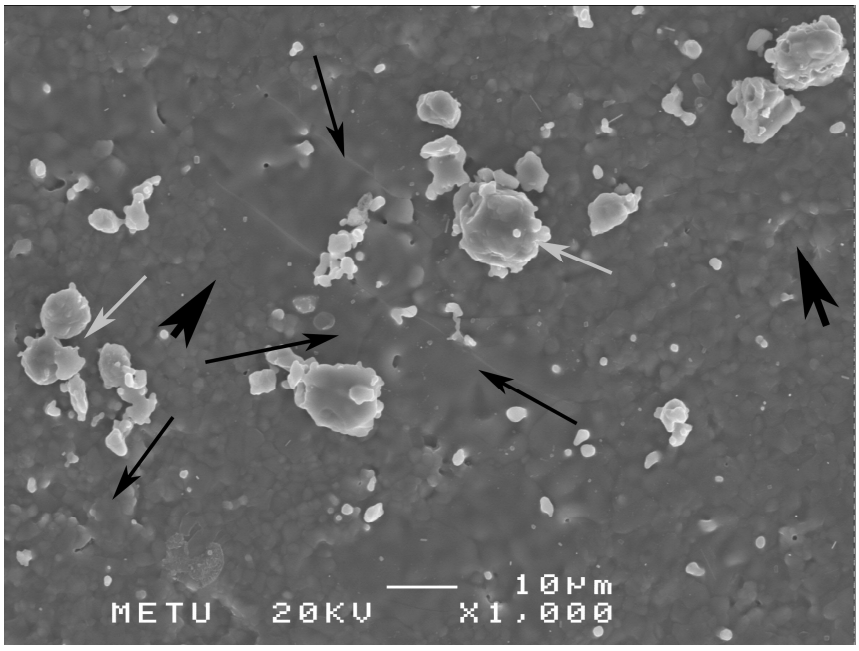

a) 5YFHA sintered at 1300°C (day 1)

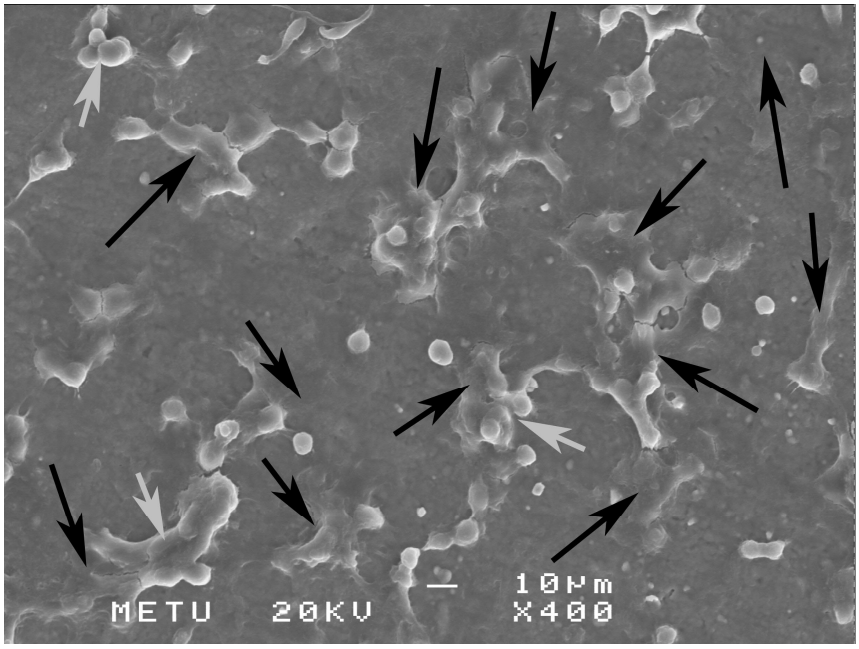

b) 5YFHA sintered at 1300°C (day 5)

Figure 3.31. SEM images of 5YFHA sintered at 1300°C after 1 and 5 days (black and white arrows show the lawn of cells and individual cells, respectively).

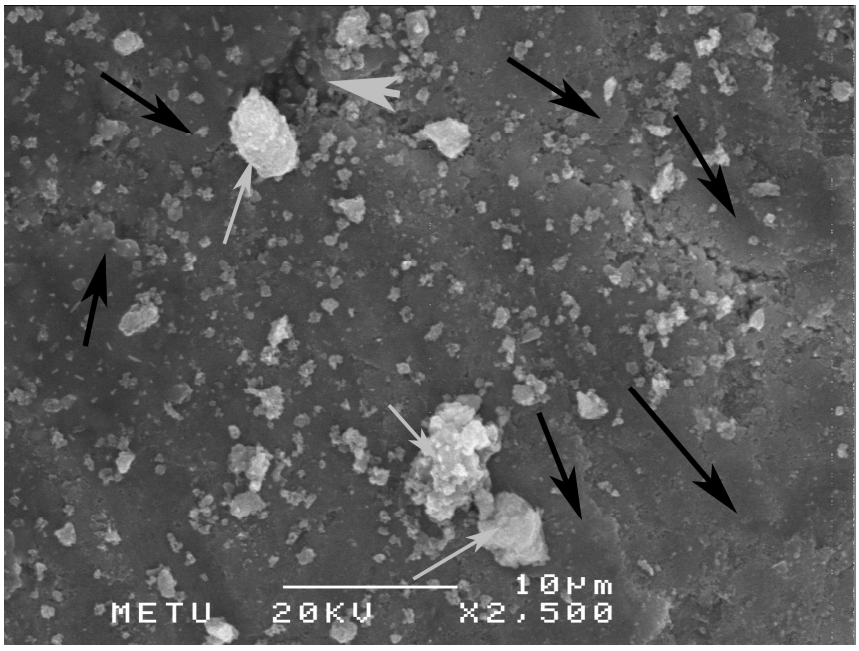

a) 7.5YFHA sintered at 900°C (day 1)

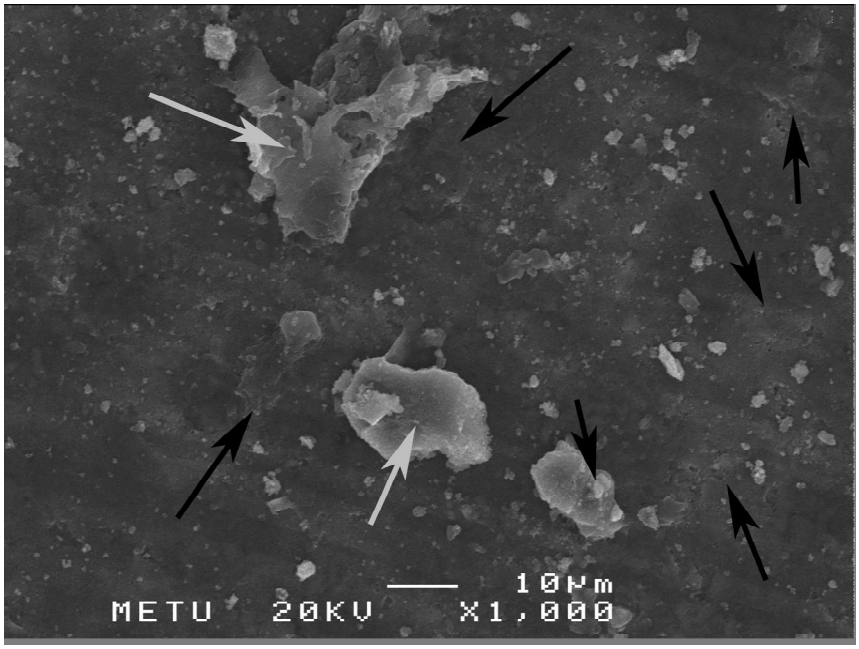

b) 7.5YFHA sintered at 900°C (day 5)

Figure 3.32. SEM images of 7.5YFHA sintered at 900°C after 1 and 5 days (narrower black and white arrows show the loan of cells and individual cells, respectively, wider white arrow show the surface of the material).

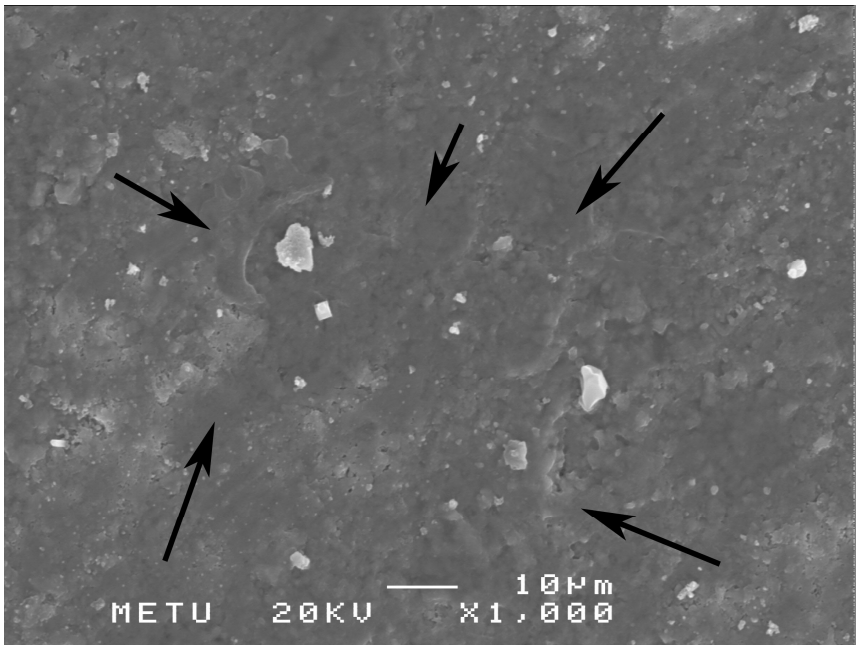

a) 7.5YFHA sintered at 1100°C (day 1)

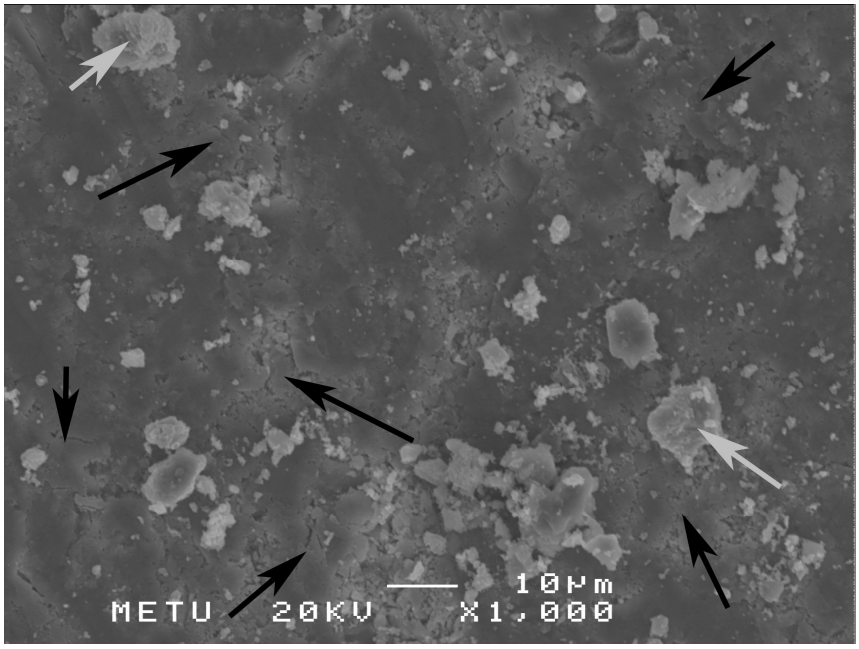

b) 7.5YFHA sintered at 1100°C (day 5)

Figure 3.33. SEM images of 7.5YFHA sintered at 1100°C after 1 and 5 days (black and white arrows show the lawn of cells and individual cells, respectively).

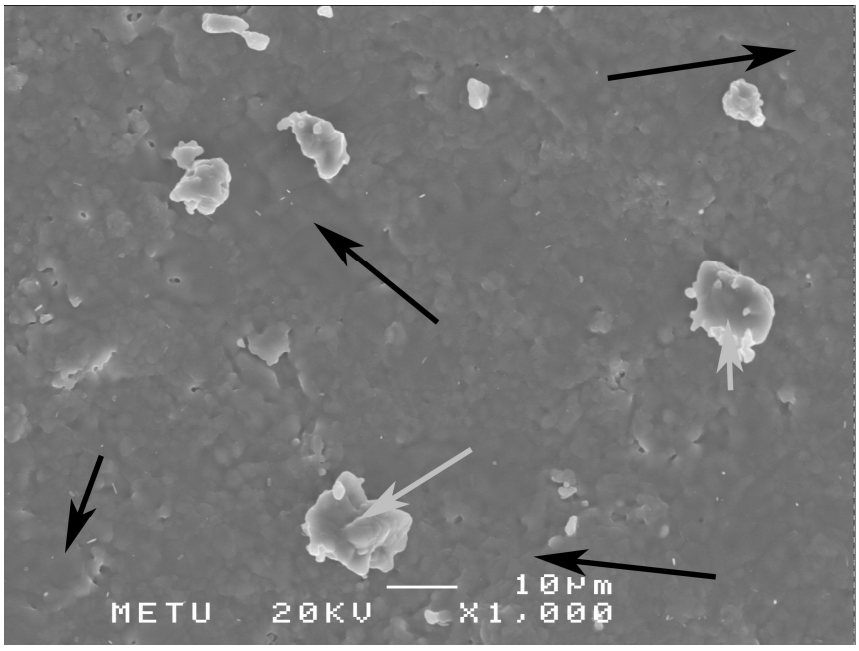

a) 7.5YFHA sintered at 1300°C (day 1)

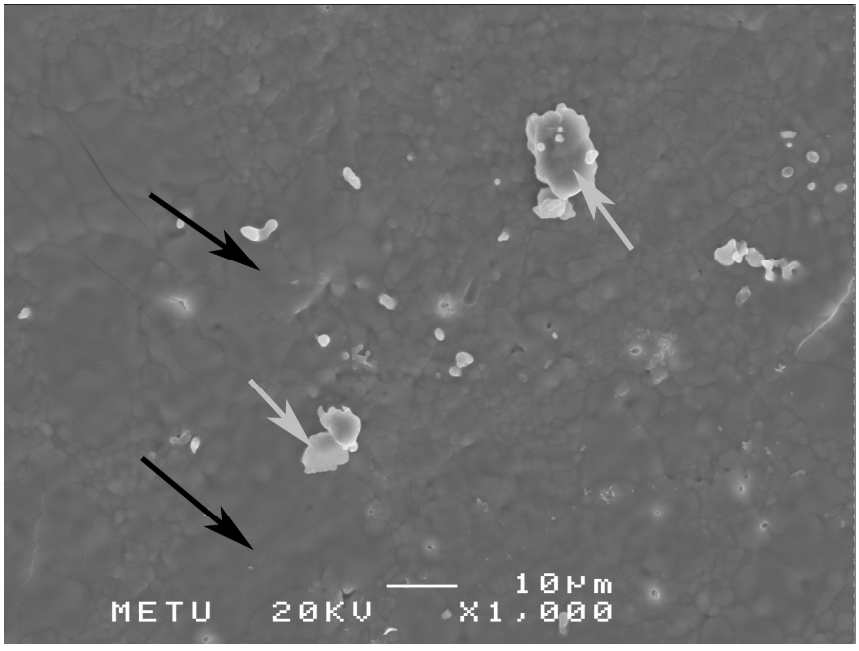

b) 7.5YFHA sintered at 1300°C (day 5)

Figure 3.34. SEM images of 7.5YFHA sintered at 1300°C after 1 and 5 days (black and white arrows show the lawn of cells and individual cells, respectively).

3.3.3 ALP Activity

Saos-2 cells were seeded on pure and yttrium and fluoride ions doped HAs discs and were cultured in osteogenic medium for up to 14 days. ALP activity, an indication of osteoblastic differentiation from non-calcium-mineral-depositing to calcium-mineral-depositing cells [131], was determined at days 7 and 14. Figures 3.35-3.37 represent the ALP activities of cells on pure and doped HAs sintered at 900°C, 1100°C and 1300°C at two incubation times.

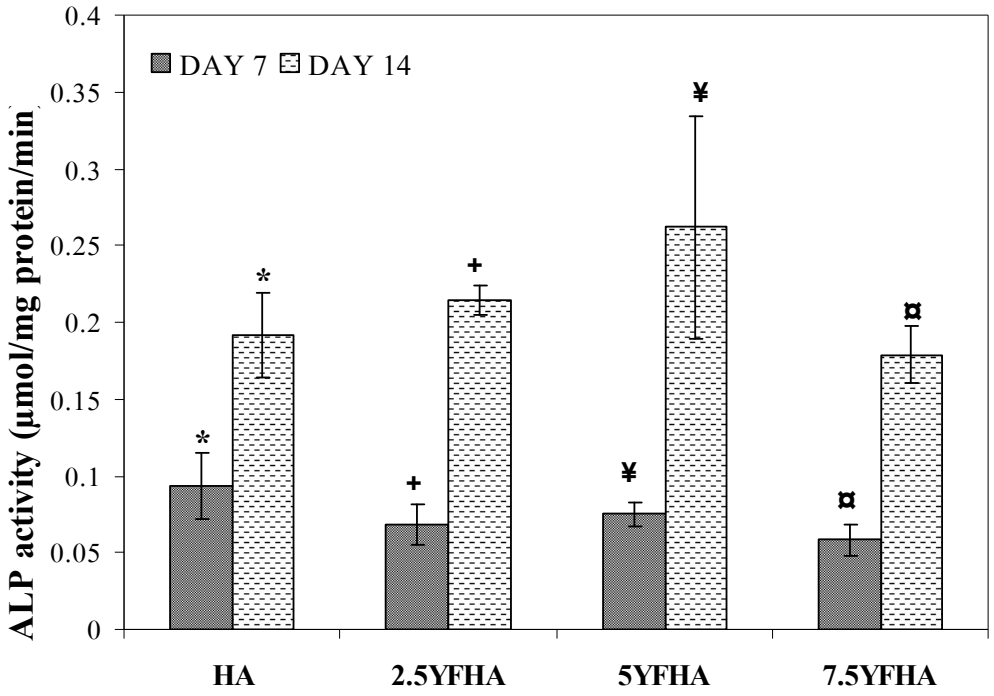

Figure 3.35. ALP activity of HAs sintered at 900°C incubated for 7 and 14 days (Significant differences between groups *, +, ¥, ¤: $p<0.05$).

As seen in Figure 3.35, ALP activity of Saos-2 cells on HAs sintered at 900°C increased with culturing time for all HAs which could be interpreted that yttrium and fluoride additions into HA sintered at 900°C have stimulated the differentiation of cells. ALP production was numerically higher than of pure HA.

However, there was no significant difference in the amount of ALP production according to the amount of dopant incorporated into HA. The cells on all HAs of incubations had similar ALP activities after 7 and 14 day. On the other hand, osteogenic differentiation was achieved and increased with culturing time.

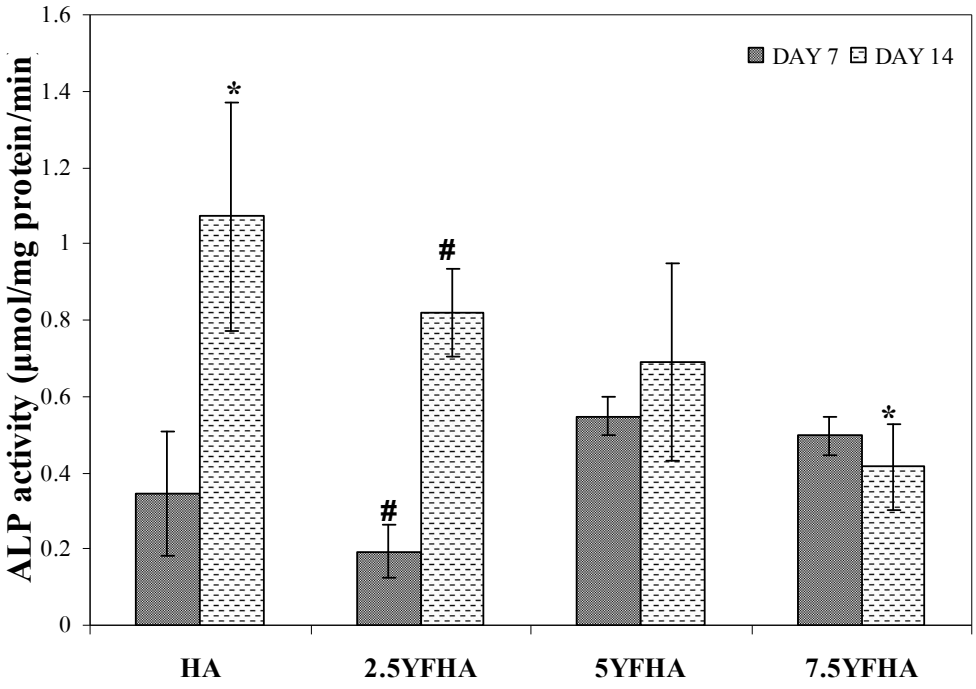

Figure 3.36. ALP activity of HAs sintered at 1100°C incubated for 7 and 14 days (Significant differences between groups #, *: $p<0.05$.

Figure 3.36 represents the ALP activity of Saos-2 cells on pure and doped HA sintered at 1100°C after incubations of 7 and 14 days. As seen in Figure 3.36, ALP activities for all HAs increased with time. At day 7, ALP activity on pure HA was lower than that measured on 5YFHA and 7.5YFHA. However, no statistical difference was determined between ALP activities of HAs. At day 14, ALP activities of cells on pure and doped HAs highly increased in comparison to measurements on day 7. The only significant increase for ALP with culture time was observed for 2.5YFHA. ALP activities measured on yttrium and

fluoride doped HAs doped with various amount were not statistically different from each other. Doped HAs except 7.5YFHA was comparable with pure HA at day 14. ALP activity of cells on 7.5YFHA was significantly lower than pure HA at day 14. This indicated that the increasing amount of yttrium in HA led to decrease in osteogenic differentiation of Saos-2 cells on doped HA.

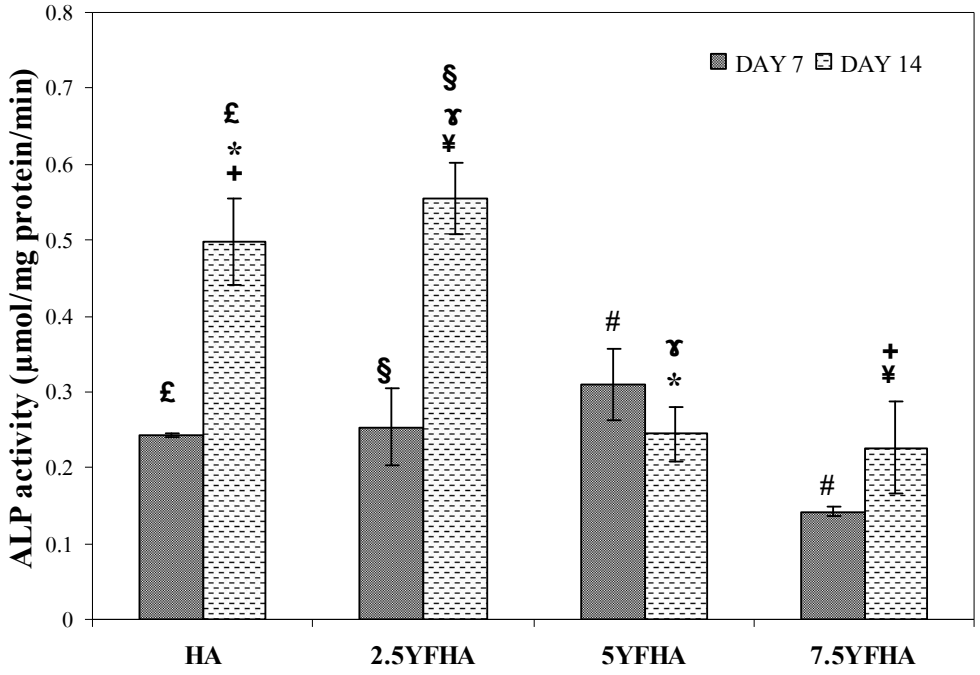

Figure 3.37. ALP activity of HAs sintered at 1300°C incubated for 7 and 14 days (Significant differences between groups £, §, +, *, ¥, ɤ, #: $p<0.05$).

Figure 3.37 shows the ALP activities of cells at day 7 and 14 on pure and doped HAs sintered at 1300°C. For day 7, ALP activities were similar for all HAs. Only 5YFHA showed a significant difference from 7.5YFHA at day 7. Time dependent increase in the ALP production was observed for pure HA and 2.5HYFA. ALP activities of pure HA and 2.5YFHA at day 14 were statistically higher than those measured at day 7. At day 14, 2.5YFHA and pure HA had similar ALP

activity. Additionally, ALP production for these groups was significantly higher than the production measured for 5YFHA and 7.5YHA after 14 days of culturing.

It was also found that ALP activities measured for HAs sintered at 1100^{o}C and 1300^{o}C were higher than of HAs sintered at 900^{o}C. Especially, pure and doped HAs sintered at 1100^{o}C, except 5YFHA revealed a significant difference in ALP activity at day 14 from HAs sintered at two other temperatures. Furthermore, ALP activities of cells on 2.5YFHA sintered at 1100^{o}C was found to be the highest among all dopant and sintering temperature groups. Cell adhesion is a prerequisite for cells to proliferate. When cell density increases to a given density, growth slows down and starts to proliferate. These cellular processes are all dependent processes. Discs with higher degree of cell adhesion showed a higher ALP activity in agreement with MTT assay results. Higher ALP production on HAs sintered at 1300^{o}C in comparison to measured at 900 ^{o}C and 1100 ^{o}C sintering temperatures was in correlation with the higher degree of proliferation.

There are many researches on the incorporation of fluoride or yttrium into HA [51, 74, 76, 132-136]. Incorporation of yttrium and fluoride ions together into HA has not been studied before in the literature. It was shown that the fluoride ions directly stimulated the osteoblast cell response in terms of proliferation and differentiation in a dose dependent manner [61, 132-135, 137]. Similarly, Qu and Wei [136] reported that lower concentrations of fluoride ions (0.231-0.313 mol F^- /mol apatite) did not result in any significant increase at day 7, but a slight increase (for 0.313 mol F^-/mol apatite) at day 14, compared to higher concentrations of fluoride (0.422-0.567 mol F^-/mol apatite). In the present study, the amount of fluoride addition was about 0.26 mol F^-/mol apatite for all doped HAs. The amount of yttrium incorporated into HA was only altered among HA doped groups. It can be suggested that the predominant effect on ALP activity could be the changes in the amounts of yttrium ions, rather than fluoride addition.

In literature, different statements were announced about ALP activities of yttrium doped HA [51, 74]. Webster *et al.* [51] stated that ALP activities of yttrium doped and pure HAs did not exhibit significant differences; furthermore decreased ALP activities were observed for 21 day incubations. The group seeded with osteoblasts on Y-doped nano HA coatings of Ti substrate were observed that the cells had greater ALP activity than those on undoped nano HA coatings [74]. As shown in Figures 3.35-3.37, ALP activities of cells on HAs were changing according to the amount of yttrium doping. In parallel with literature, lower amounts of yttrium led to increase in ALP activities; however increasing amounts of yttrium did not show any contributing effect on ALP activity. Generally, ALP activities of cells on doped HA at all sintering temperatures decreased with increasing concentrations of yttrium.

3.3.4 Calcium Deposition

Calcium deposition by osteoblast cells (or mineralization) is very crucial for quick regeneration of new bone at the defect and/or implant site. It is one of the osteoblastic differentiation markers for in vitro cell culture studies. Therefore, extracellular calcium on pure and doped HA discs was determined to investigate the effects of doping amounts and sintering temperatures on the calcium deposition of the cells. Figures 3.38-40 represent the calcium deposited by cells seeded on pure and doped HA discs sintered at 3 different temperatures after 7 and 14 day of incubations.

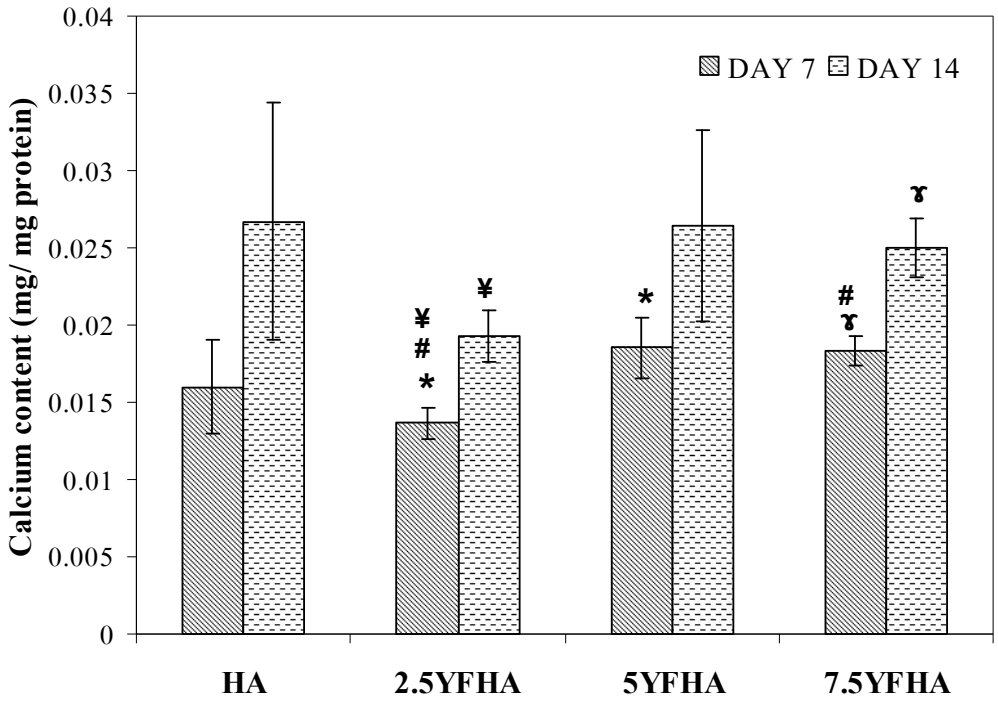

Figure 3.38. Calcium content of HAs sintered at 900°C after 7 and 14 day of incubations (Significant differences between groups *, #, ¥, ϒ: $p<0.05$).

Figure 3.38 represents calcium deposited by cells on pure and doped HAs discs sintered at 900°C after 7 and 14 day of culturing. For all HAs time dependent increase was observed for calcium deposited by cells. However, significant increase in calcium content was only observed for 2.5YFHA and 7.5YFHA. Pure HA and 5YFHA did not show any statistical increase in Ca amounts deposited with time. As seen in Figure 3.38, Ca contents for all HAs were similar at day 7. At day 14, pure HA, 5YFHA and 7.5YFHA had similar amounts of Ca deposited by cells. However, calcium deposition on 2.5YFHA was significantly lower than those on other doped HAs. As the amount of yttrium added to HA was increased higher depositions of calcium were observed.

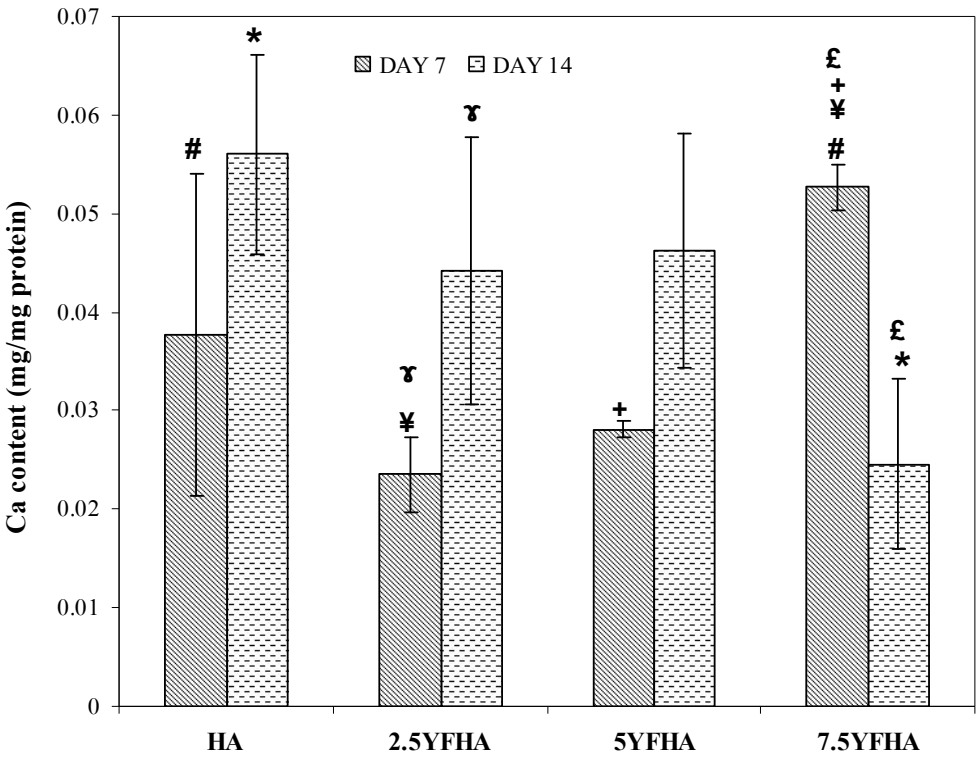

Figure 3.39. Calcium content of HAs sintered at 1100°C at 7 and 14 day of incubations (Significant differences between groups *, #, ¥, +, £: $p<0.05$).

Figure 3.39 represents the content of extracellular calcium on pure and doped HAs discs sintered at 1100°C after 7 and 14 day of culturing. In general, at day 7, amount of extracellular calcium deposited on HAs discs were statistically similar, except 7.5YFHA which had higher amount of calcium than other doped HAs. After 14 days, calcium deposition increased for all groups except 7.5HYFA. The decrease observed could be due to incomplete removal of extracellular calcium with freeze-thaw cycles for this group. The amount of calcium deposited of pure and doped HA sintered at 1100°C was about two-fold higher than the discs with same composition sintered at 900°C (Figure 3.38) in agreement with higher proliferation (Figures 3.20 and 3.21) and ALP activities (Figures 3.35 and 3.36). These findings support that sintering temperature change the surface properties of pure and doped HA and affect the cell response to the biomaterial.

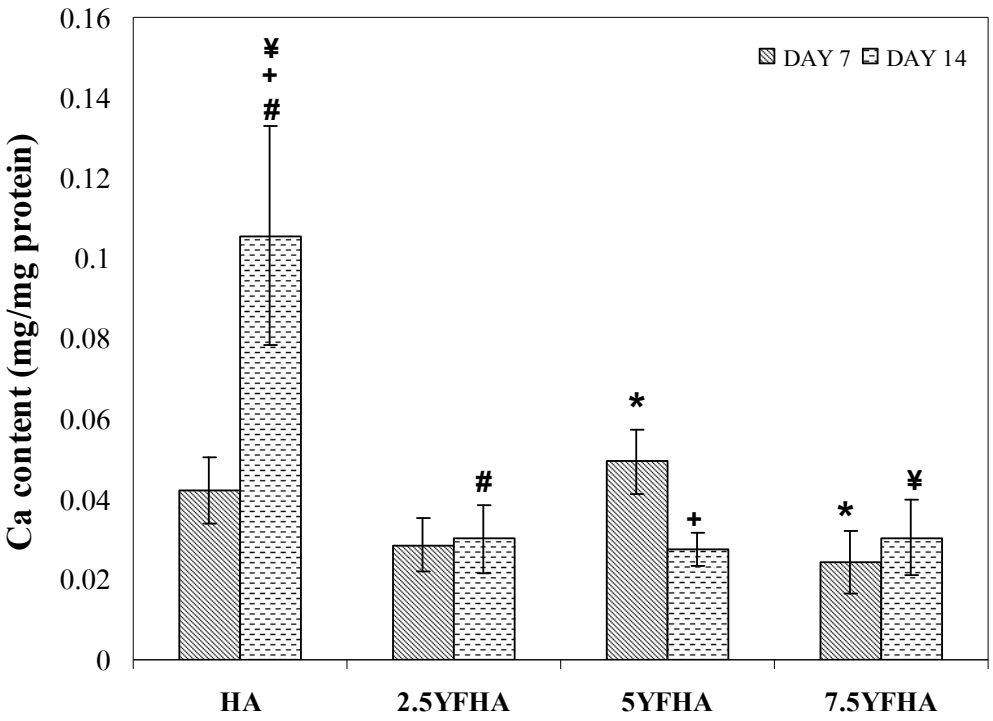

Figure 3.40. Calcium content of pure and doped HAs sintered at 1300°C at 7 and 14 day of incubations (Significant differences between groups *, #, ¥, +: $p<0.05$).

Figure 3.40 represents the content of calcium deposited by cells on HAs discs sintered at 1300°C after 7 and 14 day of culturing. At day 7, pure HA, 2.5YFHA and 7.5YFHA had the similar amount of calcium deposition. However, calcium content on 5YFHA was significantly higher than that on 7.5YFHA at day 7 day. No significant increase in the calcium amounts was observed with time for doped HAs. A similar decrease in the calcium amount at day 14 was observed for 5HYFA. Additionally, the calcium deposition on pure HA was significantly higher than that on doped HAs at day 14, indicating that dopings into HA could lead to decrease in calcium deposition, as seen in Figure 3.40. The calcium depositions of doped HAs sintered at 1300°C were similar to the ones sintered at 1100°C.

Generally, calcium deposited by cells on pure and doped HAs was not statistically significant at 7 day and 14 day of incubations for each sintering

temperatures. The least calcium content of about 0.015-0.003 (mg Ca/mg protein) at day 14 was measured on HA discs sintered at 900^{o}C. HAs discs sintered 1100^{o}C and 1300^{o}C after 14 day of incubation had calcium contents of about 0.02-0.04 and 0.04-0.06 (mg Ca/mg protein), respectively. The highest calcium content was achieved by cells on HAs discs sintered at 1100^{o}C. At this sintering temperature, 2.5YFHA had the lowest calcium content compared to other doped HAs at day 7. However, with culturing time, calcium content on 2.5YFHA increased abruptly and at day 14 all doped HAs at 1100^{o}C had similar calcium content. Also, there was no significant difference compared to pure HA. Similarly, Webster *et al.* [51] reported that yttrium doped HA did not stimulate the calcium deposition of osteoblastic cells after cell 7 and 21 days. However, they also stated that ALP activity was not enhanced by yttrium doping into HA compared to undoped HA [51]. In the current study, ALP activity of cells on doped HAs could not also be enhanced compared to undoped HA. Therefore it could be noted that the findings in this study were in parallel with literature. Also the results of ALP assay and calcium deposition assay were overlapping in this study. As for ALP activities, the best results for calcium deposition were measured for cells on HA discs sintered at 1100^{o}C.

CHAPTER 4

4. CONCLUSION

Bone is mainly composed of calcium phosphates. HA, one of the well known members of calcium phosphate family has been widely used in orthopedics due to its high biocompatibility. However, the poor mechanical properties of HA limit its application on load bearing areas. In this study, HA was doped with yttrium and fluoride elements with various amounts in order to investigate its microstructural, mechanical and biological properties. The yttrium and fluoride ions incorporations simultaneously into HA has not been investigated before.

The densification of pure and doped HAs was achieved even at low sintering temperatures. High amount of dopings caused to decrease in relative densities of HAs. However, higher sintering temperatures helped increasing the relative densities with the expense of grain growth. The degree of porosity for all HAs was under 12 % of theoretical density of HA. Almost no second phase formations were encountered in the XRD patterns of doped HAs sintered for all sintering temperatures. However, very trace amounts of β-TCP were observed in the XRD patterns of 5YFHA sintered at 1300^{o}C and 7.5YFHA sintered at 1100^{o}C and 1300^{o}C. Higher sintering temperatures and higher amounts of yttrium could result in formation of second phases, indicating that certain limitations in doping and temperature could be needed to adjust the microstructure of doped HAs. Microstructural investigations showed that the addition of elements into pure HA led to decrease in lattice parameters and unit cell volumes of doped HAs due to

substitutions of yttrium and fluoride ions. Such doping did not cause any severe decomposition of HA even at very high sintering temperatures. FTIR analysis also confirmed the substitutions of yttrium and fluoride ions into HA. SEM images revealed that pure and doped HAs were synthesized in nano size. Addition of dopings caused the grain sizes to decrease. 7.5YFHA sintered at 900^{o}C revealed the smallest grain size with 51.4 nm. The grain size of pure HA sintered at 1300^{o}C was measured as 3.5 μm, which was the highest grain size value determined in this study. As the sintering temperatures increased, the grain size of pure and doped HAs changed from nano to micron. However, even at high temperatures grain sizes of doped HAs were still lower than that of pure HA. Further addition of yttrium led to further decrease in grain sizes.

Compared to pure HA, diametral strength of doped HAs mostly enhanced with the addition of yttrium and fluoride ions due to decrease in porosity. 2.5YFHA sintered at 1300^{o}C had the highest diametral strength of 11.6 MPa with the relative density of 94.3 % of theoretical density. However, HAs with very high amount of yttrium at very high sintering temperature (1300^{o}C) showed lower diametral strengths than HAs doped with lower additions of yttrium at all sintering temperatures, probably due to the formation of β-TCP even at trace amounts. It was indicated that the main factors for determination of diametral strength was the degree of porosity and the presence of second phases. The microhardness values of doped HAs showed variations with temperatures and the amount of dopings. Microhardness values of doped HAs sintered at 900^{o}C and 1100^{o}C were generally lower than that of pure HA. For 5YFHA and 7.5YFHA sintered at 1300^{o}C, microhardness values were higher compared to pure HA. The microhardness of 7.5YFHA sintered at 1300^{o}C was the highest with the value of 5.9 GPa. Fracture toughness values of HAs were mainly influenced by the degree of porosity. Doped HAs did not show better fracture toughness compared to pure HA, except 2.5YFHA

(2.1 MPa·$m^{1/2}$) sintered at 1100^{o}C. Even tough of 5YFHA and 7.5YFHA sintered at 1300^{o}C were almost fully densified, severe grain growths might lead to decrease in fracture toughness.

Biocompatibility studies were conducted with cytotoxicity studies using Saos-2 cells. The effects of dopants incorporated into HA and sintering temperatures on cell behaviors in terms of attachment, proliferation and differentiation were investigated using MTT cell viability assay, SEM, ALP activity and calcium deposition assays. Attachment efficiency of cells on all HA, except pure HA sintered a 1300^{o}C after 24 hr incubation was above 70 %, indicating that surface properties of HAs was suitable for the attachment of Saos-2 cells. In agreement with the literature, the attachment efficiency increased with the addition of yttrium and fluoride ions. The highest cell attachment efficiency was measured for cells on 2.5YFHA sintered at 1100^{o}C. This level of yttrium incorporation along with 2.5 mol % fluoride exhibited positive effect on cellular attachment. In contrast to previous findings, this study revealed that cell adhesion on doped HAs with larger grain sizes was still high owing to the effect of yttrium and fluoride co-addition. The effect of dopings and sintering on proliferation behavior of cells on HAs was examined using MTT viability assay. These results showed that there was a significant relation between cell proliferation and sintering temperatures and amount of dopings. The best combination of yttrium and fluoride for the positive effect on proliferation was found to be 2.5YFHA. The cells on all doped HAs at all sintering temperatures proliferated, but 2.5YFHA showed the best results among all doped HAs for all sintering temperatures. Secondly, sintering temperatures also affected the proliferation on HAs doped with yttrium and fluoride ions. Cell attached on HAs sintered at 1100^{o}C and 1300^{o}C showed faster proliferation than cells on HAs sintered at 900^{o}C. These results also revealed that high amount of yttrium (7.5 mol %) along with 2.5 mol % fluoride could decrease the proliferation of cells.

Therefore, an optimization for amounts of doping and sintering temperatures is required to obtain better results for proliferations of cells. Similarly, the effects of co-substitution of yttrium and fluoride ions and sintering temperatures on osteoblastic differentiation of Saos-2 cells up to 14 days were investigated using ALP and calcium deposition assays. ALP activity assay revealed that 2.5YFHA sintered at 1100^{o}C and 1300^{o}C had positive effect on ALP production of cells on HAs. Moreover, ALP activities of cells on 2.5YFHA sintered at 1100^{o}C was found to be the highest among all dopant and sintering temperature groups. However, no significant difference was present between ALP productions of cells on pure and 2.5YFHA at all sintering temperatures for all incubation times. ALP activities of cells on 5YFHA sintered at 1300^{o}C and 7.5YFHA sintered at 1100^{o}C and 1300^{o}C at day 14 were significantly lower compared to ALP activities of cells on pure HA at those temperatures. Also, it was found that increasing sintering temperatures enhanced the ALP activity of cells on HAs. ALP activities measured for HAs sintered at 1100^{o}C and 1300^{o}C were higher than of HAs sintered at 900^{o}C. The calcium deposition amount, the other differentiation marker which was investigated in this study, was measured after 7 and 14 days of culturing. No significant differences were determined between calcium contents of pure and doped HAs after two culturing times. It was demonstrated that calcium deposition on HAs sintered at 1100^{o}C and 1300^{o}C was significantly higher than that on HAs sintered at 900^{o}C. Moreover the highest content of calcium was measured for cells on HAs sintered at 1100^{o}C. The findings in calcium deposition assay were generally in parallel with those in ALP activity assay.

When compared to mechanical properties of human cortical bone, it was seen that mechanical properties of HAs synthesized in this study was not still high enough to use this materials under load-bearing areas. Especially, mechanical strengths of HAs were still lower than that of human cortical bone. However,

greater hardness was achieved with comparable fracture toughness. Nevertheless, their excellent biocompatibility of HAs doped with yttrium and fluoride is convincing enough to state that they are very promising for future biomedical applications.

When pure and doped HA were analyzed in terms of microstructure, mechanical properties and biocompatibility, 2.5YFHA sintered at 1100^{o}C became the most outstanding material among all HAs. Therefore, further investigations should be focused on this material in order to understand the all mechanisms for future biomechanical and orthopedic applications. Additionally, since only one level of fluoride amount was added into HA in this study, investigations about yttrium and fluoride doped HAs should be extended out by using different amounts of fluoride with yttrium.

REFERENCES

[1] Vallet-Regi, M., Gonzalez-Calbet, J.M., 2004, "Calcium phosphates as substitution of bone tissues", Progress in Solid State Chemistry, 32, 1–31.

[2] Wasserman, A.J., Dunn, M.G, 1991, Morphology and mechanics of skin, cartilage and bone, in Application of Biomaterials in Facial Plastic Surgery, edited by A. I. Glasgold and F. H. Silver, CRC Press, Boca Raton, Florida.

[3] Mow, V.C., Hayes, W.C., 1991, Basic Orthopedic Biomechanics, Raven Press, Ltd., New York, Chapter 3, p 93.

[4] Rho, J.Y., Kuhn-Spearing, L., Zioupos, P., 1998, "Mechanical properties and the hierarchical structure of bone", Medical Engineering and Physics, 20, 92–102.

[5] Seer's Training Web Site, http://training.seer.cancer.gov/module_anatomy/unit3_2_bone_tissue.html:, last visited on January 2009.

[6] Bhat, S.V., 2002, Biomaterials, Kluwer Academic Publisher, Norwell, MA.

[7] Marks, Jr S.C., Hermey, D.C., 1996, The Structure and Development of Bone. In: Bilezikian J.P., Raisz L.G., Rodan G.A., editors. Principles of Bone Biology, Academic Press, San Diego, CA.

[8] Park, J.B., 1987, Biomaterials: An Introduction, Plenum Press, New York.

[9] Keaveny, T.M., Hayes, W.C., 1993, "Mechanical properties of cortical and trabecular bone", Bone, 7, 285-344.

[10] Handschin, R.G., Stern, W.B., 1995, "X-Ray diffraction studies on the lattice perfection of human bone apatite", Bone, 16 (4), 355S-363S.

[11] Young, R.A, 1974, "Implications of atomic substitutions and other structural details in apatites", Journal of Dental Research, 53, 193-203.

[12] Kalita, S.J., Bhardwaj, A., Bhatt, H.A., 2007, "Nanocrystalline calcium phosphate ceramics in biomedical engineering", Materials Science and Engineering C, 27, 441–449.

[13] Carter, C.B., Norton, M.G., 2007, Ceramic Materials: Ceramics in Biology and Medicine, New York, Springer, p. 635

[14] Holden, J.L., Clement, J.G., Phakey, P.P., 1995, "Age and temperature related changes to the ultrastructure and composition of human bone mineral", Journal of Bone Mineral Research, 10 (9), 1400-1409.

[15] Turner, C. H., Burr, D. B., 1993, "Basic biomechanical measurements of bone: A tutorial", Bone, 14, 595-608.

[16] Fung, Y.C., 1993, Biomechanics: Mechanical Properties of Living Tissues, Springer-Verlag Inc., New York, p. 500.

[17] Currey, C.D., 1983, Handbook of Composites, edited by A. Kelly and S.T. Mileiko, Elsevier Science Publishers B. V., Vol. 4, p. 501.

[18] Katz, J.L., 1980, "Symposia of the Society for Experimental Biology, Number XXXIV: The Mechanical Properties of Biological Materials", Cambridge University Press, p. 99.

[19] Katz, J.L., 1985, "The biophysical and biomechanical properties of bone, bone-mineral and some synthetic bone biomaterials", Bulletin De La Societe Chimique De France, 4, 514-518.

[20] Hench, L.L., 1991, "Bioceramics: From concept to clinic" Journal of the American Ceramic Society, 74, 1487-1510.

[21] Behiri, J.C. Bonfield, W., 1984, "Fracture mechanics of bone-the effects of density, specimen thickness and crack velocity on longitudinal fracture", Journal of Biomechanics, 17, 25-34.

[22] Praminik, S., Agarwal, K.A., Rai, K.N., Garg, A., 2007, "Development of high strength hydroxyapatite by solid-state-sintering process", Ceramics International, 33, 419-426.

[23] Antonucci, J.M., Fowler, B.O., Venz, S., 1991, "Filler systems based on calcium metaphosphates", Dental Materials,7, 124-129.

[24] Huan, Z., Chang, J., "Novel bioactive composite bone cements based on the β-tricalcium phosphate–monocalcium phosphate monohydrate composite cement system", Acta Biomaterialia, doi: 10.1016/j.actabio.2008.10.006.

[25] Prado Da Silva, M.H., Lima, J.H.C., Soares, G.A., Elias, C.N., De Andrade, M.C., Best, S.M., Gibson, I.R., 2001, "Transformation of monetite to hydroxyapatite in bioactive coatings on titanium", Surface and Coatings Technology, 137, 270-276.

[26] Kumar, M., Dasarathy, H., Riley, C., 1999, "Electrodeposition of brushite coatings and their transformation to hydroxyapatite in aqueous solutions", Journal of Biomedical Materials Research. 45, 302-310.

[27] Lu, X., Leng, Y., Zhang, Q., 2008, "Electrochemical deposition of octacalcium phosphate micro-fiber/chitosan composite coatings on titanium substrates", Surface and Coatings Technology, 202, 3142-3147.

[28] Shelton, R.M., Liu, Y., Cooper, P.R., Gbureck, U., German, M.J., Barralet, J.E., 2006, "Bone marrow cell gene expression and tissue construct assembly using octacalcium phosphate microscaffolds", Biomaterials, 27, 2874-2881.

[29] Legeros, R.Z. Legeros, J.P., 1993, in An Introduction to Bioceramics, edited by Hench, L.L. and Wilson, J., World Scientific, Singapore.

[30] Yu, D., Wong, J., Matsuda, Y., Fox, J.L., Higuchi, W.I., Otsuka, M., 1992, "Self-setting hydroxyapatite cement: A novel skeletal drug-delivery system for antibiotics", Journal of Pharmaceutical Sciences, 81, 529-531.

[31] Guo, H., Su, J., Wei, J., Kong, H., Liu, C., "Biocompatibility and osteogenicity of degradable Ca-deficient hydroxyapatite scaffolds from calcium phosphate cement for bone tissue engineering", Acta Biomaterialia, doi:10.1016/j.actabio.2008.07.018.

[32] Bauer, T.W., Geesink, R.G.T., Zimmerman, R., Mcmohan, J.T., 1991, "Hydroxyapatite-coated femoral stems: histological analysis of components retrieved at autopsy", Journal of Bone Joint Surgery, (American Edition) 73, 1439-1452.

[33] Murugan, R., Ramakrishna, S., 2004, "Bioresorbable composite bone paste using polysaccharide based nano hydroxyapatite", Biomaterials, 25, 3829-3835.

[34] Rauschmann, M.A., Wichelhaus, T.A., Stirnal, V., Dingeldein, E., Zichner, L., Schnettler, R., Alt, V., 2004, "Nanocrystalline hydroxyapatite and calcium sulphate as biodegradable composite carrier material for local delivery of antibiotics in bone infections", Biomaterials, 26, 2677-2684.

[35] Guo, L., Li, H., 2004, "Fabrication and characterization of thin nano-hydroxyapatite coatings on titanium", Surface and Coatings Technology, 185, 268-274.

[36] Legeros, R.Z., 1981, "Apatites in biological systems", Progress in Crystal Growth and Characterization, 4, 1-45.

[37] DeGroot, K., DePutter, C., Smitt, P., Driessen, A., 1981, "Mechanical failure of artificial teeth made of dense calcium hydroxylapatite", Science of Ceramics, 11, 433-437.

[38] Fang, Y., Agrawal, D.K., Roy, D.M., Roy, R., 1995, "Fabrication of transparent hydroxyapatite ceramics by ambient-pressure sintering", Materials Letters, 23, 147-151.

[39] Ioku, K., Yoshimura, M., Somiya, S., 1990, "Microstructure and mechanical properties of hydroxyapatite ceramics with zirconia dispersion prepared by post-sintering", Biomaterials, 11, 57-61.

[40] Li, J., Fartash, B., Hermansson, L., 1998, "Hydroxyapatite-alumina composites and bone-bonding", Biomaterials, 16, 417-422.

[41] Niihara, K., 1985, "Indentation microfracture of ceramics—its application and problems", Journal of the Ceramic Society of Japan, 20, 12-18.

[42] Uematsu, K., Takagi, M., Honda, T., Uchida, N., Saito K., 1989, "Transparent hydroxyapatite prepared by hot isostatic pressing of filter cake", Journal of the American Ceramic Society, 72, 1476-1478.

[43] With, G.D., Dijk, H.J.A.V., Hattu, N., Prijs, K., 1981, "Preparation, microstructure and mechanical properties of dense polycrystalline hydroxyapatite", Journal of Materials Science, 16, 1592-1598.

[44] Chen, Y. Miao, X., 2004, "Effect of fluorine addition on the corrosion resistance of hydroxyapatite ceramics", Ceramics International, 30, 1961-1965.

[45] Ergun, C., Webster, T.J., Bizios, R., Doremus, R. H., 2002, "Hydroxylapatite with substituted magnesium, zinc, cadmium, and yttrium I. Structure and microstructure", Journal of Biomedical Materials Research, 59, 305-311.

[46] Evis, Z., 2006, "Al^{+3} doped nano hydroxyapatites and their sintering characteristics", Journal of the Ceramic Society of Japan, 114, 1001-1004.

[47] Evis, Z., 2007, "Reactions in hydroxylapatite–zirconia composites", Ceramics International, 33, 987-991.

[48] Kalita, S.J., Bhatt, H.A., 2007, "Nanocrystalline hydroxyapatite doped with magnesium and zinc: synthesis and characterization", Materials Science and Engineering C, 27, 837-848.

[49] Kannan, S., Rebelo, A., Ferreira, J.M.F., 2006, "Novel synthesis and structural characterization of fluorine and chlorine co-substituted hydroxyapatites", Journal of Inorganic Biochemistry, 100, 1692-1697.

[50] Kim, H.W., Kong, Y.M., Koh, Y.H., Kim, H.M., Kim, H.M., Ko, J.S., 2003, "Pressureless sintering and mechanical and biological properties of fluor-hydroxyapatite composites with zirconia" Journal of the American Ceramic Society, 86, 2019–2026.

[51] Webster, T.J., Massa-Schlueter, E.A., Smith, J.L., Slamovich, E.B., 2004, "Osteoblast response to hydroxyapatite doped with divalent and trivalent cations", Biomaterials, 25, 2111-2121.

[52] Elliot, J.C., 1994, Structure and Chemistry of the Apatites and Other Calcium Orthophosphates, Elsevier, Amsterdam.

[53] LeGeros, R.Z., 1991, Calcium Phosphates in Oral Biology and Medicine, Karger AG, Basel, Switzerland.

[54] Posner, A.S., Blumental, N.C., Betts, F., 1984, Phosphate Minerals, in: J.O. Nriagu, P.B., Moore (Eds.), Springer, New York, p.330.

[55] Bigi, A., Compostella, L., Fichera, A.M., Foresti, E., Gazzano, M., Ripamonti, A., Roveri, N., 1998, "Structural and chemical characterization of inorganic deposits in calcified human mitral valve", Journal of Inorganic Biochemistry, 34, 75-82.

[56] Bigi, A., Foresti, E., Gregorini, R., Ripamonti, A., Roveri, N., Shah, J.S., 1992, "The role of magnesium on the structure of biological apatites", Calcified Tissue International, 50, 439-444.

[57] Bigi, A., Falini, G., Foresti, E., Gazzano, M., Ripamonti, A., Roveri, N., 1993, "Magnesium influence on hydroxyapatite crystallization", Journal of Inorganic Biochemistry, 49, 69-78.

[58] Mayer, I., Schlam, R., Featherstone, J.B.D., 1997, "Magnesium-containing carbonate apatites", Journal of Inorganic Biochemistry, 66, 1-6.

[59] Kim, S.R., Lee, J.H., Kim, Y.T., Riu, D.H., Jung, S.J., Lee, Y. ., Chung, S.C., Kim, Y.H., 2003, "Synthesis of Si, Mg substituted hydroxyapatites and their sintering behaviors", Biomaterials, 24, 389–1398.

[60] Okazaki, M., Miake, Y., Tohda, H., Yanagisawa, T., Matsumoto, T., Takahashi, J., 1999, "Functionally graded fuoridated apatites", Biomaterials, 20, 1421-1426.

[61] Farley, J.R., Wergedal, J.E., Baylink, D.J., 1983, "Fluoride directly stimulates proliferation and alkaline phosphatase activity of bone-forming cells", Science, 222, 330–332.

[62] Sivakumar, M., Manjubala, I., 2001, "Preparation of hydroxyapatite/fluorapatite zirconia composites using Indian corals for biomedical applications", Materials Letters, 50, 199–205.

[63] Gross, K.A., Rodriguez-Lorenzo, L.M., 2004, "Sintered hydroxyfluorapatites. Part I: Sintering ability of precipitated solid solution powders", Biomaterials, 25, 1375–1384.

[64] Lugscheider, E., Knepper, M., Heimberg, B., Dekker, A., Kirkpatrick, C.J., 1994, "Cytotoxicity investigations of plasma sprayed calcium phosphate coatings", Journal of Materials Science: Materials in Medicine, 5, 371-375.

[65] Nakade, O., Koyama, H., Arai, J., Ariji, H., Takada, J., Kaku, T., 1999, "Stimulation by low concentrations of fluoride of the proliferation and alkaline phosphatase activity of human dental pulp cells in vitro", Archives of Oral Biology, 44, 89–92.

[66] Lau, K.W., Akesson, K, Libanati, C.R., Baylink, D.J., 1998, "Osteogenic actions of fluoride: its therapeutic use for established osteoporosis. In: Anabolic treatments for osteoporosis. Editors: Whitfield, J.F., Morley, P., CRC Press, Boca Raton, FL, p. 207.

[67] Cheng, K., Weng, W., Wang, H., Zhang, S., 2005, "In vitro behavior of osteoblast-like cells on fluoridated hydroxyapatite coatings", Biomaterials, 26, 6288–6295.

[68] Guise, J.M., Mc Cormack, A., Anderson, P.A., Tencer, A.F., 1992, "Effect of controlled local release of sodium fluoride on trabecular bone", Journal of Orthopaedic Research, 10, 588–595.

[69] Gross, K.A., Rodriguez-Lorenzo, L.M., 2004, "Sintered hydroxyfluorapatites Part II: mechanical properties of solid solutions determined by microindentation" Biomaterials, 25, 1385–1394.

[70] Kim, H., Kong, Y., Knowles, J.C., 2004, "Fluor-hydroxyapatite sol–gel coating on titanium substrate for hard tissue implants", Biomaterials, 25, 3351–3358.

[71] Christel, P., Meunier, A., Heller, M., Torre, J.P., Cales, B., Peille, C.N., 1989, "Mechanical properties and short-term in vivo evaluation of yttrium oxide partially stabilised zirconia", Journal of Biomedical Materials Research, 23, 45-61.

[72] Owada, H., Yamashita, K., Umegaki, T., Kanazawa, T., 1989, "Humidity-sensitivity of yttrium substituted apatite ceramics", Solid State Ionics, 35, 401-404.

[73] Newnham, R.E., 1989, "Electroceramics", Reports on Progress in Physics, 52, 123–156.

[74] Sato, M., Sambito, M.A., Aslani, A., Kalkhoran N.M., Slamovich, E.B., Webster, T.J., 2006, "Increased osteoblast functions on undoped and yttrium-doped nanocrystalline hydroxyapatite coatings on titanium", Biomaterials, 27, 2358–2369.

[75] Piconi, C., Maccauro, G., 1999, "Review: Zirconia as a ceramic biomaterial", Biomaterials, 20, 1-25.

[76] Webster, T.J., Ergun, C., Doremus, R.H., Bizios, R., 2002, "Hydroxylapatite with substituted magnesium, zinc, cadmium, and yttrium: II Mechanisms of osteoblast adhesion", Biomedical Materials Research, 59, 312–317.

[77] Cullity, B.D., 1978, Elements of X-ray Diffraction, Second Edition, Addison-Wesley Publishing Company, Reading, MA, p.501.

[78] Bigi, A., Foresti, E., Gregorini, R., Ripamonti, A., Roveri, N., Shah, J.S., 1992, "The role of magnesium on the structure of biological apatites", Calcified Tissue International, 50, 439-444.

[79] Hilliard, J.E., 1964, "Estimating grain size by the intercept method", Metal Progress Data Sheet, 99-102.

[80] Thomas, M.B., Jarcho, M., Salsbury, R.L., Doremus, R.H., 1980, "Dense hydroxylapatite: Fatigue and fracture strength after various treatments, from diametral tests", Journal of Materials Science, 15, 891-894.

[81] Kamst, G.F., Vasseur, J., Bonazzi, C., Bimbenet, J.J., 1999, "A new method for the measurement of the tensile strength of rice grains by using the diametral compression test" Journal of Food Engineering, 40, 227-232.

[82] Ponton, C.B., Rawlings, R.D., 1989, "Vickers indentation fracture toughness test part I: Review of literature and formulation of standardized indentation toughness equation", Materials Science and Technology, 5, 865-872.

[83] Slosarczyk, A. Bialoskorski, J., 1998, "Hardness and fracture toughness of dense calcium phosphate-based materials", Journal of Materials Science: Materials in Medicine, 9, 103-108.

[84] Sabokbar, A., Millett, P.J., Myer, B., Rushton, N., 1994, "A rapid, quantitative assay for measuring alkaline phosphatase activity in osteoblastic cells in vitro", Bone Mineralization, 27, 57-67.

[85] Ratisoontorn, C., Seto, M.L., Broughton, K.M., Cunningham M.L., 2005, "In vitro differentiation profile of osteoblasts derived from patients with Saethre–Chotzen syndrome", Bone, 36, 627– 634.

[86] Gitelman, H., 1967, “An improved automated procedure for the determination of calcium in biological specimens”, Analytical Biochemistry, 20, 521-526.

[87] Gindler, E.M., King, J.D., 1972, “Rapid colorimetric determination of calcium in biologic fluids with methylthymol blue”, American Journal of Clinical Pathology, 58, 376-382.

[88] Akao, M., Aoki, H., Kato, K., 1981, “Mechanical properties of sintered hydroxyapatite for prosthetic applications”, Journal of Materials Science, 16, 809-812.

[89] Jarcho, M., Bolen, C.H., Thomas, M.B., Bobick, J., Kat, J.F., Doremus, R.H., 1976, “Hydroxylapatite synthesis and characterization in dense polycrystalline form”, Journal of Materials Science, 11, 2027-2035

[90] Ahn, E.S., Gleason, N.J., Nakahira, A., Ying, J.Y., 2001, “Nanostructure Processing of Hydroxyapatite-based Bioceramics”, Nano Letters, 1, 149-153.

[91] Evis, Z., Doremus, R.H., 2005, “Coatings of hydroxyapatite-nanosize alpha alumina composites on Ti-6Al-4V”, Materials Letters, 59, 3824 – 3827.

[92] Ahn, E.S, Gleason, N.J., Nakahira, A., Ying, J. Y., 2001, “Nanostructure processing of hydroxyapatite-based bioceramics”, Nano Letters, 1, 149-153.

[93] Ramesh, S., Tan, C.Y., Bhaduri, S.B., Teng, W.D., 2007, “Rapid densification of nanocrystalline hydroxyapatite for biomedical applications”, Ceramics International, 33, 1363–1367.

[94] Mobasherpour, I., Heshajin, M.S., Kazemzadeha, A., Zakeri M., 2007, “Synthesis of nanocrystalline hydroxyapatite by using precipitation method”, Journal of Alloys and Compounds, 430, 330–333.

[95] Fanovich, M.A., Porto LoPez, J.M., 1998, "Influence of temperature and additives on the microstructure and sintering behaviour of hydroxyapatites with different Ca/P ratios", Journal of Materials Science: Materials in Medicine, 9, 53-60.

[96] Shannon, R.D., 1976, "Revised effective ionic radii and systematic studies of inter atomic distances in halides and chaleogenides", Acta Crystallographica Section A, 32, 751-767.

[97] Narasaraju, T.S.B, Phebe, D.E., 1996, "Some physico-chemical aspects of hydroxylapatite", Journal of Materials Science, 31, 1-21.

[98] Lee, E.J., Lee, S.H., Kim, H.W., Kong, Y.M., Kim, H.E., 2005, "Fluoridated apatite coatings on titanium obtained by electron-beam deposition", Biomaterials, 26, 3843–3851.

[99] Cengiz, B., Gokce, Y., Yildiz, N., Aktas, Z., Calimli, A., 2008, "Synthesis and characterization of hydroxyapatite nanoparticles", Colloids and Surfaces A: Physicochemical and Engineering Aspects, 322, 29–33.

[100] Chenu, C., Colucci, S., Grano, M., Zigrino, P., Barattolo, R., Zambonin, G., Baldini, N., Vergnaud, P., Delmas, P.D., Zallone, A.Z., 1994, "Osteocalcin induces chemotaxis, secretion of matrix proteins and calciummediated intracellular signaling", Journal of Cell Biology, 127, 1149–1158.

[101] Muralithran, G., Ramesh, S., 2000, "The effects of sintering temperature on the properties of hydroxyapatite", Ceramics International, 26, 221-230.

[102] Lee, E.J., Kim, H.W., Kim, H.E., 2005, "Biocompatibility of Fluor-Hydroxyapatite Bioceramics", Journal of the American Ceramic Society, 88, 1309–1311.

[103] Amoros, J.L., Cantavella, V., Jarque, J.C., Feliu, C., 2008, "Green strength testing of pressed compacts: An analysis of the different methods", Journal of the European Ceramic Society, 28, 701–710.

[104] Vardar, O. Finnie, I., 1978, "An analysis of the Brazilian disk fracture test using the Weibull probalistic treatment of brittle strength", International Journal of Fracture, 11 (3), 495-508.

[105] Speirs, A.D.,Oxland, T.R., Masri, B.A.,Poursartip, A., Duncan, C.P., 2005, "Calcium phosphate cement composites in revision hip arthroplasty", Biomaterials, 26, 7310–7318.

[106] Brückner-Foit, A., Fett, T., Munz, D., Schirmer, K., 1997, "Discrimination of multiaxiality criteria with the Brazilian disc test", Journal of the European Ceramic Society, 17, 689-696.

[107] Marion, H., Johnstone, J., 1977, "A Parametric study of the diametral compression test for ceramics", American Ceramic Society Bulletin, 56, 998–1002.

[108] Mansur, C., Pope, M., Pascucci, M.R., Shivkumar, S., 1998, "Zirconia-calcium phosphate composites for bone replacement", Ceramics International, 24, 77–79

[109] Evis, Z., Ozturk, F., 2008, "Investigation of tensile strength of hydroxyapatite with various porosities by diametral strength test", Materials Science and Technology, 24, 274–278.

[110] Carneiro, F.L.L.B., 1943, "A new method to determine the tensile strength of concrete", Proceedings of the 5th meeting of the Brazilian Association for Technical Rules, 3rd Section, 126–129.

[111] Akazawa, T., 1953, "Methode pour l'essai de traction des betons", Bulletin RILEM 16, 13-23.

[112] Wright, P.J.F., 1955, "Comments on an indirect tensile test on concrete cylinders", Magazine of Concrete Research, 7, 87-96.

[113] Atai, M., Nekoomanesh, M., Hashemi, S.A., Amani, S., 2004, "Physical and mechanical properties of an experimental dental composite based on a new monomer", Dental Materials, 20, 663-668.

[114] Dickens, S.H., Flaim, G.M., Takagi, S., 2003, "Mechanical properties and biochemical activity of remineralizing resin-based Ca–PO_4 cements", Dental Materials, 19, 558-566.

[115] Hersek, N., Canay, S., Akca, K., Ciftçi, Y., 2002, "Tensile strength of type IV dental stones dried in a microwave oven", Journal of Prosthetic Dentistry, 87, 499-502.

[116] Zandinejad, A.A., Atai, M., Pahlevan, A., 2006, "The effect of ceramic and porous fillers on the mechanical properties of experimental dental composites", Dental Materials, 22, 382-387.

[117] Xu, H.H.K., Carey, L.E., Simon Jr., C.G., Takagi, S., Chow, L.C., 2007, "Premixed calcium phosphate cements: Synthesis, physical properties, and cell cytotoxicity", Dental Materials, 23, 433-441.

[118] Chau, K.T., Wei, X.X., 2001, "A new analytic solution for the diametral point load strength test on finite solid circular cylinders", International Journal of Solids and Structures, 38, 1459-1481.

[119] Komlev, V.S., Barinov, S.M., Rustichelli, F., 2003, "Strength enhancement of porous hydroxyapatite ceramics by polymer impregnation", Journal of Materials Science Letters, 22, 1215 – 1217.

[120] White, S.N., Yu, Z., 1993, "Compressive and diametral tensile strengths of current adhesive luting agent" Journal of Prosthetic Dentistry, 69, 568–572.

[121] Park, M.S., Eanes, E.D., Antonucci, J. M. Skrtic, D., 1998, "Mechanical properties of bioactive amorphous calcium phosphate/methacrylate composites", Dental Materials, 14, 137–141.

[122] Ishikawa, K., Miyamoto, M., Takechi, M., Ueyama, Y. Suzuki, K., Nagayama, M. Matsumura, T., 1999, "Effects of neutral sodium hydrogen phosphate on setting reaction and mechanical strength of hydroxyapatite putty", Journal of Biomedical Materials Research, 44, 322–329.

[123] Göller, G., Oktar, F.N., 2002, "Sintering effects on mechanical properties of biologically derived dentine hydroxyapatite", Materials Letters, 56, 142-147.

[124] Chenu, C., Colucci, S., Grano, M., Zigrino, P., Barattolo, R., Zambonin, G., Baldini, N., Vergnaud, P., Delmas, P.D., Zallone, A.Z., 1994, "Osteocalcin induces chemotaxis, secretion of matrix proteins and calciummediated intracellular signaling", Journal of Cell Biology, 127, 1149–1158.

[125] Ramesh, S., Tan, C.Y., Sopyan, I., Hamdi, M., Teng, W.D., 2007, "Consolidation of nanocrystalline hydroxyapatite powder", Science and Technology of Advanced Materials, 8, 124–130.

[126] Webster, T.J., Siegel, R.W., Bizios, R., 1999, "Osteoblast adhesion on nanophase ceramics", Biomaterials, 20, 1221–1227.

[127] Webster, T.J., Siegel, R.W., Bizios, R., 2000, "Enhanced functions of osteoblasts on nanophase ceramics", Biomaterials, 21, 1803–1810.

[128] Webster, T.J., Siegel, R.W., Bizios, R., 2001, "Nanoceramic surface roughness enhances osteoblasts and osteoclast functions for improved orthopedic/dental implant efficacy", Scripta Materialia , 44, 1639–1642.

[129] Webster, T.J., 2001, Nanophase Ceramics: The Future Orthopedic and Dental Implant Material, In: Ying, J.Y., editor. Advances in Chemical Engineering, Academic Press, New York, Vol. 27, p.125.

[130] Balasundaram, G., Sato, M., Webster, T.J., 2006, "Using hydroxyapatite nanoparticles and decreased crystallinity to promote osteoblast adhesion similar to functionalizing with RGD", Biomaterials, 27, 2798–2805.

[131] Guyton, A.C., 1991, Textbook of Medical Physiology, 8th ed. W.B. Saunders Company, Philadelphia.

[132] Kim, H.W., Lee, E.J., Kim, H.E., Salih, V., Knowles, J.C., 2005, "Effect of fluoridation of hydroxyapatite in hydroxyapatite-polycaprolactone composites on osteoblast activity", Biomaterials, 26, 4395–4404.

[133] Cheng, K., Weng, W., Wang, H., Zhang, S., 2005, "In vitro behavior of osteoblast-like cells on fluoridated hydroxyapatite coatings", Biomaterials, 26, 6288–6295.

[134] Wang, Y., Zhang, S., Zeng, X., Ma, L.L., Weng, W., Yan, W., Qian, M., 2007, "Osteoblastic cell response on fluoridated hydroxyapatite coatings", Acta Biomaterialia, 3, 191–197.

[135] Lee, H.U., Jeong, Y.S., Park, S.Y., Jeong, S.Y., Kim, H.G., Cho, C.R., 2009, "Surface properties and cell response of fluoridated hydroxyapatite/TiO2 coated on Ti substrate", Current Applied Physics, 9, 528–533.

[136] Qu, H., Wei, M., 2006, “The effect of fluoride contents in fluoridated hydroxyapatite on osteoblast behavior”, Acta Biomaterialia, 2, 113–119.

[137] Nakade, O., Koyama, H., Arai, J., Ariji, H., Takada, J., Kaku, T., 1999, “Stimulation by low concentrations of fluoride of the proliferation and alkaline phosphatase activity of human dental pulp cells in vitro”, Archives of Oral Biology 44, 89-92.

APPENDIX A

CALIBRATON CURVE FOR ALP ACTIVITY ASSAY

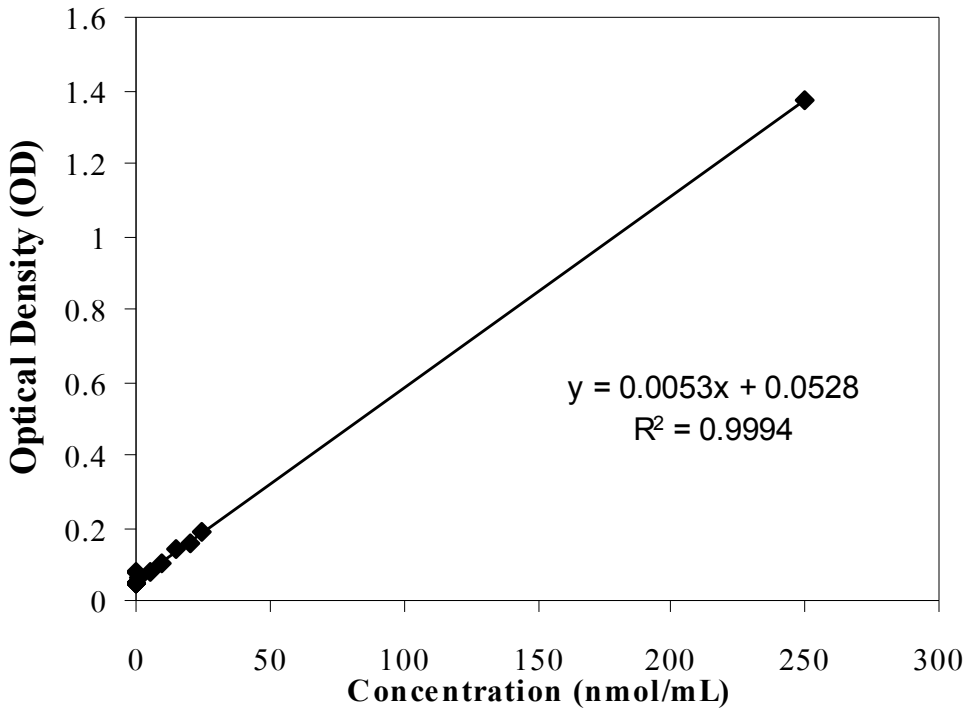

Figure A.1. The calibration curve of ALP production used in calculations of ALP activity assay.

APPENDIX B

CALIBRATON CURVE FOR BCA ASSAY

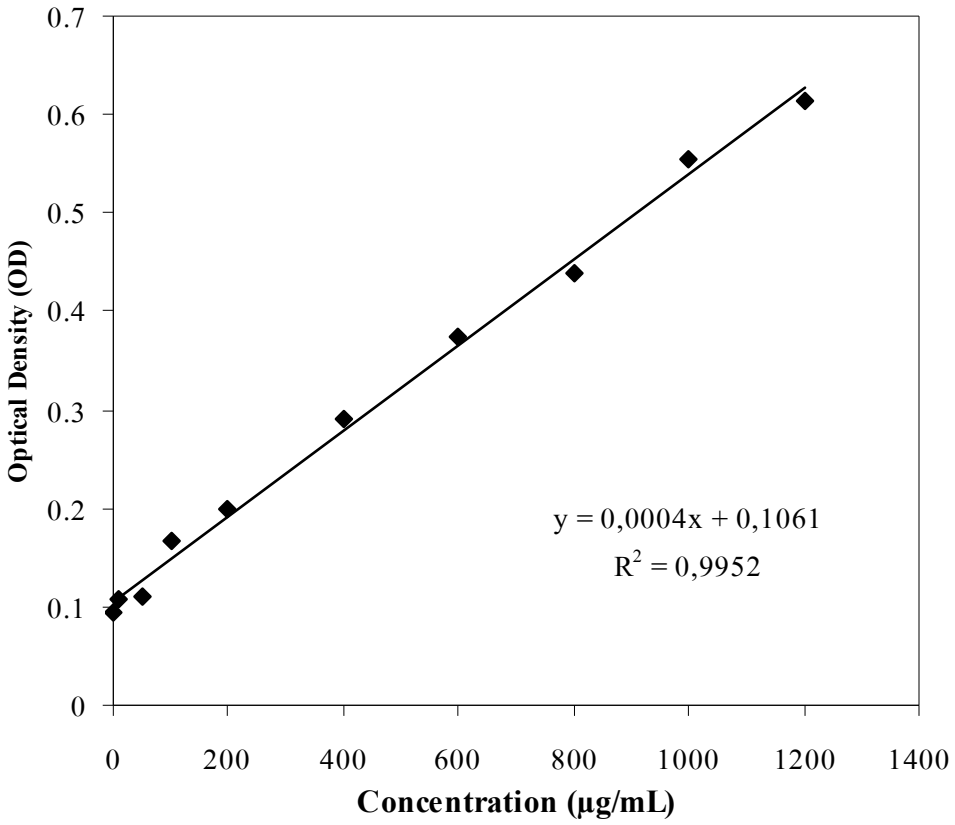

Figure B.1. The calibration curve of protein production used in calculations of ALP activity and calcium deposition assays.

APPENDIX C

CALIBRATON CURVE FOR CALCIUM DEPOSITION ASSAY

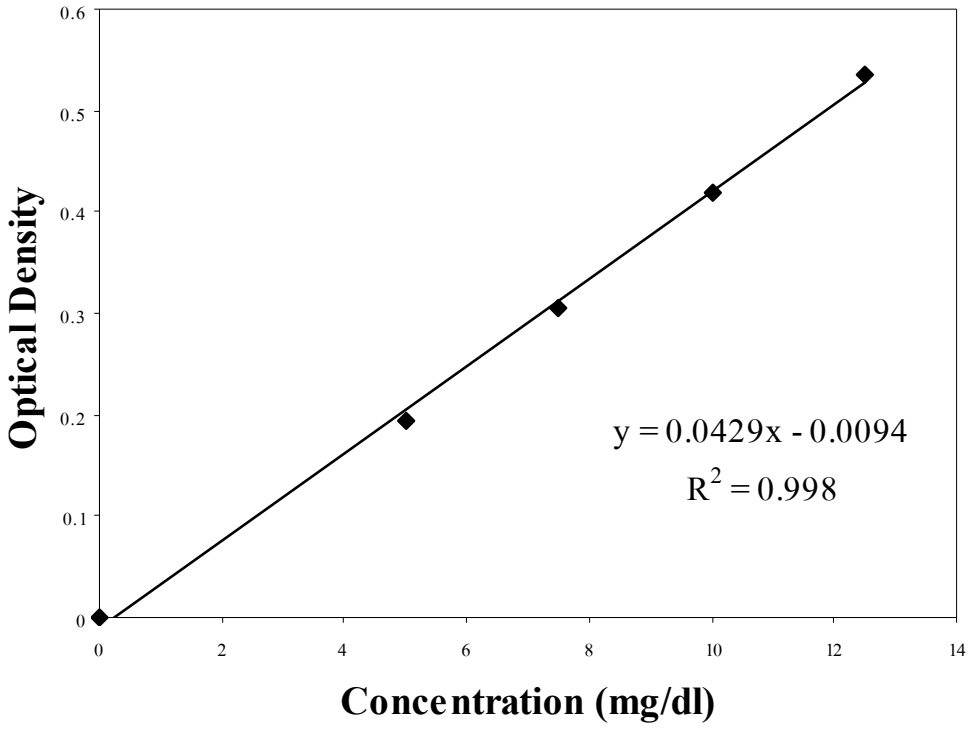

Figure C.1. The calibration curve of calcium content used in calculations of calcium deposition assay.